Stability of a Time-homogeneous System of Money and Antimoney
&
Kinetic Microscale Thermophoresis

Julian Alexander Cornelius Stein

München April 2021

Stability of a Time-homogeneous System of Money and Antimoney
&
Kinetic Microscale Thermophoresis

Dissertation

zur Erlangung des Grades
Doktor der Naturwissenschaft (Dr. rer. nat.)

an der Fakultät für Physik
der Ludwig–Maximilians–Universität
München

vorgelegt von
Julian Alexander Cornelius Stein
aus München

München, April 2021

Abstract

Human history is pervaded with financial crises. Lately, the global financial crisis of 2008 highlighted the role of uncontrolled creation of money through lending as a relevant source of financial instability. Motivated by an analogy to particle physics, time-homogeneity is imposed on monetary systems to approach and even possibly solve the associated problems. This implies a full reserve banking with a two-currency system which discriminates with an exchange rate between non-bank assets (money) and bank assets (antimoney). Payments can be made by passing on money in exchange for a good or receiving antimoney along with the good at respective price levels. Liquidity can be provided by the simultaneous transfer of money and antimoney at a negotiated exchange rate between money and antimoney, also termed the liquidity price. In this system, interest rates and credit creation are replaced by a varying price for liquidity. Here, the economic stability of such a system with an agent-based random economy model is studied, in which households and firms are urged by random boundary conditions to apply stochastic exchanges of goods via a limit order book mechanism, implementing the trading scheme of stock markets. The comparison of the market simulations for equilibrium and external shock scenarios of the prevailing monetary system with the money–antimoney system highlights two core aspects: First, the need of debt-limiting boundary conditions in order to equilibrate markets and second the similarity of the price dynamics of the studied systems as an indicator of fundamental functionality of the money–antimoney system.

The formation, stability and dissociation of biological ligand-binder systems play a fundamental role in nearly all aspects of living matter. Whereas the binding affinity is well described for many molecular ligand-binder interactions, their kinetic association and dissociation rates are far less well studied, due to lack of comprehensive experimental techniques. Here, Kinetic Microscale Thermophoresis KMST is established, which allows for a purely optical, immobilization-free and quantitative analysis of kinetic rates of biological ligand-binder processes. In a KMST measurement, the kinetic fingerprint is extracted from the fluorescence change back to equilibrium within a formerly IR laser-heated spot. Kinetic relaxation time constants between 0.01–$0.5\,\mathrm{s}^{-1}$ can be measured, allowing for the determination of on-rates 10^4–$10^6\,\mathrm{s}^{-1}\,\mathrm{M}^{-1}$ and off-rates 10^{-4}–$10^{-1}\,\mathrm{s}^{-1}$ in principle. For Cy5-labeled DNA strands, the expected exponential dependence of the off-rates on salt concentration, strand length and inverse temperature, respectively, was confirmed and measurements in crowded solutions were performed. The measured on-rates show linear dependence on salt concentration but weak dependence on strand length and inverse temperature. For biological reaction processes with sufficient enthalpic component, KMST offers a suitable immobilization-free determination of kinetic rates.

Zusammenfassung

Finanzkrisen treten in der Geschichte der Menschheit frequent auf. Die globale Finanzkrise machte 2008 im Besonderen die Rolle unkontrollierter Kreditschöpfung als relevante Quelle finanzieller Instabilität deutlich. Motiviert durch eine Analogie zur Teilchenphysik wird Zeithomogenität auf ein Geldsystem angewandt, um die mit Kreditschöpfung verbundenen Probleme zu mindern und möglicherweise auch zu lösen. Das führt zu einem Vollgeldsystem mit zwei distinkten Währungen: Nichtbankaktiva (Geld) und Bankaktiva (Antigeld). In diesem Geld–Antigeldsystem können Zahlungen durch Entgegennahme von Geld gegen eine Ware oder durch den Transfer von Antigeld zusammen mit der Ware zum jeweiligen Preis abgewickelt werden. Liquidität kann durch den gleichzeitigen Transfer von Geld und Antigeld zu einem ausgehandelten Liquiditätspreis zwischen Geld und Antigeld bereitgestellt werden. Der variierende Liquiditätspreis ersetzt Zinssätze und Kreditschöpfung. Die wirtschaftliche Stabilität eines solchen Systems wurde mithilfe eines agentenbasierten Zufallsökonomiemodells untersucht. In diesem handeln Haushalte und Unternehmen stochastisch Güter auf einer zentralen Limit-Orderbuch Börse äquivalent zu Handelsschemata an Aktienmärkten. Der Vergleich der Marktsimulationen für Gleichgewichts- und externe Schockszenarien des vorherrschenden Geldsystems mit dem Geld-Antigeld-System verdeutlicht zwei Kernergebnisse: Erstens, die Notwendigkeit individueller schuldenbegrenzender Randbedingungen, um effiziente Gleichgewichte in den Märkten zu erzielen und zweitens eine ähnliche Preisdynamik zum vorherrschenden Geldsystem, die auf eine grundlegende Funktionalität des Geld–Antigeldsystems hinweist.

Die Bildung, Stabilität und Dissoziation biologischer Liganden-Binder-Systeme spielen eine fundamentale Rolle in fast allen Aspekten belebter Materie. Während die Bindungsaffinitäten für viele molekulare Liganden-Binder-Systeme gut beschrieben sind, sind die kinetischen Assoziations- und Dissoziationsraten weniger gut erforscht. Mit der weit verbreiteten Microscale Thermophoresis Technik MST, werden mittels mikroskaliger Temperaturgradienten die Affinitäten von Ligand-Bindersystemen bestimmt. Durch eine im Vergleich zur MST Technik um eine Größenordnung verbesserte thermische Anbdingung des Samples können mit der neuartigen kinetische mikroskalige Thermophorese Technik KMST zusätzlich quantitativ die kinetischen Raten auf rein optischer und immobilisationsfreier Basis bestimmt werden. Bei einer KMST-Messung wird der kinetische Fingerabdruck aus der Fluoreszenzänderung zurück zum Gleichgewicht innerhalb eines zuvor IR-laserbeheizten Spots extrahiert. Gemessene kinetische Relaxationszeitkonstanten zwischen 0.01–$0.5\,\mathrm{s}^{-1}$ lassen die Bestimmung von Assoziationsraten 10^4–$10^6\,\mathrm{s}^{-1}\,\mathrm{M}^{-1}$ und Dissoziationsraten 10^{-4}–$10^{-1}\,\mathrm{s}^{-1}$ prinzipiell zu. Für Cy5-markierte komplementäre DNA-Stränge wurde die erwartete exponentielle Abhängigkeit der Dissozitationsraten und Dissoziationskonstanten von Salzkonzentration, Stranglänge und inverser Temperatur bestätigt und Raten in makromolekular gedrängten Lösungen gemessen. Die gemessenen Assoziationsraten weisen eine lineare Abhängigkeit von der Salzkonzentration auf, eine schwache Abhängigkeit von der Stranglänge und der inversen Temperatur. Für biologische Reaktionsprozesse mit ausreichender enthalpischer Komponente bietet KMST eine immobilisationsfreie Bestimmung der kinetischen Raten.

Contents

List of Figures

List of Tables

Part I

Stability of a Time-homogeneous System of Money and Antimoney

Chapter 1

Introduction

In this part of the thesis, the stability of a time-homogeneous system of money and anti-money is studied. The time-homogeneous system of money and antimoney is an alternative approach to the current monetary system, targeting the problems associated with credit creation. Simulation results of an agent-based random economy allow stability analysis and comparison of the money–antimoney system with the prevailing monetary system. The findings of necessary debt limitations as a stability boundary condition are discussed[1].

1.1 Debt relationships in human history[2]

As long as humans have lived in communities outgrowing natural living environment such as the family or tribe, debt-relation systems have played a crucial role in societies. In Mesopotamia, since 3500 BC the first organized cultures have been reported to track debt-relationships as obligations for future payments onto clay tablets. These clay tablets are not only one of the first evidences of human writing sources but also the first reported currency, in which payments could be made. The tablets could be sealed and circulated amongst citizens, serving as a promissory note. They were favoured over cattle, cowry shells, salt, or even slaves because they were durable and portable. The invention of metal money furthermore made payments easily divisible, which enabled the administration of the temples and settlements to introduce an accounting measure which served as a commodity to pay taxes.[3]

In Ancient Greek, Alexander the Great borrowed money from creditors with which he paid and provisioned his troops. Melting down gold and silver plundered after victorious battles, he minted his own coins and paid his creditors back. The conquered peoples were forced to slavery and partly worked in mines to guarantee future liquidity support for the victorious power.[4] In Ancient Rome, conquered populations were forced to adopt the Roman currency (coins) to facilitate the collection of taxes. To fight crises having risen

---

[1]Parts, Tables and Figures of this (1), the methods (2), results (3) and discussion (4) section contain works of me that were previously published in[1] and are reproduced with permission by ©Elsevier

[2]This section (1.1) follows my master's thesis section 'Debt Relationships in Human History'[2]

from excessive indebtedness or liquidity shortages, military expansion was an accepted mean to fight them. But once, new money supplies dried up and the foreign imports excessed exports, money (coins and metals) left the Roman Empire and as a consequence armies to defend the borders could not be afforded. This among other reasons led to the Fall of the Roman Empire.[5]

In the Late Antiquity, numerous invasions by various tribes destabilised many Middle European regions and trade decreased dramatically. Trading opportunities were limited by a lack of secure trade routes. In many regions available goods and services were limited up to the ones which were providable by the inhabitants. Due to the lack of acceptance (there were hardly any services, which could be bought by money), coinage disappeared in some regions and was replaced by old commodities, such as tallies, tokens or local coinages.[3,5]

In the Middle Age, religious institutions influenced the relation of debt and money to societies. European Christian societies returned to hierarchical structures of power: Priests, Warriors and Farmers. In contrast to splendidly equipped churches and magnificent cathedrals – actual gold and silver was increasingly laid in sacred places –, ordinary people living under the protection of Catholic Church were taught a modest live. Inevitably, arguments about wealth and markets became arguments about debt and morals. Debts between the stands were considered threatening because they implied the potential of equality. Everything that could lead to excess (vast concentrations of capital, commerce or usury) and could throw the entire social order out of its balances, was therefore condemned.[3] With Marco Polo introducing paper notes from his travels to China, the first banknotes-precursors were used as promissory notes, enabling the transport of large amounts of money over long distances.[6]

In Medieval Italy, a banking system developed in which gold ingots or coins could be deposited and stored at a bank. Keeping track over all transactions, bookkeeping mechanisms were invented and whenever demanded, the bank had to pay off the creditor. Thus a new form of money was invented: *book money*. Families like the Medici and later Fugger dynasties set up large banking-systems developing social and political influences – e.g. by financing wars – all over Europe. These banks also were lending institutions for wealthy citizens. Despite usury was prohibited by the Catholic Church – openly charged interest rates were forbidden – interest charges were hidden in bills of exchange as a workaround.

The first central banks were established in the 17th century, e.g. the Early Bank of Amsterdam. It was governed by the state and fulfilled three functions that are routinely carried out by central banks today: operating a large-value payment system, creating a form of money not directly redeemable for coin and managing the value through open market operation.[7] In 1844, the Bank-Charter Act established that the notes issued by the Bank of England were fully backed by gold reserves.[8] This monetary system is called *gold standard*. With the Age of Revolutions – the Industrial, the American and French Revolutions – almost all elements of financial apparatus that are associated with *capitalism* – central banks, bond markets, short-selling, brokerage houses, speculative bubbles, securization, annuities – came into being not only before the science of economics but also

before the rise of factories and wage labour itself.[3] Financial institutions prepared the way for industrialization and from the mid 1800s the ordinary man could now acquire credit and it became possible to access financial markets. Though, millions of laborers starved in proletarian living conditions, being forced to sell their work for a living, not elementarily differing from ancient slavery.

With the United States prospering in the beginning of 20th century, the first worldwide financial crisis arose. The crisis had been preceded by a credit bubble, in which not only banks, share holders but also ordinary people lost huge amounts of their savings due to rampant speculation.[9] As seen by the majority of economists, the crash on the stock markets in October 1929 led to the *Great Depression*, lasting until the mid 1930s. The prices fell and holding money seemed profitable. As a result the overall demand decreased and the unemployment rate rose. Importantly, the monetary supply contracted by 35%. Economists have proposed various attempts of explanations, defending contrary positions. The policy of the Federal Reserve Bank (FED) is a major controversial issue. Keynesians[10] and Monetarists[11] proposed the central bank should have poured liquidity into the banking system to accelerate spending in order to keep the nominal money stock and total nominal demand from collapsing.[12]

One reason for the FED to not increase liquidity in the early 1930s was the gold standard which limited the amount of credit the FED could issue. Required by the Federal Reserve Act, FED had to back up 40% of the FED notes issued. After the Great Depression, more and more countries left the gold standard and recovered from the crisis. They imposed the so called *gold exchange standard*, which fixed their exchange rate relative to the U.S. Dollar, which was still remaining on the gold standard until 1971. Then, Richard Nixon ended the international convertibility of the U.S. Dollar to gold, making the international monetary system a pure fiat money system, again as a mean to finance the Vietnam War.[3]

Since the Great Depression, one of the worst financial crisis was the financial crisis of 2008, the *Great Recession*.[13] It started as the *subprime crisis* in the U.S. housing market, in which banks granted loans to individuals who could not pay the credits back. In fear of losing money, banks aggregated credit contracts and sold those bonds to other banks, in the hope they would have sold all faulty credits before the bubble burst. The strategy did not succeed and the crisis spread to a global financial crisis, damaging trust in the whole financial sector. Banks did not lend money to each other and the collapse of large financial institutions had to be prevented the bailout of banks by national governments. The causes for the crisis are manifold and a deregulated financial sector in combination with uncontrolled creation of credit seemed to have played a crucial role.[14–16] The huge amounts of billions of Euro and U.S. Dollars needed to back up collapsing banks are just one example of the inconceivable *free game of the market*. The global network of money has gone beyond comprehension of many, if not all humans,[17], far away from its initial purpose to track economic transactions and debt-relationships.[3]

Recent technological advances not only gave rise to payment methods such as *electronic cash* but also to parallel non-state *crypto currencies*, like *Bitcoin*.[18] These currencies are

used as a medium of exchange, using digital cryptography to secure transactions and control the creation of new units. A major difference is the decentralized control of the currency, e.g. the bitcoin's block chain transaction database.[19] However, the not yet resolved sources of large fluctuations against the dollar and the crash of many digital currencies in December 2017 highlighted that these alternative forms of monetary systems do not provide stable currencies.[20]

Taken together, monetary systems in human history have not sustained for long periods and often revealed their weaknesses when greed came into play. Money and debt are closely related to almost the entire newer history of mankind. In contrast to previous crises, mankind now faces the fundamental question whether the current monetary system can stop the exploitation of the planet and provide a basis for sustainable economic action. It remains unclear if the multiple deficiencies of the prevailing monetary system are targeted sufficiently by the authorities. This gives rise to the question, if alternative monetary systems could counter the outlined deficiencies and how the alternative monetary systems could be designed.

1.2   Relevance of stability of monetary systems

The scientific discipline of physics studies and successfully characterizes the stability conditions of numerous systems from subatomic to cosmological scale. The understanding of the underlying principles allows to predict these systems' evolutions. The field of econophysics tries to bridge the gap between physics and economics by applying methodologies, concepts and principles of the physical science in the economic framework. It targets a deeper understanding of economic problems from a complementary point of view.

This work aims for a deeper understanding to which extent the application of physical conservation laws and mechanisms could increase the stability of monetary systems. In the so-called money–antimoney system, conservation laws and the particle–antiparticle analogy are applied on the relation of money and debt. To test if such an alternative monetary system could provide an increased stability in comparison to the prevailing monetary system, simulations of each system within an agent-based market economy are conducted. Although direct application of the found stability conditions may be impractical (there is no antimoney currency in the economic system), the study of the stability-imposing boundary conditions provides insights into price formation and market efficiency that can be related to the prevailing monetary system to improve its stability.

1.3   The modern monetary system

1.3.1   Functions of money

A general definition of money is difficult, since money performs a wide range of functions and there are many different monetary systems. In order to understand the concept of

money, its functions and the different types of money that exist and circulate in the modern economy are introduced. The functions of money can generally be defined threefold:[21] First, money serves as a store of value. As seen throughout history, money – in its various forms like gold or silver – was used to store economic value over a long time. On the one hand it needed to be non-perishable so that no value could be lost due to processes of expiry. On the other hand, to keep its value it must be hard to make and should not be easily copyable. Second, money is the unit of account in which prices are expressed, that is today usually a currency. Third, money is used as a medium of exchange. Money enables two parties to trade without the double coincidence of barter. The role of money as a medium of exchange was seen as the predominant role by many economists.[22]

These functions of money are linked closely to each other. For example, it is efficient for the unit of account to be also the medium of exchange:[23] the prices for services and goods within a country would ideally be expressed in the currency of the country so that a purchase can take place without a calculation of exchange rates. Not all assets would serve as good money-substitutes, i.e. although houses or real estate might be a good store of value, they are not easily transferable between agents.

The function-oriented definition does not comprise the inherent meaning for humans. From history, it is known that a major task of money was to serve as a memory of (past) economic transactions.[24,25] Whoever did something in the past and was given money for her or his service, money could be seen as the means to memorize economic action of the past. Someone who created a lot of economic value in the past could track this value creation by the accumulation of money for offering the services (or selling the goods). This view is opposed by other economists, who argue that anonymity enables agents to 'always start anew with a fresh identity'[26] and thus keeping debt track of individuals would not be beneficial.

1.3.2 Different types of money

Over centuries, humans used a large variety of non-financial assets (e.g. cowry shells, copper, gold) which served as a means to fulfill the above-defined functions of money. Non-financial assets are things that can produce goods an services for their owner, e.g. land, houses, machinery, etc. However, not all non-financial assets the people used served as good moneys. Cowry shells for example only could be used as a store of value in regions distant to the sea, where the shells could not easily be collected (at the sea) but had to be traded in for goods. When non-financial assets or goods would be valuable for other purposes than money, they are known as *commodity money*.[23]

In contrast, financial assets are claims on someone else in the economy, e.g. an IOU (I owe you) to a person, a company, a bank or a government. Because financial assets are claims on someone else in the economy, there is a corresponding financial liability. When two parties agree on the issuance of an IOU, they create a financial asset and an equal financial liability on the same service or good. In fact one could also imagine a financial world without money and only IOU from everybody to anybody, so that money

would cancel out.[27] In the following, the term asset generally refers to both financial and non-financial assets.

Because the assets and liabilities of an institution vary over time, it is desired to keep track of them. Therefore, assets and liabilities can be written in balance sheets. Typically, assets are written in a column (left) next to the liabilities (right) and their changes are noted along the vertical axis downwards. In order to show the current balance sheets of an institution, the different types of assets and liabilities are usually written below each other in the respective column.

Money is a special financial asset, because money provides a solution to the lack of *trust*. In this sense money is a social institution.[28,29] It is an IOU which is accepted by every participant in an economic system as a means of payment and thus serves as a medium of exchange, stores economic value and is the unit of account. Money in the modern economy is *fiat money*, lat. *fiat*: 'let it be done'. Fiat money is declared by a government to be legal tender .[30]. It has no intrinsic value (fiduciary money) and its value is not related to any physical quantity[31] and by law can not be converted into any other thing. Fiat money can be held by three groups: central banks, commercial banks and consumers (consumers in this context are individuals and firms), which all trust in the system. In a fiat money system, three different types of money can be distinguished: Currency, bank deposits and central bank reserves. The balance sheets, which keep track of the assets and liabilities, for the money-holding groups are shown in Fig.1.1.

Currency (blue) is made up of bank notes and coins and it is issued by the central bank to the commercial banks. Commercial banks can buy bank notes and coins from the central bank and give them to the consumers. Currency is a liability of the central bank and an asset for commercial banks and consumers. When a commercial bank buys bank notes from the central bank, it usually pays with central bank reserves. It is fundamental that consumers trust in the purchasing power of the currency so that the value of the currency is stable over time.

Deposits (light green) are money from consumers that are stored electronically in bank accounts of commercial banks. If a consumer makes a deposit of currency with a commercial bank, the consumer swaps its claims against the central bank for claims against the commercial bank. The commercial bank's currency holdings are increased and at the same time it credits the household's deposits. In this way, deposits are a liability of the commercial banks and an asset of consumers and express how much the bank owes to its consumers.

In order to meet the frequent deposit inflows and outflows, (only) commercial banks are allowed to hold digital central bank reserves (dark green) to carry out the large volume transactions between the commercial banks.[23] Thus, reserves are assets of the commercial banks and liabilities of the central bank.

The assets of the central bank are its loans given to commercial banks, securities of the central bank (e.g. bonds) and foreign assets (e.g. foreign exchange reserves). The central bank's liabilities are the reserves, the currency and the central bank's capital. Further commercial bank's assets are loans lent out to the households and other assets

Current monetary system balance sheets

Figure 1.1: Balance sheets of the three money-holding gropus in the modern monetary system. The assets of the central bank are the loans to banks, securities and bonds and the holdings of foreign currency reserves. The central bank's liabilities are the reserves of the commercial banks, its capital and the bank notes which are hold by the commercial banks and households as their assets. The commercial banks assets are their reserves at the central bank, the loans hold by the households and other assets, e.g. bonds. The liabilities of the commercial banks are the deposits of the households, the loans from the central bank, other liabilities and the bank's capital. Figure reproduced from[1].

(e.g. bonds, immovable property). Other commercial banks' liabilities are loans from the central bank, their capital and other bank liabilities (e.g. loans from other banks). Consumers posses other assets (e.g bonds) along with their deposits and currency held. Lastly, the liability of the households are their loans from commercial banks and other liabilities.

The identification of the different types of money can also be viewed from a hierarchical perspective:[32,33] what is seen as money at one level of the hierarchy can be seen as credit from the institution above: The central banks are at the top level, holding gold and securities as their assets which are not a liability to anybody else in the system. The currency issued by the central banks are the central banks' liabilities and at the same time the assets of the institutions below the central banks, namely the commercial banks. The deposits, that are liabilities of commercial banks, are the assets of the consumers. In this sense, deposits of the consumers extend the commercial banks' credits and are promises to pay currency on demand. At the bottom of the hierarchy, the consumers can hold liabilities, for example 'securities [that] are promise to pay currency (or deposits) over some time horizon in the future, so they are even more attenuated promises to pay'.[32]

1.3.3 Measurement of the quantity of money

How much money is there in the economy? This question naturally arises, after the different types of money are introduced. Unfortunately, this question can not be answered boldly. The complex structure of modern monetary systems demands for a careful approach. When money is quantitatively assessed, difficulties arise which different types of money should be counted as money.

It is the responsibility of the central banks to oversee their respective monetary systems. Therefore, the central banks define various measures to quantify the total amount of money
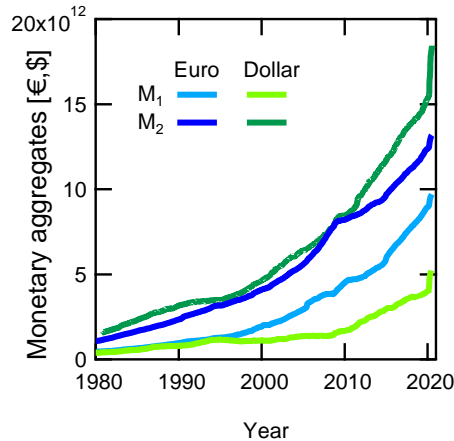
Figure 1.2: Monetary aggregates of Euro and Dollar currencies M_1 and M_2 from[34,35]

within their monetary systems. The definitions of measures for the quantity of money vary according to the information the central banks want to obtain. *Narrower aggregates* focus more on the liquid assets, which can easily be transferred within the economy. *Broader aggregates* include less liquid assets and highlight the function of money as a medium of exchange. To set monetary policies (e.g. to increase or decrease the quantity of money in circulation or setting the interest rate), central banks use the measures of money to gather information about the growth of the economy and the risk of inflation.

The definitions of the central banks, e.g. the Federal Reserve (central bank of the Unites States of America), the European Central Bank (ECB) or the Swiss National Bank differ slightly. According to the ECB, the money quantities can be defined as follows:[36]

M_0 is the sum of currency (notes and coins) in circulation held by non-banks and the central bank.

M_1 is the sum of currency in circulation and consumer sight deposits. These are deposits which can be withdrawn from banks in a very short period, e.g. checking accounts of individuals or business accounts. M_1 is a narrow monetary aggregate and can provide information about spending in the economy, as the money covered by M_1 is largely used for processing payments for goods and services in the economy.

M_2 is the sum of M_1 plus deposits with an agreed maturity of up to two years and deposits redeemable at notice of up to three months. This broader monetary aggregate can serve as an incremental indicator for future spending in the economy.

M_3 is the sum of M_2, plus repurchase agreements (a so called *repo* is the sale of securities, that is usually government debt, tied to an agreement to buy the securities back later), money market fund shares (money market funds are institutions that invest in short term debt instruments such as commercial paper and government bonds close to expiry, e.g. short term gilts and treasury bills[37]) and debt securities with a maturity of up to two years.

Central banks regularly publish data on the monetary measures. Fig.1.2 shows the historic development of M_1 and M_2 for the Euro and the Dollar.[34,35] The monetary aggregates increase exponentially over time. Not only the physical currency M_1 increases, but also the bank deposits M_2 and consequently, the bank credits increase. To justify the increase of monetary aggregates, the equivalence of value of economic goods and services and the money supply is made.[38] In this view, clearly, technological advances increased the value of all goods and services over time and consequently, the monetary base was increased, see[39] for discussion. The increase of the quantity of money is significantly driven by the process of credit and deposit creation by commercial banks.[40]

1.3.4 Credit creation in the modern monetary system and its limitations

In the modern monetary system, credit can in principle be created by central banks (*quantitative easing*[27]) and commercial banks. Commercial banks create credit by expanding their balance sheets by creating loans and deposits. To later understand the role of credit creation, the exact process on the bookkeeping level is described in detail as follows, adapted from.[27]

Assume two consumers (agents), a buyer who wants to buy an asset of the seller. Each agent has an account at a commercial bank. First, the buyer's bank creates a loan and respective deposit and credits the buyer's account the deposit and loan. The buyer pays the seller by exchanging the deposit with the house. The buyer is left with the house as an asset and the newly created loan as a liability. In the seller's assets, the house has exchanged with deposits. The balance sheets of the buyer and seller consumer are shown in Fig.1.3a. The balance sheets of the involved banks are shown in Fig.1.3b: After the buyer's bank simultaneously creates the loan-deposit pair, it needs to transfer the newly created deposit (which is a liability of the buyer's bank) to the seller's bank. Because deposits are liabilities of the banks, the seller's bank will not accept the deposit without receiving a balancing asset. The typical asset type banks accept as payment for loans on a large scale are the reserves. It would be unsustainable, if the buyer's bank settled all transactions by transferring reserves along with deposits to other banks, because it would run short on reserves. Thus, the buyer's bank would seek to attract new deposits along with reserves to not run short on reserves, see Fig.1.3c. This implies four limitations on the bank's lending quantity:

First, the competition in the credit market limits the credit creation of banks. The buyer's bank can choose to transfer central bank reserves (which are banks' assets) along with the deposit to the seller's bank. If there are many consumers asking for a credit, the buyer's bank would run short on reserves when creating many new loans. This is not favorable for a bank as a shortage in reserves limits its liquidity and could lead to an insolvency. In order to attract new reserves, the bank can try to attract new deposits. Then the bank of a consumer who owns deposits with the other bank would transfer the deposits along with reserves to the reserve-seeking bank. However, consumers probably

Money creation in the modern monetary system
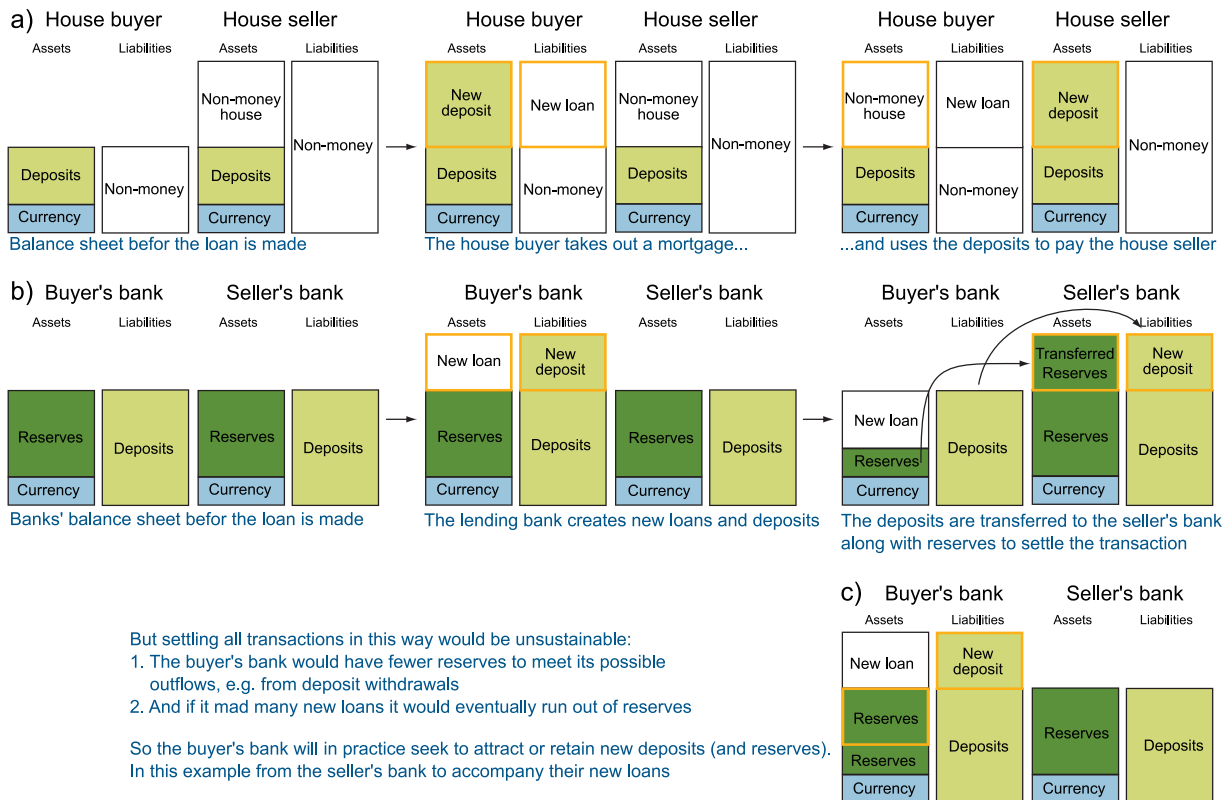
Figure 1.3: Money creation in the modern monetary system a) The balance sheets for a household (house buyer) which takes a credit at his bank (buyer's bank) to pay the house seller. When the buyer is granted the new deposit the buyer's bank also adds the loan to the buyer's liabilities. The buyer then uses the newly created deposit to pay for the house. b) The balance sheets for the buyer's bank and the seller's bank. The buyer's bank simultaneously creates the loan-deposit pair. It then needs to transfer the newly created deposit (which is a liability of the buyer's bank) to the seller's bank. The seller's bank will only accept the newly created deposit if the seller's bank also transfers reserves along with the deposit. It would be unsustainable, if the buyer's bank settles all transactions by transferring reserves along with deposits to other banks, because it would run short on reserves. c) Thus, the buyer's bank would seek to attract new deposits, e.g. from individuals withdrawing their deposits from the seller's bank, because then the seller's bank has to transfer its deposits along with reserves to the buyer's bank. Figure adapted and granted permission from [27].

only transferred the deposits, if the deposit-seeking bank would offer a higher interest rate to the deposit than the other bank. In order to compete with the other banks in the credit market, the bank has to operate in a profitable corridor between the interest rate it charges on granted loans and the interest it pays on deposits.[41] Thus, money creation is limited by the competition for loans and deposits with the other banks.

Second, the risk management of the bank limits the credit creation. The bank faces the risk of liquidity shortage, if large amounts of deposits are withdrawn at once. This stems from the associated reduction of reserves when a deposit is withdrawn by a consumer. Therefore, the bank has to ensure to possess enough reserves at each time point. To counter this risk, banks usually try to lend for longer periods, which fixes the amount of deposits for a negotiated period of time and facilitates the liquidity calculations of the banks. Banks also need to incorporate losses of defaulting loans, which they implement with higher interest rates they charge on loans if the expectation that the borrower could not repay the loan, e.g. when the ratio of loan to value (of a mortgage) is high. Then the bank would suffer more if the creditee defaults. In order to control the credit default associated risk, banks are encouraged to limit credit creation.

Third, the consumer's behavior in response of the granted credit influences the limitation of credit creation, e.g. if the house seller uses the received deposits to terminate a previously taken credit. Then the deposits of the house buyer are annihilated together with her or his loans. The buyer's bank removes the loans and deposits from its account. According to the *reflux theory*, the system returns to the state like it had before the creation of the credit.[42] But if the house seller chooses to spend the money elsewhere in the economy, the limitation on credit creation is less pronounced. If the money is passed through economy, e.g. through increased spending by the house seller, the inflationary pressure could possibly increase.[43] This means that prices may increase due to the increased demand for goods and services by households and firms. In this case, the creation of credit is not in general limited.

Fourth, the monetary policy set by the central bank can limit credit creation. The aim of the central bank is to provide price stability and set the inflation target. Therefore it sets the key interest rate for reserves. As the central bank is the monopole provider of central bank money, the interest rate on central bank reserves has a strong impact on many money markets: the interbank lending rate, that is the rate with which banks lend money to each other and finally the interest rate with which commercial banks grant loans to consumers. However, the central bank focuses on the stabilization of prices by primarily setting the interest rate for reserves and subordinately the choice of the quantity of reserves.

1.3.5 The role of banks in credit creation

The role of banks in credit creation in the modern economic system has been controversially debated for over a century:[40] Three main views on credit creation by commercial banks can be distinguished in economic literature. First, *financial intermediation theory of banking* views banks as intermediaries which lend out the deposits, they receive from households. According to this theory, banks do not *create* additional money and do only play a minor role in the economy by allocating liquidity needs and supplies. The theory became dominant under the influence of John Maynard Keynes, who played an important role for current macroeconomic research, and is taught in higher education textbooks.[44]

Second, according to the *fractional reserve theory*, individual banks can not create money on their own but the banking system on the systemic level can. The legal requirement to keep a fraction of the bank customer's deposit permits a bank to lend out unlimited loans. But by dispersion of deposits of one bank to an other bank, that is when one bank lends its excess reserves to an other bank, the increased reserves of the other bank allow it to lend out further loans. Accordingly, the total money supply depends on the reserve requirement or reserve ratio.

Third, *credit creation theory of banking* views banks as creators of money and liability pairs as 'fairy dust' out of 'thin air'. In contrast to the previous two theories, the credit creation theory of banking was the only one empirically proven up to now by Werner:[40]

> "When a real world bank grants a credit, it does not take the money away from internal or external accounts but 'invented' the funds by crediting the borrower's account with a deposit, although no such deposit had taken place... Thus it can now be said with confidence for the first time possibly in the 5000 years' history of banking - that it has been empirically demonstrated that each individual bank creates credit and money out of nothing, when it extends what is called a 'bank loan'. The bank does not loan any existing money, but instead creates new money. The money supply is created as 'fairy dust' produced by the banks out of thin air. The implications are far-reaching."

A discussion of the implications that arise from the credit creation theory of banking can only be sketched. The subject of the field is far reaching and the controversy strong, e.g. that this mechanism grants commercial banks profits in the order of billions each year.[45] The view of the Bank of England also supports the credit creation view by clarifying and supporting the role of credit creation as introduced above.[23] Recent admittance of central banks, that the role of banks in the money creation process was underestimated, fuels hope of clearance of the controversy. Importantly, credit creation, with the created money (and credit) not being a scarce good but being created by keystrokes, poses social questions: how can the role of banks be justified as producers of money, whereas large parts of society are permitted to create money?[46]

1.3.6   Challenges of credit creation

The *Cantillon Effect*

Credit creation leads to non-local shifts of monetary wealth.[39] This effect has been first described by Richard Cantillon in the 18th century.[47] The so called *Cantillon Effect* describes the loss of monetary wealth for agents that are not involved in a credit creation process but suffer from the associated increase of the quantity of money. The effect can be formally described by following the balance sheets of agents before and after credit is created[3].

---

[3]The description given in this section closely follows[39]

The assets and liabilities that agent k holds at time t_n are denoted $a_k^{(n)}$ and $l_k^{(n)}$. The money supply at time t_n is

$$M^{(n)} = \sum_{k=1}^{N} a_k^{(n)} = \sum_{k=1}^{N} l_k^{(n)} \tag{1.1}$$

Electronic bookkeeping prevents monetary units from being lost or destroyed. If agent i buys some good from agent j, and they agreed on a price Δ, agent i has several payment methods, see Fig.1.4a. Given that the trade happened between t_1 and t_2 and no other transactions occurred in that time period and the agents have chosen payment via direct asset transfer, the asset holdings after the trade will be

$$a_i^{(2)} = a_i^{(1)} - \Delta \qquad a_j^{(2)} = a_j^{(1)} + \Delta \qquad a_k^{(2)} = a_k^{(1)} \tag{1.2}$$

where $k \neq i, j$ are agents that are not involved in the trade. The liabilities are not affected in this case. The relative monetary wealth $\omega_k^{(n)} = \left(a_k^{(n)} - l_i^{(n)}\right)/M^{(n)}$ after the trade at $t^{(2)}$ is

$$\omega_{i,j,k}^{(2)} = \begin{cases} \left(a_{i,j}^{(1)} - l_{i,j}^{(1)} \mp \Delta\right)/M & \lessgtr \omega_{i,j}^{(1)} \\ \left(a_k^{(1)} - l_k^{(1)}\right)/M & = \omega_k^{(1)} \end{cases}. \tag{1.3}$$

Clearly, the monetary wealth of agent k is not affected by the payment. This is not the case if i chooses to pay by credit creation. In that case, the relevant changes of the agents' accounts are

$$l_i^{(2)} = l_i^{(1)} + \Delta \qquad a_j^{(2)} = a_j^{(1)} + \Delta \qquad a_k^{(2)} = a_k^{(1)}. \tag{1.4}$$

But now, the total money supply that can be used in trades has increased: $M^{(2)} = M^{(1)} + \Delta$. Then agent k suffers from a non-local shift of monetary wealth due to the increased money supply:

$$\omega_{i,j,k}^{(2)} = \begin{cases} \dfrac{a_{i,j}^{(1)} - l_{i,j}^{(1)} \mp \Delta}{M^{(1)} + \Delta} & \lessgtr \omega_{i,j}^{(1)} \\ \dfrac{a_k^{(1)} - l_k^{(1)}}{M^{(1)} + \Delta} & < \omega_k^{(1)} \end{cases}. \tag{1.5}$$

The shift in relative monetary wealth then reads

$$\Delta\omega_k = \omega_k^{(2)} - \omega_k^{(1)} = -\left(a_k^{(1)} - l_k^{(1)}\right)\frac{\Delta}{M^{(1)} \cdot \left(M^{(1)} + \Delta\right)}. \tag{1.6}$$

Thus, credit creation is potentially beneficial for debtors and adversely affects creditors. Only in the case of $a_k = l_k$, non-involved agents are unaffected by credit creation. Indeed, as $\sum \Delta\omega = 0$, there is an indirect transfer of monetary wealth from creditors to debtors.

Increase of financial instability

History has shown that the increase of credit to consumers, in particular rapid credit extension, can lead to economic crises[48] and is a major predictor for economic crises.[15] Increased credit sentiment can drive business cycles and have an impact on the real economy,[49–51] with high costs for the economy associated with boom-bust credit cycles.[14] Boom-bust credit cycles are economic time cycles in which the quantity of money increases 'booms' and decreases 'busts'. One example of a credit boom was the time between 2002 and 2007 in the US housing market,[52] where banks expanded credits for individuals although they could not repay their loans. This led to the subprime crisis, being one of the causes for the Global Financial Crisis of 2008.[53] Credit expansion is strongly associated with risks for the banking sector. Systemic risks rise, when all banks simultaneously try to increase granting loans. They would do so when they overestimate the economic perspective and underestimate the risks of consumers to default.[54,55] Notably, the expanded lending may stem from the misaligned incentives for executive employees,[56] also appreciated by the shareholders.[57]

Destruction of economic information

Viewing money from an information storage viewpoint, it can be argued that money serves as a special type of memory to track past economic transactions.[25] When money, in this view memory, can be created without a service done or good created in the past, the memory of the already existing gets flawed. In other terms: economic information is destroyed by credit creation, limiting the capability of money to serve as an (imperfect) memory of past economic transactions.[24]

Inflation

Credit creation leads to increasing price levels, also termed inflation.[15,58] Other sources of inflation are technological advances, the increase of real demand and production capacities. Whether the plethora of effects, that inflation has on society, are beneficial or harmful has been an ongoing debate for decades[38,59] and exceeds the scope of this thesis. At the bottom of the monetary policy debate the question is: do the positive effects of inflation, which are conjectured to be price stability[60] and fueling growth[61] up to a certain inflation rate, outperform the negative consequences, like the risks of high[62] and hyperinflations[63] for growth? The impact of inflation on unemployment rates is inconclusive.[64] However, for small inflation rates $< 2\%$, the range of positive effects seems weighing about the negative ones, still depending on region and time.[65,66]

1.4 The time-homogeneous money–antimoney system

1.4.1 From classical bookkeeping to antimoney

A natural starting point for the search of an alternative monetary system is to look at elementary bank bookkeeping, which is the mandatory measurement of money.[67] With reinterpreting money from the viewpoint of theoretical mechanics, bank bookkeeping processes translate to elementary particle physics interactions and give rise to a new field of studies, *bookkeeping mechanics*.[68]

Bookkeeping is an adding and subtracting scheme of assets and its negative counterpart liabilities. In particle physics, particles carry and exchange momentum with other particles. An analogy assigns assets to moving particles with positive momentum and liabilities to moving anti-particles (=antimoney) with negative momentum.[68,69] Each agent's monetary assets and liabilities are accounted for by a distinct money and antimoney account, respectively. Payments can either be made by passing money or by accepting antimoney along with the received good or service. Hence, two different price levels establish, one for each method of payment. Accounts may not be transferred between agents, only asset and liability units may change their owner. This corresponds to an exchange of momentum between particles in the particle frame.

Looking at the elementary process of money creation reveals that money and liabilities are always simultaneously created or annihilated as a money-liability pair. Analogously, a particle-antiparticle can only be created or annihilated in particle-physics. Consequently, the distinction of the money currency and the liability currency similar to particles and antiparticles resembles a generalization of bookkeeping. Assets and debts do not necessarily have to be accounted for in the same currency. In contrast, traditional bookkeeping neglects this relation and connects both sides with no other reason than tradition.

The visualization of T-account bookkeeping translates to Feynman graphs of interacting particles. Bookkeeping has four elementary transactions: transfer of assets, transfer of liabilities, creation of credit and termination of credit. All transactions follow the principles of a balanced state *'For every asset there must be a corresponding liability'*.[70] This principle corresponds to the physical law of momentum conservation – in a closed system, the sum of particle momentum at any time must be zero. All transactions can be interpreted as an interaction of two particles, see Fig.1.4 (1) – (4). A transfer of assets (1) or liabilities (2) is mapped to the translation of momentum of a moving (anti)particle to another particle or antiparticle, respectively. Assets and liabilities are never added or subtracted directly but only symmetrically created or terminated. Therefore the creation (3) and termination (4) of credit is implemented by a particle-antiparticle pair creation and annihilation, respectively. No other interaction between a particle and antiparticle is allowed.

To calculate profit in bookkeeping, changes of assets and liabilities are recorded over a fixed time interval. Profit increases, if assets increase or liabilities decrease. Likewise profit decreases, if assets decrease or liabilities increase. In the mechanical picture, the same results are obtained by calculating the momentum change over time for the asset
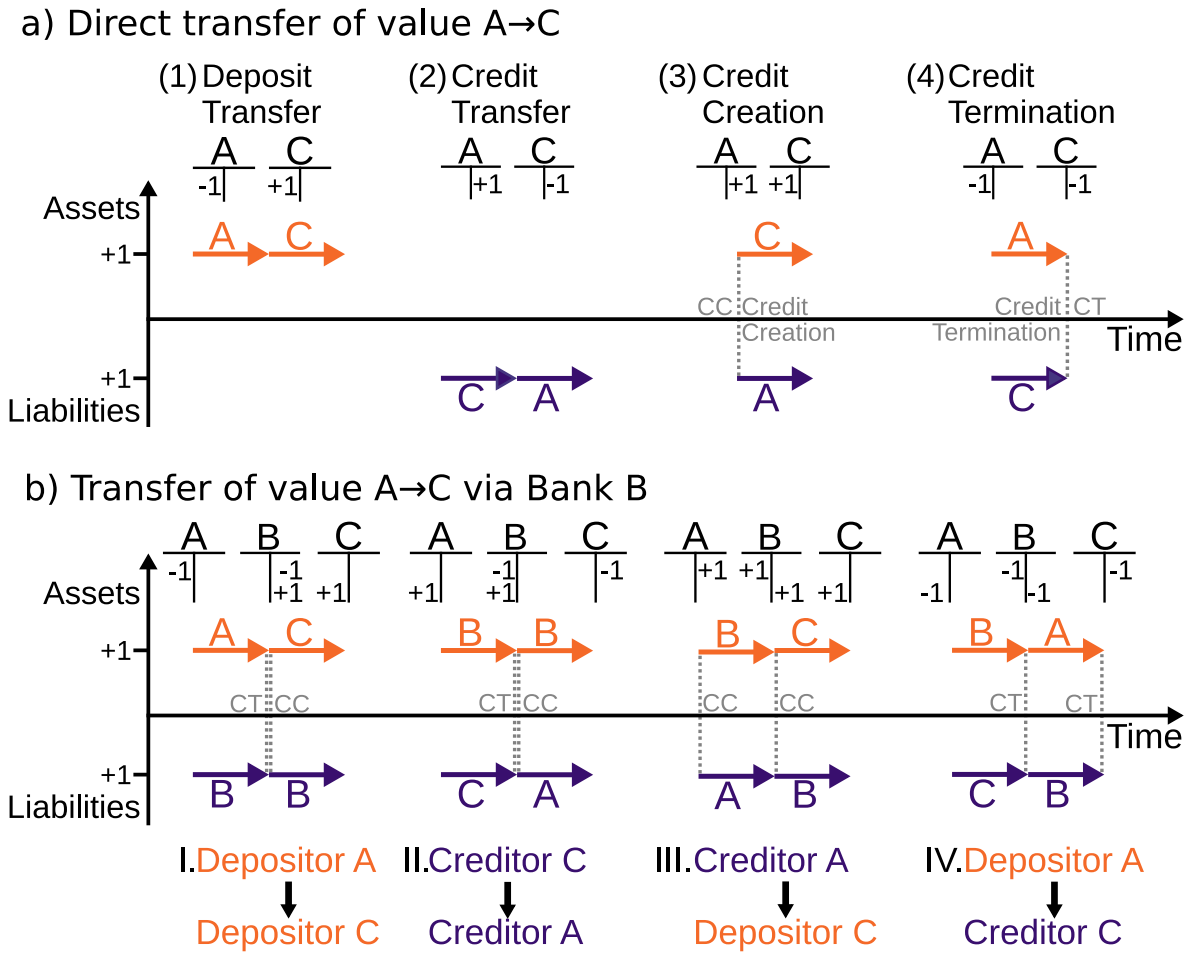
Figure 1.4: Bookkeeping mechanics and corresponding agents A,B and C T-accounts of assets and liabilities. The colors correspond to assets (orange) and liabilities (violet). In the T-accounts, time axis goes vertically from top to bottom. **(1)** − **(4)** elementary bookkeeping processes for payments. Assume C has done something for A and A directly wants to compensate monetarily. (1) A directly gives assets to C, (2) C gives liabilities to A along with the good or service it has done for A, (3) A and C agree on a payment by credit creation. C gets the created asset and A is left with the liability part of the creation. (4) Credit termination, A gives away the asset and C terminates a liability. **I** − **IV** Payment methods for agents A and C via a bank B. When C has done something for A and A wants to pay C. The method of payment depends on the accounts of A and C, if they are depositors or creditors at the bank. (I) Deposit transfer between two depositors, (II) credit transfer between two creditors, (III) deposit transfer from depositor to creditor and (IV) credit transfer from creditor to depositor. Resting particles are not shown.

particle and liability particle of an agent. Since momentum change over time is the physical definition of a force, the profit of an income statement is derived from the forces, which accelerate and decelerate the agent's asset and liability particle.[69] Connecting to statistical

physics, forces that drive particles in physical systems can be implemented in economic systems as changes of an agent's asset and liability holdings.

1.4.2 Bank bookkeeping with money and antimoney

Payments between two parties are usually performed via commercial banks. The money-antimoney system is compatible with the traditional bank bookkeeping framework. The interaction of depositors, creditors and banks can be described by the combination of the transaction, creation and termination processes. The fundamental statement that a depositor's assets are a bank's liabilities and a creditor's liabilities are a bank's assets is well-reflected by the strict distinction between the asset and liability currencies. The four fundamental bookkeeping transactions of depositors, creditors and banks are shown in bookkeeping accounts and particle graphs, see Fig. 1.4 (I–IV). Assume agent C has done something for A and A pays C for the service by transferring monetary value to C. The agents A and C can chose between the four different methods of payment and four price levels would establish, respectively. The payment methods are a deposit transfer (I) from A to C, a credit transfer (II) from C to A or a credit creation (III) or termination (IV). From the graph it gets clear, that an asset of the bank is a liability of an agent and vice versa. As later energy conservation will be imposed on the system, only a transfer of either assets or liabilities will be allowed. Two price levels establish: one for payment with assets (I) and one for payment with liabilities (II). Note, the direction of liability units at a payment: When C pays A by a transfer in liabilities, C gives the service along with an amount of liabilities to A.

1.4.3 Principles of the time-homogeneous money–antimoney system

Inspired by the Noether theorem,[71] conservation laws are imposed on the money–antimoney system. The Noether theorem connects symmetries of actions of physical laws with the conservation of physical quantities. The symmetry of passing on and receiving money and antimoney units takes the physical law of momentum conservation into account.[68] The conservation of momentum is equivalent to the invariance of the laws of physics under a spatial transformation. That means that in a closed system, the transfer of momentum is independent of the particles, the direction of the transfer and the point of space. In traditional bookkeeping, momentum conservation is known as the principle, that the total sum of money must equal the sum of all liabilities at each time point: *'For every asset, there must be a corresponding liability.'*[70] Similarly, to conserve momentum in the money-antimoney system, the sum of money must equal the sum of antimoney at each time point. This means that the passing of money is independent of the involved agents and the direction of the transfer. However, the total sum of money and antimoney may change by the simultaneous creation of a money-antimoney pair, which does not violate

momentum conservation, as the sum of money equals the sum of antimoney at each time point.

The Noether theorem connects time-homogeneity with the conserved quantity of energy in the physical context. When a system obeys time-homogeneity, an interaction is independent of the time point of the interaction. In the context of the money–antimoney system, the quantity of energy corresponds to the total quantity of money and antimoney.[72] When time-homogeneity is applied on the money-antimoney system, the arbitrary creation and annihilation of money and antimoney is prohibited and thus the total quantity of money is conserved. An important consequence is that the time point of a transaction then is not dependent on the time point of the transaction. Based on the conservation of the quantity of money and antimoney, three major differences to the prevailing monetary system (in which money may be created) arise.[39,68,69,72,73]

First, the conservation of the quantity of money and antimoney forbids any kind of money (credit) creation. This fixes the money and antimoney supply throughout time and credit granting is decoupled from an increase of the quantity of money. This corresponds to a full-reserve banking system (also narrow or 100% banking system), which was proposed by Irving Fisher.[74] Fisher claimed four major advantages, which were recently supported by an analytic and simulation study.[75] These are (1) a reduced amplitude of business cycle fluctuations, (2) the elimination of bank runs, (3) highly reduced public and (4) private debt levels. Extended research has to explore the coherence of the money-antimoney system with Fishers claims. The the simulation results below, see Fig.3.6, will show that the response to production and credit shocks is similar to a single currency system, which may indicate support for Fisher's first claim.

Second, the conservation of money and antimoney mitigates non-local shifts of monetary wealth (Cantillon Effect):[39] In the prevailing monetary system, credit creation leads to non-local shifts of monetary wealth for agents which are not involved in the creation process, see Sec.1.3.6. But the fixed money supply of the time-homogeneous system of money and antimoney prevents such non-local shifts of monetary wealth. In the time-homogeneous systems of money and antimoney, $\Delta = 0$ and the non-involved agent's money and antimoney holdings M_i and A_i are not affected by a liquidity trade between two other agents. This means that the date of a trade does not have an influence on the system, contrary to the prevailing monetary system. Single currency systems with constant money supply have been reported to be unstable because liquidity shortages can arise easily.[76] Simply introducing an arbitrary second currency does not solve the problem, as the increase of one of the money supplies leads to a change of the exchange rate and subsequently triggers inflation.

Third, the liquidity shortages accompanied with a fixed money supply[33,77] are targeted by the introduction of a liquidity providing mechanism. Liquidity provision in the contemporary monetary system is ensured by the creation of book money by commercial banks. Usually, long-term credit contracts are made between a commercial bank and a creditor. The price of liquidity is determined by the payment of interest, which is often fixed for a long time span. In the money–antimoney system, liquidity can be obtained at

a liquidity market by a simultaneous transfer of money and antimoney at a free floating exchange rate from seller to buyer. If agent A seeks for liquidity and agent C provides it, agent C will simultaneously transfer an amount of money ΔM and antimoney ΔA at a negotiated liquidity price $\phi = \frac{\Delta A}{\Delta M}$ to agent A. Thus, liquidity provision turns into an ordinary purchase and the liquidity mechanism is decoupled from money creation. No long-term credit contracts, that charge interest rates, have to be signed and interest rates are turned into varying prices for liquidity.[39]

The prevailing monetary system couples growth to the creation of credit (and money), but voracious creation of money can harm the economy.[15] Thus, it is highly questionable, if the catalysis of growth should be induced solely by money creation. Further, it is not clear, if the current money creation mechanism is the proper fundamental mean to target growth questions. Although mainstream economic literature widely holds the view that full reserve banking could not account for growth,[78] growth can be accounted for in the time-homogeneous system of money and antimoney as follows: to enable growth, the money–antimoney system couples money and antimoney to the number of individuals who act within the economic system. Growth is still possible, first through an increase in the population: every agent who enters the system is initially endowed with the same amount of money and antimoney. Conceptually this would increase the total amount of money and antimoney and thus break time-homogeneity. The justification of this break in time-homogeneity is the entrance of a new economic subject, a new acting person which increases the potential (and thus energy) of the system . A debate if this view is more desirable than the coupling of the amount of money to the amount of goods needs to be carried out in the future. Second, growth can be achieved through the active use of the liquidity mechanism, which is not yet included in the simulations. For example, an agent who wants to invest would ask for liquidity, then use the received money to make the investment and later has to sell the newly created capacities in antimoney (which he/she got along with the money in the liquidity trade). A future question is, how exactly the money–antimoney system behaves under economic growth and which impact the liquidity mechanism has.

1.4.4   Balance sheets of the money–antimoney system

Having introduced the basic principles of the money–antimoney system and its differences to the prevailing monetary system, the balance sheets of the money–antimoney system are introduced. This is one possible way to embed the money-antimoney system in the existing economic framework of central banks, commercial banks and households. Fig.1.5 shows the balance sheets with the major items of the central bank, commercial banks and households for a) the current monetary system, adapted from literature,[67,79] b) the money-antimoney system and c) the later introduced model economy. For simplification, only non-government related items are listed.

The current monetary system's balance sheet is shown in Fig. 1.5 a), as introduced above. In the money–antimoney system, see Fig. 1.5 b), the central bank holds securities

a) Current monetary system balance sheets

Central Bank (CB)	
Assets	**Liabilities**
Loans to banks	Reserves
Securities & bonds	Capital
	Bank notes
Foreign assets	

Commercial Bank	
Assets	**Liabilities**
Household loans	Household deposits
Reserves	Loans from CB
Bank notes	Other bank liabilities
Other bank assets	Capital

Households	
Assets	**Liabilities**
Deposits	Loans
Bank notes	
Other assets	Other liabilities

b) Money-antimoney system balance sheets

Central Bank	
Assets	**Liabilities**
Loans to banks	Reserves
Securities & bonds	Capital
	Other central bank liabilities
Foreign assets	

Commercial Bank	
Assets	**Liabilities**
Household loans	Household deposits
Reserves	Loans from CB
Other bank assets	Other bank liabilities
	Capital

Households	
Assets	**Liabilities**
Deposits	Loans*
Other assets	Other liabilities

c) Model economy balance sheets

Bank	
Assets	**Liabilities**
Household loans	Household deposits

Households	
Assets	**Liabilities**
Household deposits	Household loans*

Accounted in ▢ money ▢ antimoney

*For the limited money-antimoney system the individual loans are limited

Figure 1.5: Balance sheets for the current and the money–antimoney system. (a) Shows the above introduced balance sheets of the current monetary system. (b) In the money–antimoney system, no banknotes exist, as money and antimoney are directly issued digitally to the households by the commercial banks. The central banks tasks would not differ largely from the current tasks. However, the commercial banks issue the money and antimoney to the households and are not allowed to create money. This assigns the commercial banks a pure intermediary role. (c) Shows the simplified model economy's balance sheets for the central bank and households, there are no commercial banks involved. Figure reproduced from [1].

and foreign assets, maintains reserve accounts for commercial banks and could possibly lend loans to the commercial banks. There is no issuance of bank notes through the central bank, as money and antimoney are digital currencies. However, the money–antimoney system focuses more on the directly issued deposits (digital money) and loans (digital antimoney) from the commercial banks to the households, e.g. every time a new human is born she/he is endowed the same amount of money and antimoney. The role of commercial banks in the monetary system is different from their role in the current monetary system. Because the money–antimoney system is a full reserve banking system, commercial banks are not allowed to create a money–antimoney pair and lend the money to households. Thus, the role of commercial banks shifts from financial actors which in the past triggered a multitude of economic crises,[14–16,40,50] but was assigned only a minor or none role of

allocating credit supply and demand[40,80] – to pure intermediaries who do not pose a systemic threat to economic stability. They can only allocate the deposits and loans from their customers but not expand the money and debt in circulation. The assets and liabilities of the households are money and antimoney, respectively. Fig. 1.5 c) shows the balance sheets for the agent-based model economic system, which includes one bank and the households. The bank initially issues equal pairs of money and antimoney to the agents (households & firms), but does not further interact in the simulations with the agents.

The risk monitoring is not carried out by the central bank by applying policy rules or setting interest rates but by all market participants simultaneously. The decentralized risk monitoring of the commercial banks in the current monetary system multiply was shown to fail.[15] Also the centralized risk monitoring and managing of the central banks, especially after 2008, did not sustainably stabilize the monetary system.[81] This particularly shows that neither banks nor central banks have thoroughly succeeded in ensuring stability and decreasing risks for society. Instead, in the money–antimoney system the monitoring, sharing and managing of risk is carried out by all agents simultaneously by negotiating the liquidity price. Every agent has access to the central liquidity market and thus can evaluate the values of the past (debt = antimoney) with the values of the future (savings = money) in real time. This does not exclude commercial banks a priori, which could establish themselves as an intermediate matching aggregate supply and demand for credit.

1.4.5 Transfer potentials shape wealth

In order to make predictions about economic quantities within a money-antimoney framework, the statistical properties were studied under random money transfers. Statistical physics of random money transfers have gathered an increased attention since the computational power for simulations has increased.[82,83] The underlying assumption that random boundary conditions of an economy force agents to act in a random way can be well-implemented by using the strong methods of statistical physics modeling boundary conditions. Economic quantities such as an agent's asset and liability holdings can be translated to fundamental statistical variables. For example, an agent's asset holdings a and liability holdings l, can be assigned to the microeconomic quantity of wealth $\omega = a - l$. The macroeconomic quantity of money $M = \langle M \rangle = \int_{-\infty}^{\infty} n \, |\omega| \, d\omega$, with $n(\omega, t)$ the density of monetary wealth, can be derived from the microeconomic variable ω.

Initial studies focused on the monetary part of a most simple model economy and confirmed various wealth distributions depending on the exact boundary conditions:[72] In the studies, agents are initially endowed with an equal amount of money and liabilities and a central bank holds the complementary liability and money pairs. Agents randomly exchange money and liabilities via one of the four introduced methods of transfer. Interestingly, random economies reach economic equilibria, if boundary conditions limit central quantities, e.g. the quantity of money or an agent's maximum liability holdings. Boundary conditions can be imposed locally by transfer potentials $U(\omega)$ that act on an agent's wealth

by the force $F(\omega) = -\nabla U(\omega)$ via additional transfers of monetary units. Another implementation covers global boundary conditions, that forbid certain transfers (e.g. credit creation that would increase the quantity of money above a limit). One important finding is that local wealth transfers and global boundary condition can yield for the same wealth distribution.

1.4.6   Money- and debt-side quantity theory

Quantity theory connects the total money supply with the gross domestic product (GDP). GDP measures the value of all (monetary) transactions carried out within a defined period. The natural question arises, if quantity theory holds in the agent-based random economy. Quantity theory states that

$$M \cdot V_M = GDP_M = \sum_i p_{M,i} \cdot q_{M,i} \tag{1.7}$$

for the total money supply M, the money circulation velocity V_M, the monetary GDP_M, all good types i, all money prices $p_{M,i}$ and respective money-good quantities $q_{M,i}$. For the money–antimoney system, quantity theory is expanded by formulating a money and antimoney-side quantity theory.

$$M \cdot V_M = GDP_M = \sum_i p_{M,i} \cdot q_{M,i} \qquad A \cdot V_A = GDP_A = \sum_i p_{A,i} \cdot q_{A,i} \tag{1.8}$$

with total antimoney units A, the antimoney circulation velocity V_A, the antimoney GDP_A, all good types i, all antimoney prices $p_{A,i}$ and respective antimoney-good quantities $q_{A,i}$ and money-side quantity theory as stated above. In this way, the monetary GDP_M accounts for all transactions carried out by payment of money and the antimoney GDP_A accounts for all transactions carried out by payment in antimoney.

The distinction of a money-related GDP_M and debt-related GDP_A might contribute to a better understanding of money and debt flows in economic systems. Measuring distinct money and debt sides of the GDP could serve as an indicator of overheated economies and economic crises. Supposed that many agents need to carry out payments in antimoney, due to little money holdings and indebtedness (high antimoney holdings) an increase of transactions in antimoney then leads to an increase in the GDP_A with probably increasing antimoney good-prices $p_{A,i}$ and antimoney good quantities $q_{A,i}$. An increase of the GDP_A could then indicate an upcoming crisis.

The expansion of quantity theory for a money side and debt side for systems of distinct money and debt flows was proposed in earlier works:[84] In a system of random money / debt transfer and money-debt creation process, the equiblibria conditions were achieved for limited money supply by required reserve regulations. Equilibria were characterized by money circulation and debt circulation. Money circulation in these systems depended on earning and spending of traders, whereas debt circulation was formed by loan granting and repayment. In contrast, the results of random money transfers in systems that allow unrestricted creation of money and liability pairs show that quantity theory did not hold.[69]

1.4.7 Statistical mechanics in a random economy

By applying time-homogeneity on a money-antimoney system, the quantity of money and antimoney and thus energy is conserved. Credit creation and termination are prohibited thoroughly. Recent studies with a time-homogeneous system of money and antimoney in a random economy yielded promising results to target sources of instability:[39] In the economy, agents initially are endowed with equal money and liability holdings, a central bank owns the counterparts, respectively. Because the total quantity of money is conserved, payments are restricted to either passing money or receiving antimoney. Thus two price levels establish p_a for a payment in assets and p_l for a payment in liabilities. The agents randomly exchange amounts x_j, $j \in \{m, l\}$ of money m or liabilities l, respectively, according to an exponential distribution $p(x_j) = \frac{1}{p_j} \cdot \exp\left(-\frac{x_j}{p_j}\right)$ with the respective price level p_j. The particular choice is motivated by observations, that in real economies low prices are encountered much more often than high prices.

Dragulescu and Yakovenko have shown that the equilibrium monetary distribution in a closed single currency system is given by a Boltzmann-Gibbs distribution for a wide range of random transfer schemes, namely those that have time-reversal symmetry.[85] As the money and antimoney holdings are independent of each other – not yet a liquidity mechanism is introduced – the expected Boltzmann-Gibbs distribution can be found. The probability P_j of finding an agent with monetary units x reads $P_j(x) = \frac{1}{T_j} \cdot e^{-\frac{x}{T_j}}$ with the parameter $T_j = \frac{M_j}{N}$ being equivalent to a temperature in statistical physics. M_j is the total amount of money or liability units and N the total number of market participants. An agent's relative monetary wealth is defined by $\omega = \frac{m-l}{M}$ its asset m and liability holdings l and M the money supply. The monetary wealth distribution separates from the monetary asset and liability distributions and turns out to be a Laplacian. A fundamental question is, if agents could hoard large amounts of antimoney. To partially address the issue, a liability limit $\hat{\omega}$ on individual debt can be imposed. The underlying asset distribution remains unchanged, but the liability distribution changes its temperature due to the cutoff.

There have been few attempts to study the role of credit extension in random economies. Chen et al[86] adopted the money–antimoney framework and allowed for money and credit creation as a means of payment. They find that the monetary aggregate increases up to an upper externally-set limit due to local credit creation of the agents. If an agent possesses enough money it will simply transfer it to the other agent. But if an agent, who hast not enough money – needs to pay another agent, and as long as credit creation is allowed, the random choice of payment due to micro circumstances will (at least stochastically) lead to an increase of the money supply. These findings stress the importance of credit restriction, as the system only reaches equilibrium when an upper monetary aggregate limit is imposed.

1.5 Choice of a suitable economic modeling approach

The preceding studies on the money–antimoney system mainly focused on analytical approaches investigating statistical physics properties of the system.[39,68,69,72,73] Because monetary systems have a fundamental influence on real economies, it is desired to test the stability of the money–antimoney system in a real world implementation. Ideally, a federal bank would issue a persistent digital money and antimoney currency, which could be used for the payment of real goods and services within a country. In this way real economic data could be obtained and analyzed. Unfortunately, this implementation lies over the scope of non-institutional research and thus exceeds the available capacities. The next best option is a game-theory experimental laboratory, in which humans interact with each other in the framework of a model economy. To obtain preliminary insights into such a modeling approach, a simulation setup is designed in order to define the boundary settings of the economic framework.

There are several requirements for the economic framework. First, the model has to reflect a real but simplified economy with a clear structure of input and output variables and quantities, independent of side-effects due to the structure. Second, the measurement and comparison of monetary stability of single currency and bi-currency systems has to be possible. Third, the model has to be easily adaptable: On the one hand it should be easily integrable to other economic models. On the other hand, game theoretical experiments with real people shall be conductible. To decide which model should be used, a standard economic theory model and the alternative agent-based model are shortly discussed. First, a standard economic theory approach is sketched and its drawbacks are highlighted. Second, a complementary econophysically-inspired *agent-based model* approach is introduced and compared to the economic standard approach.

1.5.1 Addressed issues of standard economic DSGE models

Standard New Neoclassical Synthesis predominantly describes economic systems with Dynamic Stochastic General Equilibrium (DSGE) models.[80,87–90] Firms rent capital and labor to produce goods and sell them in perfectly clearing markets to infinitely-lived households. The households maximize a utility consumption function under an intertemporal budget constraint, including consumption, cash holdings and work labor. A fiscal authority sets a monetary policy by levying taxes and a global interest rate is set by a central bank. Commercial banks, if any, are implemented as financial intermediates, allocating asset and credit resources. Households and firms are aggregated, resulting in a single *representative* household and firm agent. All agents form their expectation rationally.[91] Optimality conditions are imposed and interactions between the actors are modeled as sets of transition equations covering stochastic processes. Parameters used to model the equations are estimated and the system is calibrated. The system's response to exogenous technological, financial and price shocks can be studied, to infer monetary and fiscal policy recommendations. However, DSGE models suffer from some serious weaknesses, regarding the realism of their assumptions. The Great Recession served as a natural experiment for

economic analysis and showed the inadequacy of standard theory's predominant frameworks. Some critics of mainstream economic theory view the economic crisis of 2008 as crisis for economic theory.[13,92–95] Six major pitfalls of economic mainstream DSGE models are discussed, based on.[96–98]

First, *Rational expectations*, introduced by[91], states that agents know about the 'true model' of the economy and optimize their utility with all available information to forecast the future free of systemic biases; also all agents know that every other agent acts and reacts in every possible situation.[98] These assumptions do not take into account that human behavior and action in an economic framework is not solely an optimization problem. Individual decisions may be better described by taking reciprocity, fairness, identity, money illusion, loss aversion, herding, and procrastination into account.[99] Recent studies try to incorporate bounded rationality; agents do not perfectly calculate their expectations, but use rules of thumb,[100] apply 'trial and error' learning[101] or start to include heterogeneous expectations.[102]

Second, the concept of the *representative agent* has been critically questioned for decades.[13,95,96,103–105] Macroeconomic foundations face difficulties justifying the assumption of the aggregate representative agent fourfold: First, the justification for the assumption that the aggregate of individual (maximizing) decisions can be governed by a representative agent is not thoroughly plausible, if not absent.[103] The behavior of rational individual interacting units does not imply a rational aggregate acting agent and vice versa. Second, the reaction (due to a shock, e.g. a change in policy) of a representative agent may not be the same as the aggregate reaction of the individuals it represents.[103] The fact that economic shocks do not affect all agents at once but diffuse through the various parts of economic systems with different speeds, affecting various agents at varying times in a different manner. Also cascades of e.g. bankruptcies in a credit network are not reflected.[96] Third, even if the first two doubts were dispelled – that is when the representative individual is a utility maximizer and its choices coincide with the individuals' choices – there may well be the case that in two situations of which the representative prefers the first to the second, every individual prefers the second to the first.[103] The preferences of the representative individual cannot legitimately be used to decide whether one economic situation is *better* than another. Fourth, the interaction of heterogeneous individuals with each other is completely ruled out by the representative agent, neglecting all distributional issues which were one of the major cause of the Great Recession.[95] Increasing indebtedness of a large part of a population paved the way to the subprime mortgage crisis.[96,106] It is hard to believe that an economy could be properly described by a representative agent while not incorporating distribution issues.

Third, DSGE model assume and require economic systems to be in *equilibrium.*[80,87–90] Due to an inability to cope with non-linearities in the model equations, the simplification of log-linearization[107] is applied, which imposes the system to be in an equilibrium state.[13,108] To justify this simplification, it is pointed that an economy, that is kicked out of equilibrium, quickly returns to equilibrium due to some adjustment processes.[109] In stark contrast, it has been shown that such adjustment processes do not exist under

general conditions and the equilibria are neither unique[105,110] nor stable.[13,111–113] Also the dynamics governing the adjustment of prices (due to a shock) lack intrinsic logic.[97,112,114] After a shock kicks a system out of equilibrium, the system needs time to recover towards equilibrium. The Walrasian auctioneer calculates prices and sets equilibrium before trades take place. Real economies work the other way round. Agents meet at markets discovering (equilibrium) prices as a result of trading. Price formation therefore has to be the result of trading and not its precondition.[112–114]

Fourth, identification,[115,116] estimation[115] and empirical validation[117] of DSGE models' parameters face various difficulties. DSGE models capability to reproduce empirical stylized facts such as fat tails or rare economic shocks is doubtable, since the models on the one side make too simplifying estimations[117] and pay too much attention to the identification of the structural model without testing the potential misspecifications of the underlying statistical model.[118] Thus it is questionable, if DSGE results can be used to address policy and economic questions.[115]

Fifth, the concept of perfect markets, as assumed in standard DSGE models, states that demand equals supply and the markets clear efficiently. To address this critique, recent models have incorporated frictions in markets.[119] Yet, they do not account for an actual interaction of agents within a market and miss to include asymmetrical information distribution, strategic interaction, expectation formation on the basis of limited information, mutual learning, social norms, externalities, market power, predation, collusion and the possibility of coordination failure.[105]

Sixth, the role of the banking sector is underestimated or even not included in many DSGE models.[40,120] Banks are assigned only an intermediate role, reallocating resources by collecting deposits and lending credits. Although recent DSGE models incorporate financial markets,[119] the effects of the creation of money (similar to *fairy dust out of thin air*[40]) are not sufficiently included. Basic DSGE models[80] assume a non-monetary, non-banking system, in which the representative agent is perfectly creditworthy and never default. DSGE models did not have the capacity to incorporate shifts of risk premia and credit constraints, hoping that authorities could quickly restore normal conditions to make the standard model usable again.[121]

1.5.2   Econophysic framework of an agent-based random economy

Econophysics can be viewed as a complementary approach to standard textbook economics. Its name results from 'economics' and 'physics'.[122] Econophysics views economic systems as complex evolving systems, populated with heterogeneous agents, whose far-from equilibrium interactions continuously change the structure of the system.[123,124] Econophysics has developed for the last 30 years in the fields of complex systems,[125] financial markets,[123,126] wealth and income distributions.[83] Also a sister-field of sociophysics[127] has been established. Many fundamental assumptions made by econophysic approaches differ from the above mentioned assumptions of DSGE models and lead to al-

ternative methodologies. The motivation to apply econophysics-motivated methodologies is to counter the above discussed deficits of the standard economic approaches.

First, monetary systems are seen as complex economic systems. When complex economics are studied, *agent-based models* (ABM)[13,128,129] provide an appropriate method to describe economic systems from a bottom-up perspective:[98] Aggregate properties emerge out of repeated – inherently non-linear – interactions among heterogeneous entities (agents) differing in behavior, strategies, actions, wealth, types, time scales and others. Agents live in complex systems that evolve through time far from rationality and equilibrium. To reflect real-world complexity and the inability of agents to act hyper-rationally, agent-based models allow agents to behave as boundedly rational entities with adaptive expectations. Typically, agents are assigned a type, like household, firm, bank, etc with a defined set of actions, e.g. placing orders within a market and consuming/producing goods, and an (adaptive) strategy, defining the concrete actions. The characteristics of an agent critically depend on the economic framework, in which it 'lives'.

However, agent-based models are still in their infancy and some issues remain open. The number of parameters to describe an ABM is prone to become large, reducing the explanatory power of the model. Typically the specifications of agents' behavioral rules are injected by many parameters, to meet as much as possible what is observed in reality.[98] Especially, when an ABM reproduces stylized facts, how can one be sure that it represents the minimal mechanism capable of the system? Thus ABM modelers try to keep the number of parameters within their model as small as possible and use reasonable simplifications, in order to avoid relics of over-parametrization.

Second, the interaction of the agents is set to take place at markets. The importance of the understanding of markets was highlighted by the crashes of the Great Recession, when the loss of trust in the global financial system led to worldwide price corrections at stock exchanges. Of course, research on markets is not a specific econophysic approach but has been carried out by standard economic theory for a very long time. According to an economic definition of markets,[130] 'a market opposes buyers and sellers, and the prices which resolve this conflict are the input but also in a sense the outcome of the agents' economic calculations'.[131] But the econophysic approach to characterize markets with a mechanistic order processing logic departs from standard economic approaches. In contrast to DSGE models, where market maker algorithms match supply and demand side, the econophysic approaches to model markets focus on order books. In order books, the atomistic placement and cancellation of supply and demand orders drives the prices. From an econophysic viewpoint, these order book processes show similarities with reaction–diffusion processes[132] and have been studied in depth.[133,134] They serve as a simple tool to determine prices and are applicable for good–money trading and for good–antimoney trading.

Third, the actions of the agents are defined. The agents are equipped with behavioral rules, which define their actions, e.g. set an order price and amount. Economic theory focuses on the optimization of individual utility functions when defining the actions of agents. From an econophysic perspective, not the optimization of potential outcome

but the randomness of natural processes plays a dominant role for setting the agents'
actions. In so called 'random economies',[39,73] the agents are assigned only little intel-
ligence. This reflects a non-strategic trading behavior, like the agents' behavior in the
random economies, in which they are forced by their environment to act in a random way.
A connected field of study are markets with *zero intelligence* traders.[135] These types of
traders do not base their decisions on any observation but randomly act without memory
of past actions. Zero Intelligence traders were studied in the works of Cliff et al.[136–138]
Interestingly, *Zero intelligence Plus* traders which are equipped with a memory and are
able to sense their environment and adapt to it, outperform human traders in market
experiments.[139]

1.5.3 Choice of an econophysic modeling approach

The description of economic systems from the economic perspective and the econophysic
perspective deviate in many respects. To find a suitable framework for a test simulation
environment for the money–antimoney system both approaches are compared. The choice
of the econophysic approach is justified by the following points: The econophysic approach
provides reasonable methodology, reductionism, notion of uncertainty within the models
and the consideration of extreme events.[140]

Most economic models are based on an *a priori* methodology that invents economic
reality. Economics do not aim for describing the real world but develop abstract models
and characterizing their parameters. This interpretation is highly questioned by econo-
physics, which aims for describing economic reality with models that are based on empir-
ical data.[98,117] Economic theory is not an empiric discipline and has not seen itself as a
such.[141,142] Because monetary systems have a real impact on societies and general theoretic
findings have already been drawn – indicating an overall stability of the money-antimoney
system[39] – an econophysic approach is chosen. Within the econophysic framework of an
agent-based model the money-antimoney system can be simulated and in principle be
compared to human experimental data.

Economics apply *atomistic reductionism*, i.e. use of the representative agent imply-
ing that the macro level equals the micro level and neglecting the dynamics of inter-
acting agents in markets. The use of the representative agent in economics could not
account for the recent economic crisis. By contrast, econophysics focus on the interac-
tion of heterogeneous populations of agents,[105] known as *interactive reductionism*. The
macroeconomic output emerges endogenously from the microeconomic interaction.[95] An
agent-based model serves well as a framework to study the response of markets within a
money-antimoney system due to shocks. Taking a close look at the interaction of agents
suffering from a shock can give insight in the stability conditions for markets.

In economic models the notion of uncertainty is a priori reduced to risk within a
Gaussian world of statistical models, independent of reality. Uncertainty then is usu-
ally measured with the probabilistic approach of the standard deviation. In contrast,
econophysics try to provide a collection of operational instruments to study uncertainty of

economic systems. Thus econophysics becomes to a more *uncertainty-oriented* discipline than economics.[124,143] The actions of individuals in real world are often governed by their uncertain environment. The introduction of traders that act randomly meets these needs.

In economics, extreme events like the latest financial crisis, are not considered but stable equilibria are ensured by the architecture of the models.[140] In contrast, econophysics is founded on the universality of statistics and takes extreme events – with a significant probability – into account. Since the crisis, especially monetary systems have undergone extreme events. To study the stability of the money–antimoney system, it is therefore reasonable to use a framework that takes the occurrence of extreme events into account. The framework of a random economy agent-based model allows for simulation of such extreme events.

Recently, rational expectations are questioned within economics.[102,144] In contrast to economics, econophysics studies models that assume that agents do not to form rational expectations[145] and thus act randomly – forced by their chaotic environment.[146] The aim of a real world implementation of a money-antimoney system motivates to apply random behavior in simulations, as agents randomly exchange money, see above. Then, the random simulations can be compared to empirical data and even more interestingly, the influence of human behavior on the stability of monetary systems can be evaluated. The choice of a random economy is also motivated by the finding that details of money exchange do not appear to be essential.[85] The irrational decisions of the agents are a maximal probe for the stability of the money-antimoney system.[1]

It is also highly questionable if the economy is in the state of an equilibrium, as argued above. Therefore the agent-based approach does not impose equilibrium as such but has a highly increased flexibility and equilibrium is only one possible outcome.[98]

1.6 Outlook: Multi-flavor money-antimoney system

Going one step further, the concept of the money–antimoney system can serve as a starting point to explore novel monetary systems. The concept of the money-antimoney system can be expanded to multiple private currencies, in which each individual issues its own unique money and antimoney currency and in which corresponding liabilities are stored at a central bank. The fundamental idea behind multi-flavor money-antimoney systems is the following: On the micro level, money is discrete; there is a smallest amount of money which can be exchanged. On the macro level, that is in an agent's wallet, the discrete states overlay and form an ensemble of money. The wallet of an agent can store all flavors of moneys and antimoneys, respectively and the monetary wealth of an agent would be the sum of all moneys minus all antimoneys of the agent's wallet. This can be compared to the superposition of light of various frequencies to obtain 'white' light on the aggregate level. In the beginning, all $\mathcal{N}$ agents start with the same amount of all flavors of money and antimoney units. Now there are not only 2 markets for each type of good, but $2 \times \mathcal{N}$ markets per good. The agents can make payments in the flavor they desire.

The system has three major advantages over the prevailing monetary system: first, it is time-homogeneous and thus the negative consequences associated with the creation of money are mitigated. Second, debt defaults can be tracked back to its origin, after a highly indebted agent exits the system. This means that a creditor is liable for its granted credits. When an agent defaults, it exits the system together with its unique money/antimoney units. Third, the liquidation algorithm for the exiting agent is a simple retraction of all of its (indexed) flavored money and antimoney units from all other agents' accounts and mitigates problems of complicated reversal transactions when an agent exits a single money-antimoney system. Adding new agents to the system is easy: when a new agent enters the system, all agents simply add the initial amount of money and antimoney of the new unique flavor to their wallet.

However, it could be argued that a system of multi-flavor money and antimoney would not be considered as a monetary system. To fulfill the requirements of a monetary system, first the agents would need to like to accept each unique flavor of money and antimoney to reflect the storage of value. Second, the money and antimoney units need to be the measure of account, which is obviously fulfilled as prices can be expressed in each flavour. Third, the multi flavor moneys and antimoneys need to be medium of exchange, which would be possible as a digital currency. Clearly, the first requirement is the most difficult to prove and would need empirical studies to show the applicability.

Having introduced the time-homogeneous system of money and antimoney and argued why the stability of such a system should be studied with an agent-based, random economy, the next chapter introduces the used simulation techniques.

Chapter 2

Methods

2.1 Economic model system

2.1.1 Setup of agent-based model economy

In the round-based agent-based model, a central bank initially created the money–anti-money pairs and N agents acted as firms and households. The central bank did not interact otherwise, see Fig.1.5**c**) for the balance sheets of the bank and the agents. The endowments for each agent were initially 10 money and 10 antimoney units. The corresponding bank liability and bank money parts were held by the central bank. The state of an agent was determined by its money and antimoney holdings, its good stocks, its utility and a set of harvestable (producible) goods. The economy did not exhibit growth but stayed in a stationary state with constant harvest. Testing the stationary stability was crucial for potential dynamic state equilibrium research, because if no equilibria were found in the stationary state, presumably no equilibria could be found in a growing economy. Extending the equilibrium from the stationary state to a sufficiently slowly-growing economy, stationary boundary conditions would apply and thus stability could be inferred.

The flowchart of the round-based economy is shown in Fig.2.1. At the beginning of each round, each firm harvested goods at zero costs and then tried to trade them at central good exchanges. After trading, the households consumed the purchased goods, increasing their utility. Firms harvested h out of G different types of consumption goods at zero cost. All simulations were conducted for an economy with $h = 2$ and $G = 4$, resulting in $\binom{G}{h} = \binom{4}{2} = 6$ different sub populations. Each of those harvested a different set of goods. The agents harvested the fixed amount of 0.5 goods per good type per round. For each good type $N/2$ agents produced the good and the complementary $N/2$ agents could consume the type. Agents could store infinitely many goods without storage costs. Importantly, each single agent represented both a household and a firm at once. When it could produce a good, it supplied it at the money or antimoney-good market (firm). When, it could not produce the good type (this means in the complementary markets), it demanded for it in the respective markets (household). A firm could not consume self-

harvested goods, which forced all agents to trade on the markets in order to increase their utility. The utility accumulated over the rounds and increased by the consumption of goods with $\Delta U = 1 - \exp(-\frac{1}{c}\Sigma_i x_i)$ with x_i the consumed goods per good type i and a curvature factor which was set $c = 7$.

The aim of the studies were the comparison of the prevailing monetary system with the money–antimoney system. Therefore simulations of a single money, a two money system and the money–antimoney system were conducted. Simulations of a single money system provided a reference to compare the results for the other systems. The results of the single money system served as a baseline to validate the results of the chosen parameters. The comparison of results of a two-money system with the money–antimoney system provided answers to the question to what extend the money–antimoney system differs from a two-money system.

2.1.2 Limit order book characteristics

The goods were traded sequentially at stock exchange markets with a memory-less conventional limit order book mechanism (LOB), also used by Schewe et al.[147] to model crop market price developments. Models of agent-based order books were used to study various systems and provide a widely-used tool in the world's economic markets by a suitable bottom-up approach.[148] Individual actions have an influence on the markets, no market maker is needed and the prices evolve endogenously through the interaction of the agents.[148] To simplify the simulations, the LOB did not have a memory. In this way, the study focused on the price and volume movements without exhibiting artifacts as bid–ask spreads and other typical continuous order-book mechanisms.

The agents tried to place a new limit order bid every round. The order was defined by the amount, the price per unit and the good type-dependent demand or supply type. The markets were traded in sequential good-type order and for each good, first the money-good then the antimoney-good market were processed. For demand bids, households submit a maximum price per unit they were willing to pay and for supply bids, firms submitted the minimum price per unit for which they were willing to sell. For demand bids, the amount of goods d and for supply bids, the amount of goods s were submitted. When a submitted bid exceeded an agent's money budget, the bid did not enter the order book. The prices were rounded to the price grid with smallest tick 1×10^{-5}. The order book collected all valid bids and determined the aggregate demand and aggregate supply per price. The aggregate demand (supply) curve is determined by summing over all amounts of bids that accept higher (lower) prices. The trading price P_{tr} was set to be the price that maximized the minimum of the demand and supply curve. The corresponding trading volume is V_{tr}. In good-money markets, this price was equal to the intersection of the supply and demand curve, because the demand curve was monotonously decreasing and the supply curve monotonously increased.
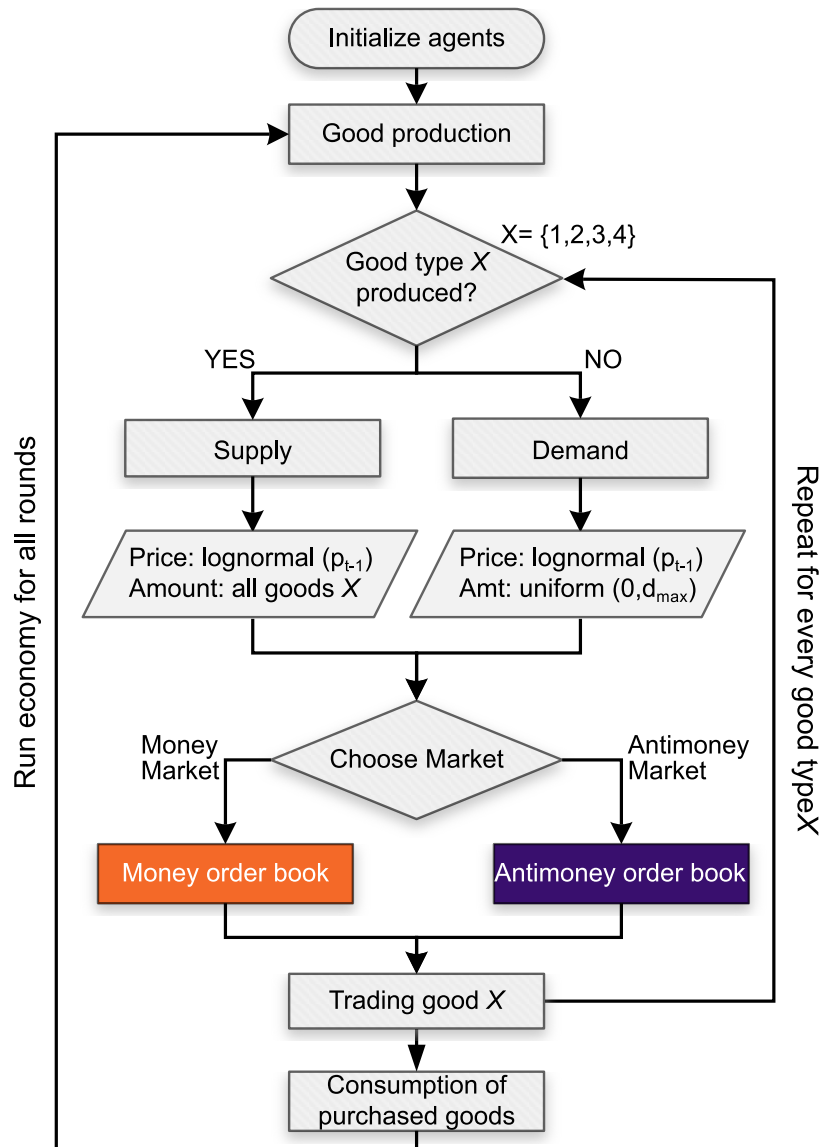
Figure 2.1: Flowchart of the random economy setup. The agents and the economy are initialized. In the turn-based economy, the agents produce (harvest) goods, trade them at respective markets and consume the purchased goods. Figure reproduced from [1].

2.1.3   Limit order book – antimoney supplies

Conversely to the money-good order book, in which the demand is limited by the agents'
budgets, the order book for good–antimoney markets exhibits a supply-bid limitation. In
contrast to the money market, where a supplier could easily accept a higher price, a seller
in the antimoney market faced problems with arbitrary high prices: it could not give
away more antimoney units (together with the goods) than it currently possessed. An
antimoney-supply order at price P_{sub} and amount s, that exceeded the agent's antimoney
holdings A, that means $P_{sub} \cdot s > A$, did not enter the order book. The mechanism of the
aggregate supply function also had to take into account that for higher prices, an agent
may not have possessed enough antimoney holdings to sell at arbitrarily higher prices
$P^* > P_{sub}$. In the following P^* refers to prices higher than the price of a submitted bid of
an agent.

A simple algorithm called (*resizing order book*) was applied to calculate the supply
curve. The order book mechanism checked for all submitted prices $P^* > P_{sub}$, if the
agent's antimoney holdings A were large enough to satisfy $s \cdot P^* < A$. If the relation was
true, the supply order entered the supply curve. That means that the bid's amount was
added to the total bids for the price P^*. If the agent did not have enough antimoney,
that is when $s \cdot P^* > A$, the agent's supplied amount s was resized to $s^* = \frac{A}{P^*} < s$.
This changed the shape of the supply curve and the supply curve lost its monotonously
increasing character, in general. The trading price was still determined to be the price that
maximized the minimum of the demand and supply curve. But in fact, both curves do
not necessarily intersect at all. If there were more than one price maximizing the trading
volume, the trading price was randomly chosen from these prices.

Minimal example   The following minimal example illustrates the non–monotonicity of
the supply curve and sketches the implementation of a strict order book, which would only
accept supply orders of agents which have enough antimoney at respective prices to sell
their goods. However, the strict order book was not implemented in the model. Consider
agents $A - E$ with goods g_i and antimoney holdings A_i according to table 2.1, willing to
place a supply-order with supply amount s_i and price p_i in the good–antimoney market:

Agent	Antimoney A_i	Good amount to be supplied s_i	Price p_i
A	5	2	2.5
B	6	2	3
C	12	3	4
D	5	1	5
E	24	4	6

Table 2.1: Agents' $A - E$ antimoney holdings and intended supply bids with supply amount s_i
and p_i.

The supply side of the order book was filled, starting at small prices. Agent A's order was placed first, see Tab.2.2. The supply side of the order book consists of a price column (Price p_i), the total supplies at the given price (Total supplies), the amount of supplies at the respective price (Amount supplies) and the respective agent of the order (Agent orders).

Agent orders	Amount supplies	Total Supplies	Price p_i
A	2	2	2.5

Table 2.2: Order book: Agent A's bid is placed on the supply side

Strict antimoney order book

Now B's order at price $p_B = 3$ had to be placed. Then the problem arose, how agent A's supply order should be treated. On the one hand A was willing to accept a price higher than $p_A = 2.5$. On the other hand A had not enough antimoney to pass its 2 goods at prices $P^* > 2.5$, because $A_A = 5 < P^* \cdot s_A = 3 \cdot 2 = 6$. A 'strict' the order book (which is not implemented) would add A's order to the order book and the total supplies for higher prices, *only* if $A_A > s_A \cdot P^*$. In this case, the full order book would look like Tab. 2.3. A

Agent orders	Amount supplies s_i	Total supplies	Price p_i
A	2	2	2.5
B	2	2	3
C	3	3	4
D	1	1	5
E	4	4	6

Table 2.3: In a strict implementation of the good–antimoney order book, orders of agents who did not have enough antimoney A_i (see Tab.2.1) to pass along with the submitted goods s_i for each price $P^* > P_{sub}$, were ignored, leading to a non-monotonic supply function in the order book

main weakness of this implementation was that it is very strict in the way accepting orders only if an agent's full order could be processed. As the placement of an order depended on the antimoney holdings of the supplier, the supply function (total supplies) was in general not monotonically increasing. Also it was not taken into account that A and B were *willing* to sell goods at high prices, although they would accept them. Considering these arguments, the strict order book was not applied in the simulations.

Resizing supply bid antimoney order book

The chosen implementation to process supply orders for the good–antimoney order book was a resizing of the supplied amounts s_i for $P^* > P_{sub}$ so that every order of every agent

entered the book with $s_i = A_i/P^*$. After C's order had entered the book, it had the form of Tab.2.4. The order book mechanism had to check for all submitted prices, if the supplying

Agent orders	Amount supplies s_i	Total supplies, with resized individual $s^\star$ supplies	Price p_i
A	5	**2**	2.5
A, B	2	$\frac{5}{3} + 2 =$ **3.6$\bar{6}$**	3
A - C	3	$\frac{5}{4} + \frac{6}{4} + 3 =$ **5.75**	4

Table 2.4: Resizing Order Book: The total amounts were resized for increasing prices for agents A - C and the supply function gets smoothed.

agents possessed enough antimoney to supply together with the supplied amount of goods. This kind of order book differed from the strict order book in a number of respects. A's and B's orders were taken into account at higher prices than their budgets of antimoney would have allowed by reducing the amount of supplied goods. The respective supplied amounts were $s_A = A_A/P^* >$ and $s_B = A_B/P^* >$. In this way A and B could have sold a fraction of their goods at higher prices, making a supply order more independent from the antimoney holdings of a supplier. To complete the entry of the supply orders, the orders of agents D and E entered the book, see Tab. 2.5. Notably, also a high price entered by a demander led to a resized order book for suppliers, who did not have enough antimoney to pass along with the amount at the higher price.

Agent orders	Amount supplies	Total supplies, with resized indiv. $s^\star$ suppl.	Price p_i
A	2	**2.00**	2.5
A, B	2	**3.6$\bar{6}$**	3
A - C	3	**5.75**	4
A - D	1	$\frac{5}{5} + \frac{6}{5} + \frac{12}{5} + 1 =$ **5.60**	5
A - E	4	$\frac{5}{6} + \frac{6}{6} + \frac{12}{6} + \frac{5}{6} + 4 =$ **8.6$\bar{6}$**	6

Table 2.5: Complete resizing order book with multiple local maxima of trading volumes at prices $p = 4$ and $p = 6$. Note that the supply function ('Total supplies') was <u>not</u> monotonically increasing for increasing prices!

The resizing order book had two decisive advantages: First, the resizing smoothed the supply function. In the strict order book, large jumps of the supply curve between the prices could occur, as agents who could not supply at higher prices were not considered for higher prices and their (large) supply orders dropped out immediately if the agent did not possess enough antimoney units to submit at (slightly) higher prices. Second, in the resizing order book every bid of every supplying agent was taken into account to calculate the supply curve. This increases the toal amount of supply bids and thus

maximizes the trading volume to increase the market's efficiency. The bids of supplying agents accepted all prices higher than the submitted price. In the strict implementation, only prices $p_{sub} < P^* < A_i/s_{sub}$ were accepted, limiting the prices to a possibly narrow interval.

A qualitative illustration of order book supply curves is shown in Fig.2.2. It shows the shape of the supply curves in the resizing good–antimoney order book. Fig. 2.2a) shows a typical conventional order book of a good-money market. The supply curve increased monotonically and the trading price was the price of the intersection of demand and supply curve. For the resizing good–antimoney order book, the supply curve did not necessarily increase monotonically but exhibited single maxima, see Fig.2.2b, or multiple local maxima, see Fig.2.2c). The determination of the trading price and trade volume was carried out according to Section 2.1.2. For every price, the maximal trade volume (which was the minimum of the demand curve and supply curve at the respective price) was calculated. Fig.2.2 also shows the maximal trade volumes for each case. The global maximum of the maximal trade volumes per price was then set as the trade volume and the respective price is the trading price at which all orders clear.
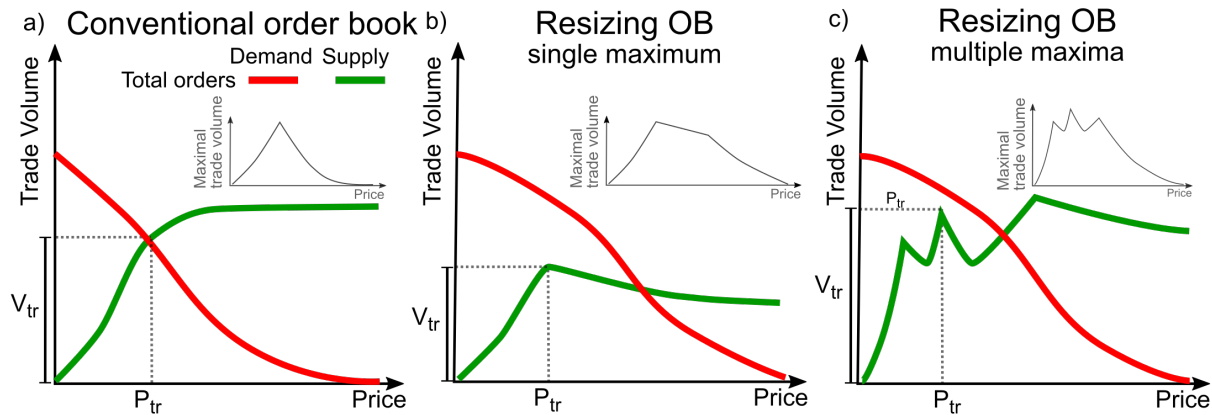
Figure 2.2: a) shows a conventional order book with no resizing for good-money markets. The demand curve monotonically decreased and the supply curve monotonically increased. The trading price and trade volume were determined by the intersection of the supply curve and the demand curve. b) shows a resizing order book for a good-antimoney market for the case that the supply function has one local maximum. c) shows a supply curve with multiple maxima, where price of the global maximum of the supply curve was not identical with the trading price. The inset figures show the maximal trade volume per price. The global maximum of each inset curve was then determined by the trading price that maximized the trade volume. The determined trading prices is not necessarily the price of the intersection of the demand and supply curve.

Opposed to the supply side, there were no effects as described above on the demand side of antimoney-involved markets. If a higher price enters than an agent's limit price, the order with a lower price was not taken into account when the total amount was calculated. Orders with lower prices than an agent's submitted price were also not critical, as accepting
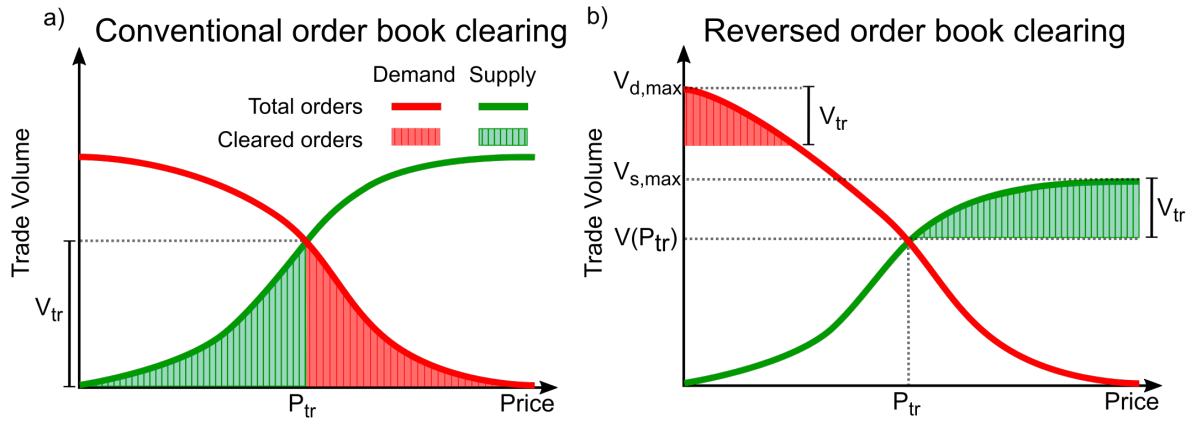
Figure 2.3: a) Conventional order book clearing mechanism: All supply oders with a smaller price than the trading price (green area) and all demand orders with a higher price than the trading price (red area) are cleared successfully. In the reversed order book (not implemented), all demand orders with a smaller price (red area) and all supply orders with a higher price (green area) than the trading price are cleared up to the total trade volume.

less antimoney than the submitted limit price had no consequences for the agent or the order submission.

2.1.4   Limit order book – order clearing

After the trading price had been determined, the orders were cleared. In the clearing process, the successful demand and supply bids were determined and executed. Starting point for the clearing was the trading price P_{tr}, the total trading volume V_{tr} and the submitted orders. Two different clearing mechanisms were tested: A conventional clearing mechanism and a reversed clearing mechanism. The clearing mechanisms differed in the way, which of the submitted orders were successfully executed.

For the conventional order clearing mechanism, all demand orders which would have accepted a higher price than P_{tr} were executed. The orders with the highest price was executed first. For the supply orders, orders which would have accepted a lower price than the trading price P_{tr} were executed. Fig.2.3 a) illustrates the conventional order book clearing.

The reversed order book clearing mechanism was motivated by the instability of unconstrained antimoney markets. In these markets trading froze due to high prices and small trade volumes. Also, there were few agents who possessed hundred-fold the initial antimoney holdings, see Fig.3.1. An approach to solve the problem of freezing good–antimoney marktes was to reduce the amount of antimoney which is passed to agents whose demand orders were successfully executed. In contrast to the conventional order book, in which the demand orders with high limit prices were more likely to be successful, the reversed clearing mechanism took the demand orders with the smallest demand

prices into account first. The supply orders with the highest supply prices were executed first. The trading price was determined similarly to the conventional order book, but the trading volume was determined as follows: The actual trade volume V_{tr} was the difference of the trade volume at the trading price $V(P_{tr})$ and $\min_p(V_{d,max}, V_{s,max})$, the minimum of the maximum trade volume of the demand and the maximum of the supply curve. Index p of the minimum denoted the price dependence of the minimum trade volume. Fig. 2.3 b) illustrates the case, where the supply curve had the smaller maximum trade volume $V_{tr} = V_{s,max} - V(P_{tr})$.

After the successful orders had been determined, the orders were executed. In the money market, an agent who had submitted a successful demand order receives goods in the demanded amount of d and therefore payed $d \cdot P_{tr}$ money units. An agent who had submitted a successful supply order received $s^* \cdot P_{tr}$ money and its good stock of the specific type was reduced by s. In the antimoney market, a successful demand agent received d goods along with $d \cdot P_{tr}$ antimoney units. A supplying agent's good stock was reduced by the resized amount of goods s^* (for the respective price P_{tr} and its antimoney units are reduced by $s^* \cdot P_{tr}$.

The inverse order book did not show significant deviations from the results with the conventional clearing mechanism (results not shown). The conventional order book clearing mechanism was used in the further studies because it rewards the agents who were willing to sell (buy) at the lowest (highest) price and led to higher V_{tr} in the studied cases.

2.1.5 Agent antimoney holdings limitation

The equilibration of monetary systems critically depends on their boundary conditions on individual monetary holdings.[1,72,73,85,149,150] The effects of global monetary constraints on monetary stability and distributions were studied for various model systems[72,73,85] and with respect to a required reserve ratio.[149] The application of these boundary conditions reflected real circumstances of credit granting. In real world credit granting, the creditor (typically commercial banks) has to evaluate the ability of the debtor to repay the debt before the debtor exits the system.

Two types of antimoney limits were implemented. First, for a global antimoney limit $\hat{A}$, agents who submitted a demand order in an antimoney-good market, which successful execution would have exceeded the agent's antimoney holdings above the global limit, the order did not enter the order book. Second, an individual life-time dependent antimoney limit, imposed a local constraint. All agents were assigned an equal lifetime τ and a maximum antimoney limit $\hat{A}$. The current (local) antimoney limit of an agent calculated as follows:

$$A(t) = \frac{A_0 - \hat{A}}{\tau} \cdot t + \hat{A} \tag{2.1}$$

The antimoney limit $A(t)$ decreased linearly over time t from the maximum limit $A(t = 0) = \hat{A}$ to the initial endowments $A(t = \tau) = A_0$.

This reflected the fact that real world agents have different ages at which they are differently credit-worthy: the agents started with a uniformly distributed $t \in (0, \tau)$. When

an agent reached its lifetime, it died and was immediately replaced by a child agent, which inherits the mother agent's money and antimoney units, its good stock and its utility and starts with $t = 0$.

2.2 Agent strategies

The main idea behind the strategy setting of the agents was that it would not cause artifacts in the monetary systems stability analysis. To keep the amount of parameters as small as possible, agents only submitted the market bid and set their consumption. The strategy of an agent within one round was thoroughly defined by the bid price, the bid amount, the type of bid (demand or supply) and the amount of consumed goods. The application of random strategies was incorporated by random probability distributions, from which the agents draw the respective quantities. The strategy was defined as follows: Firms tried to sell all of their goods per good-type, in order to not hoard them in their storages. The households demanded for a uniformly-distributed amount between zero and d_{max}. The choice of prices p solely depended on the price of the last round and was drawn with probability P from

$$P(p) = \exp\left(\ln a + \mathcal{N}\left(0, b^2\right)\right). \tag{2.2}$$

$\mathcal{N}$ is the normal distribution with mean zero and standard deviation $b = 0.3$ and a is the price of the last round. The prices of the first round were set to 1 for all good types. Agents did not have a preference for either market and chose the good-money or good-antimoney market with 50% probability. At the end of each round, all households consumed all bought goods.

This made the strategy especially well-suited for shock scenarios and specifically a hard measure for shocks, as the price dynamics were strongly reflecting the evolution and were not trying to reach (an artificial) equilibrium. During equilibrium, the strategy relies on the equilibrium fluctuating price. This implies the rejection of the idea of intrinsic value. This is in contrast to earlier order book studies which applied different agent types and set the demand and supply prices according to a private information reservation value.[151] This would imply that every agent 'knew' the intrinsic value of a good and could assign a price equal to the intrinsic value plus a price premium. The intrinsic value of the goods is set to zero and assignment of intrinsic value to the goods is rejected for two reasons: First, the harvesting agents would have to pay the intrinsic value to a central harvest providing agent which does not exist. Nature, from which the goods are extracted, does not have a bank account to which payments could have been made. It could be argued that extraction of goods from nature would be free, but this causes and maintains inequality states.[152] In addition,to stay in the intrinsic value framework, utility would need to be mapped to the amount of consumed goods, which seems difficult if one thinks about measuring happiness/fullness quantitatively. Second, when agent strategies get the parameter of intrinsic value, an optimization would be desired. This would introduce additional parameters to the ABM and make the simulations vulnerable to design-related footprints,[153] which are sought to be avoided.

2.3 Production and credit boom & shock scenarios

To study the impact of structural changes of the model economy and analyze economic stability, economic standard theory models structural shocks (and booms) which hit equilibrated economic systems.[90]To compare the stability of the money–antimoney system with a single money and a two-money system, distractions from equilibria by production shocks, production boom and credit shock scenarios were conducted. In each simulation, the monetary systems were equilibrated and then at a defined round, the system experienced the respective shock. The response of the the prices, the trade volumes and the money distributions were recorded.

For all three monetary systems, the scenarios were conducted similarly: Production shock and boom scenarios were conducted with 90 initial rounds of market equilibration under normal conditions. Then, for 3 rounds, the external shock/boom hit the economy and the harvest was boosted by 50% (boom) or reduced by 50%. After the shock/boom the harvest was set to its level before the shock/boom.

The time (measured in rounds) it took to recover from the production shock was an indicator for the monetary systems' recovery capabilities. It was defined by the time constant C_2 of the fitted exponential price recovery $p(t) = C_0 + C_1 \exp(t/C_2)$ between the shock and round r. Round r is the round, at which the price had reached its pre-shock value again. Round r was defined by the round in which the gradient $g = (p * f)'$ falls below the threshold 0.02. The function f is a rectangle of length 5 and height 1 which is convoluted ($*$) with the price p.

For the credit shocks, the systems were similarly equilibrated as for the good shocks. For the single money and the two-money system, the credit shock was simulated by a single increase of every agent's money holdings (only M_2 holdings in the two-money system) by the initial amount of money in the first round of the shock. In the last round of the shock, all agents' money holdings were halved. The credit shock in the money–antimoney system was simulated by a temporary increase of the agents' antimoney holdings by the initial amount of antimoney holdings. Simultaneously, the maximum antimoney limit of the agents was doubled. In the last round of the shock, all agents' antimoney holdings were halved. In all credit shocks, the amount of money (single), M_1, M_2, money and antimoney before and after the shocks was equal.

2.4 Simulation parameters

The simulations were conducted with $N = 9000$ agents, to obtain a large enough sample. Each agent was initially endowed with $M_0 = 10$ money units and $A_0 = 10$ antimoney units and zero goods. All simulation parameters are shown in Tab. 2.6. The quantitative comparison of the monetary systems (single money, M_1-M_2 and money-antimoney) was established by simulating each scenario in each monetary system. In the two money system, two money currencies (M_1 & M_2) were issued and the agents applied the same strategy as in the money–antimoney simulations.

Global economic parameters	Variable	Value	Trading parameters	Variable	Value
Agent population size	N	9000	Price distribution		Lognormal
Different good types	G	4	Lognorm. distrib. shape param.	a	0.3
Harvestable goods per agent	h	2	Lognormal distrib. median	p_{t-1}	Price of last round
Harvested goods p. ag. p. round		0.5	Demand amount	d_i	Uniform $(0, d_{max})$
Utility gain curvature	c	7	Excess supply		0.5
Consumption per round	x_i	All goods	Excess demand	d_{max}	1.5, 2.5, 4
Initial money per agent	M_0	10	Fraction of supplied goods		1.0
Initial antimoney per agent	A_0	10	Boom & shock scenario	Variable	Value
Initial trading price	p_0	1.0	Rounds to equilibrate system		90
Agent lifetime	τ	50, 200	Duration of shock/boom		3 rounds
Maximum antimoney limit	$\hat{A}$	$2.8 \times A_0$	Change in harvested goods		± 0.25
Price tick		1.0^{-5}	Change in monetary holdings		± 10

Table 2.6: Overview of simulation parameters. The economic, trading and scenario-related parameters are shown. Note that excess demand d_{max} parameter is fixed within a respective simulation, but differs for the various simulations, accordingly. Table reproduced from [1].

Chapter 3

Results

The results are organized as follows: First it is shown that symmetric trading strategies led to asymmetric money and antimoney price levels. Second, antimoney limits, that set an upper bound on the agents' antimoney holdings were introduced to equilibrate the antimoney market. Simulations showed that quantity theory is fulfilled. Third, the systems' responses to deflections from equilibrium by supply and credit shocks hitting an equilibrated system indicated their fundamental functionality. Lastly, simulations of a multi-flavor money and antimoney system for excess demand and supply scenarios are shown.

3.1 Stability of money and antimoney markets

3.1.1 Diverging money and antimoney markets for symmetric strategy

For excess supply simulations $d_{max} = 0.5$, the money and antimoney markets quickly reached a symmetric equilibrium in which prices decreased to about the smallest price tick 10^{-5}, see Fig. 3.1a) and the mean trading volumes were about equal for money and antimoney markets, see Fig. 3.1c). The markets equilibrated and the agents' money and antimoney holdings changed little, due to money and antimoney prices near zero.

For excess demand $d_{max} = 2.5$, the money prices and trading volumes reached an equilibrium level, see orange lines Fig. 3.1b,d). In contrast, the antimoney market showed a non-linear transition into an extremely inefficient non-equilibrium state, see purple line Fig. 3.1b,d): near to zero trades are made on the antimoney market, as the prices exploded three orders of magnitude. Instead, the trade shifted from the antimoney market towards the money market, where it flourished at high volumes and low prices. A detailed look into the money and antimoney order books explained the divergence of the markets, see Fig. 3.2a). Following the price explosion for money and antimoney prices, see Fig. 3.2b,c), respectively, the order book's supply (green) and demand (red) curves for one good of selected trading rounds showed distinctly different behavior. First the antimoney market
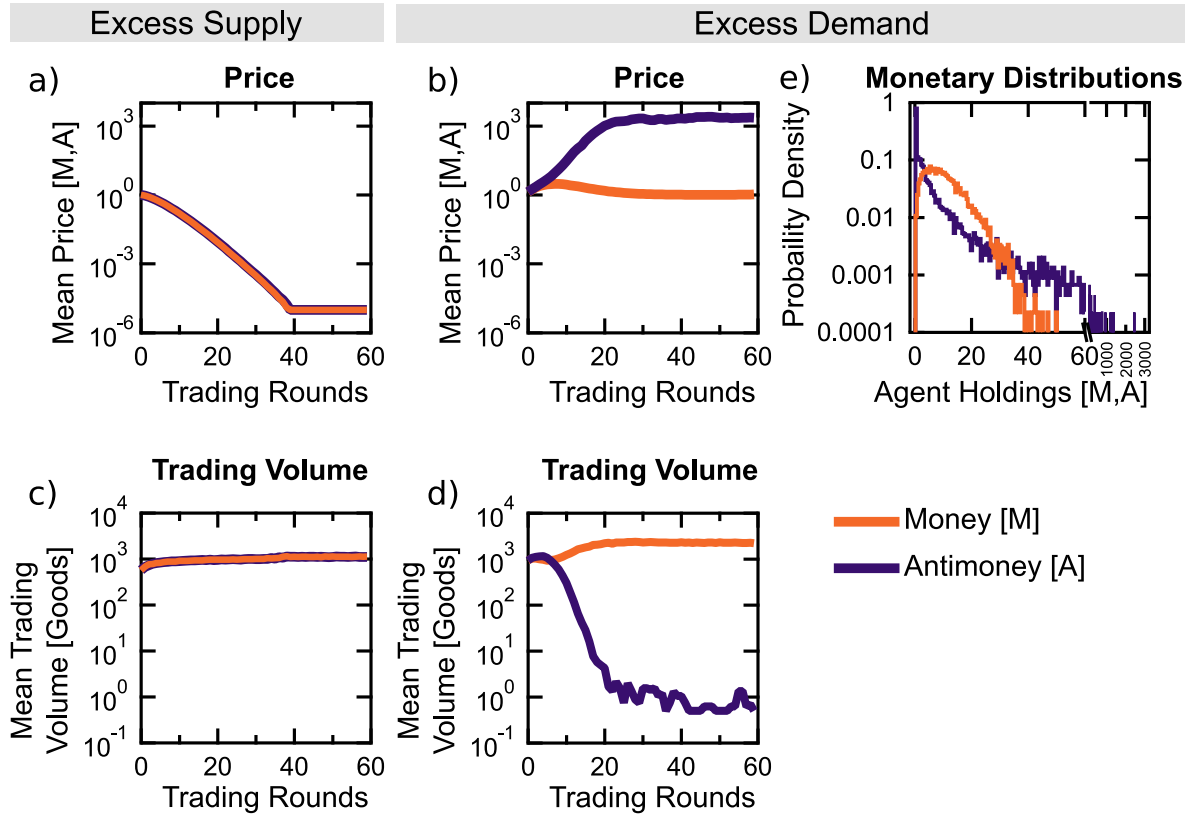
Figure 3.1: Prices, trading volumes, money and antimoney distribution for excess supply $d_{max} = 0.5$ and excess demand $d_{max} = 2.5$. (a) For excess supply, the prices dropped to about the smallest tick 10^{-5} and (c) a symmetric constant trading volume for money and antimoney was reached. (b, d) For excess demand, the money prices quickly equilibrated at a constant trading volume. Astonishingly, the antimoney prices exploded while the trading volume dropped to near zero. (e) Shows the money and antimoney distributions for all agents in the last round (60) on a semi-log scale for excess demand. While the money was narrowly distributed, antimoney was distributed much broader, with a large peak at zero antimoney holdings. The money and antimoney distributions for excess supply are not shown, as the system reached an unrealistic state in which goods were traded with devalued money and antimoney currencies. Figure reproduced from [1].
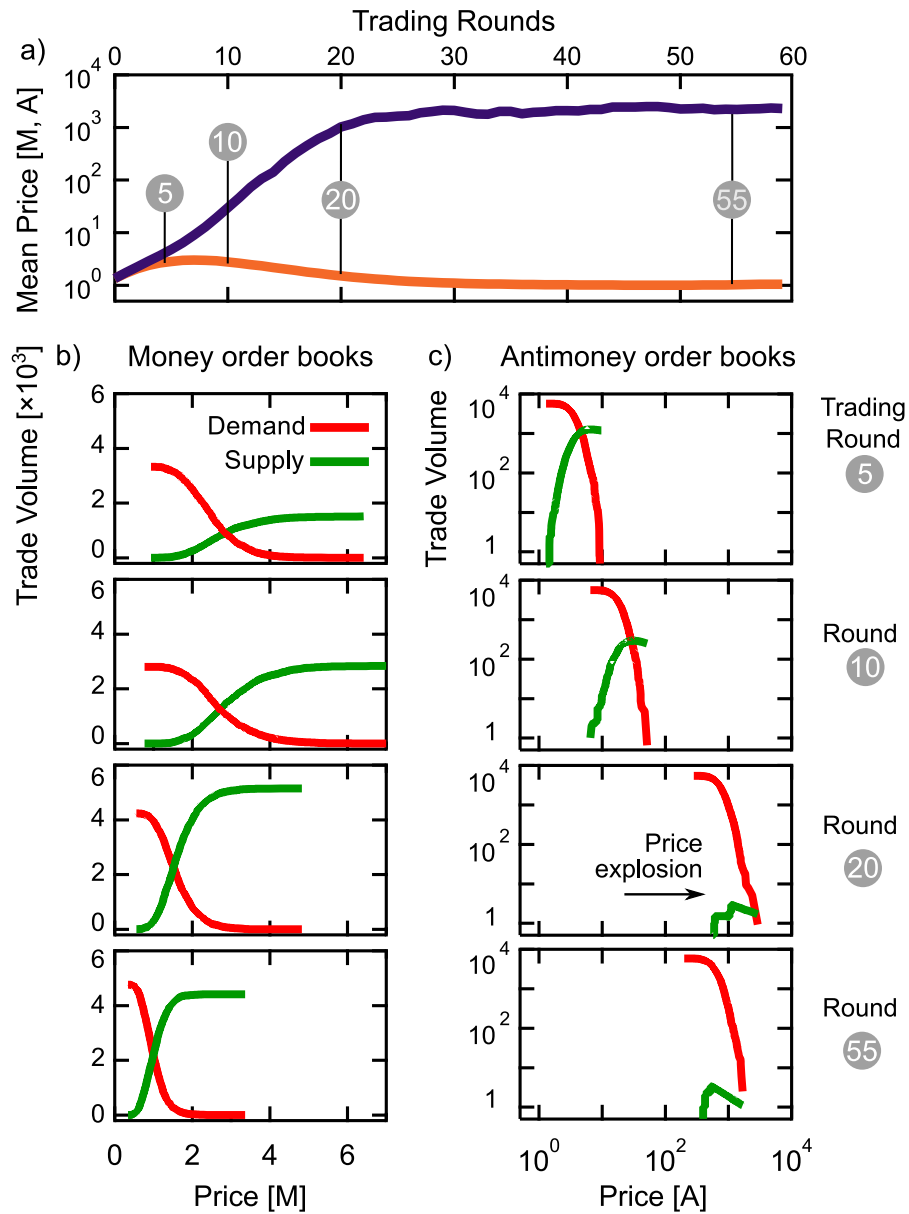
Figure 3.2: Price equilibrium for money order book and price explosion in antimoney order books. The order book demand (red) and supply (green) curves for an excess demand scenario are diffent for the money and antimoney markets in selected rounds. (a) The mean prices over time for the money and antimoney markets. (b) The demand and supply curve in the money market equilibrated at a price of about 1. (c) The uninhibited demand curve in the antimoney market drove the prices to levels which were three orders of magnitude higher than in the money market. The supply curve declined and was not monotonically increasing for higher prices, as only very few agents possessed enough antimoney to sell them along with their goods. Note that the trading price in round 20 and 55 was determined by the maximum of the supply curve, even if demand and supply curve did not intersect, see Section 2.1.3. Figure reproduced from [1].

prices explode and subsequently, the trade swaps over to the money market with high trading volumes and small price. Notably, the money market is in equilibrium after the trade has shifted.

First, the antimoney prices increased quickly within 10 rounds more than three orders of magnitude due to the uninhibited demand curve in the order books, see Fig.3.2c). The shape of the demand curve was scale-invariant for low and high price levels. This stems from the fact that the strategy of the agents does not adapt and that there was no budget constraint. Demanders could accept unlimited antimoney units and ask for goods at arbitrary high prices. With increasing prices, the fraction of suppliers and the supply curve declined, because only few agents possessed enough antimoney units to pass along with the goods. The supply curve is not necessarily monotonously increasing, see Section2.1.3. The resulting highly inefficient state was equivalent to a frozen antimoney market in which too high prices permit the agents to find back to an efficient market. The price fluctuations at high levels were a mere relict from very few agents which could trade by chance.

Second, the shift of the trading volume from the antimoney market to the money market was an artifact of the trading strategy. As all agents always tried to sell all of their goods, an agent which could not sell its goods in the antimoney market, would by chance later choose to sell in the money market. The supply curve in the money market increased, see Fig. 3.2b), and the money prices decreased, resulting in an increased trading in the money market. The empirical probability density of the agents' money and antimoney holdings for excess demand at the end of the simulation (at 60 trading rounds) differed from each other, see Fig.3.1e). While monetary units were distributed narrowly between zero and $\sim 6 \cdot M_0$, the antimoney holdings exhibited a peak at zero (if an agent succeeded to sell in antimoney, it got rid of all its antimoney) and a much broader tail (when an agent succeeded in buying in the antimoney market at high prices, it obtained many antimoney units), with agents hoarding more than hundredfold A_0.

The implicit budget constraint in the money market by the declining demand curve for increasing prices had no equivalent constraint in the antimoney market. This finding was in agreement with previous research, stating that the lack of boundary conditions did not necessarily yield for equilibrated monetary systems.[69,72,149,150] In conclusion, the absence of a budget constraint in the antimoney market resulted in non-efficient and non-equilibrated good-antimoney markets.

3.1.2   Symmetric equilibration of antimoney and money markets

In order to equilibrate the antimoney market, three solutions could be considered. First, the strategy of the agents could be changed to aim for equilibrium markets. However, this study focused on monetary stability and did not look for stabilizing agent strategies and therefore was not taken into account. Second, systemic constraints like global or local antimoney limits can be imposed, influencing the demand curve. Third, implicit transfer mechanisms could lead to a limitation of antimoney hoarding which may equilibrate
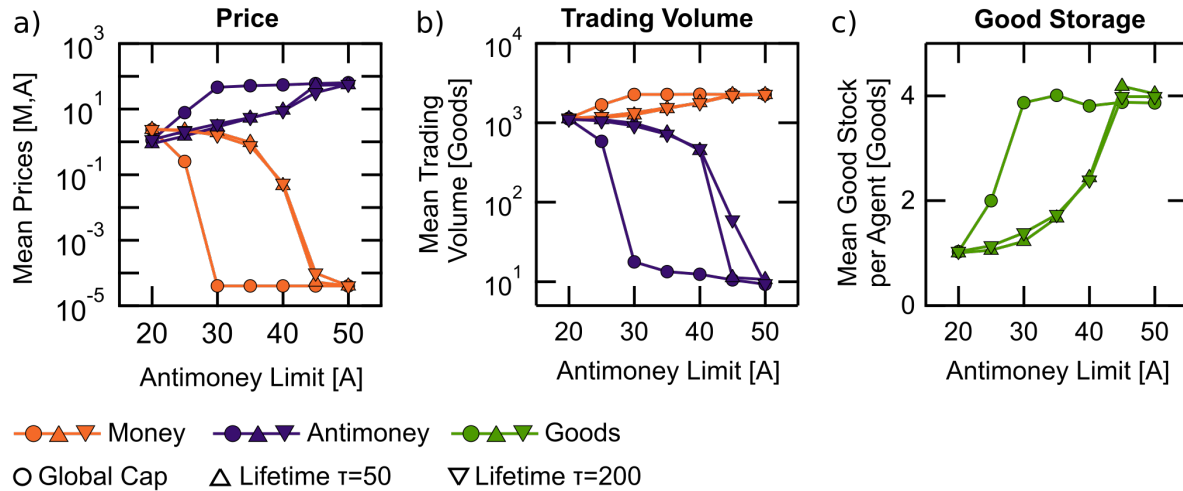
Figure 3.3: Symmetric equilibration of money and antimoney markets by imposed global ($\circ$) and local antimoney limits (lifetime $\triangle \tau = 50, \bigtriangledown \tau = 200$) for excess demand $d_{max} = 1.5$. (a) For high antimoney limits – larger than about three times the initial money endowments $A_0 = 10$ – the mean money prices (orange) dropped near to the smallest tick and the antimoney prices (violet) rose to three orders of magnitude above money prices. For decreasing antimoney limits the antimoney market became functional: the money prices increased and the antimoney prices decreased. For an agent life-time dependent antimoney $\hat{A} \approx 2.8 \cdot A_0$ the prices and trading volumes became symmetric. (b) For high antimoney limits, the mean trading volumes shifted towards the money market while the antimoney market froze. For decreasing antimoney limits the money trading volumes decreased and the antimoney trading volumes increased. (c) For decreasing antimoney limits, the good stocks decreased, indicating an increase of the market efficiency. Overall, an agent lifetime-dependent antimoney limit ($\triangle, \bigtriangledown$) had a stronger effect than a global antimoney ($\circ$) limit, reducing (increasing) the antimoney (money) prices and increasing (decreasing) the antimoney (money) trading volume. The results were similar for different agent lifetimes $\tau = 50$ ($\triangle$) and $\tau = 200$ ($\bigtriangledown$). For antimoney limits > 40 an equilibrium was not yet reached – money prices had not yet dropped to 10^{-5} and antimoney trading volumes had not yet dropped to about zero. Figure reproduced from[1].

the antimoney market. Transfer mechanisms in the framework of the money-antimoney system were already previously studied and could be mapped to the constraint of monetary quantities.[72,73] In the following, a global and local antimoney limit were applied to equilibrate the markets with respect to prices and trading volumes.

The application of a global and local antimoney limit equilibrated the antimoney markets for slight excess demand $d_{max} = 1.5$, see Fig.3.3. The agents' life-time dependent antimoney limit had a larger impact on the reduction of antimoney prices than a global antimoney limit, see Fig.3.3a). Still, for high antimoney limits, the market fell in the previously analyzed non-equilibrated state with exploding antimoney prices and trading volumes approaching zero. As the trading then shifted almost completely to the money market, the money market showed an excess supply and the money prices dropped near to the smallest tick, see orange lines in Fig.3.3a) for high antimoney limits. The smaller the antimoney limits got, the more the mean antimoney prices decreased, Fig.3.3a), the trading volumes increased, Fig.3.3b) and the good stocks per agent decreased, see Fig.3.3c). The system resulted in a functional, stable and equilibrated state, indicating efficient money and antimoney markets.

The money and antimoney market prices and volumes could be symmetrically equilibrated for an antimoney limit of $\hat{A} \approx 2.8 \cdot A_0$. For smaller antimoney limits, the antimoney price was higher than the money price, at the same trading volume. The results suggest that the antimoney market reached an equilibrium by the setting of a natural antimoney limit and the antimoney limit controlled the antimoney market's functionality. Different agent lifetimes did not have a relevant impact. The symmetric equilibrium was the starting point for the following analysis.

3.1.3 Quantity theory in equilibrated markets

To study the application of quantity theory in the money–antimoney system with simulations, the price dependence on the initial amount of money (and antimoney) was analyzed under the above introduced antimoney-limited equilibrium condition. Comparison of the prevailing monetary system with the money–antimoney system was achieved by simulations of a single money system M_S, a two money currency system M_1-M_2 (e.g. euro and dollar) and a money–antimoney system $M_{M,A}$.

The results of the two money system were used as a reference for the money–antimoney system. The results for the monetary systems showed that quantity theory applied for the two cases of constant q_{const} and proportional $q \propto M$. Fig.3.4a,b) show that the mean price and mean trading volume depended on the initial money endowments per agent. To compare the results, the single money market's volume was normalized by dividing by two, as the agents in the other systems chose at which market to trade with 50% probability. The money velocity V_M and antimoney velocity V_A was constant for all simulations, as the frequency of trades per round and the average trade volume was equal for all simulations. For constant trading volume q_{const} the prices of all systems were proportional to the initial endowments M_0. When trading volume was proportional to the money supply $q_{prop} \propto M$,
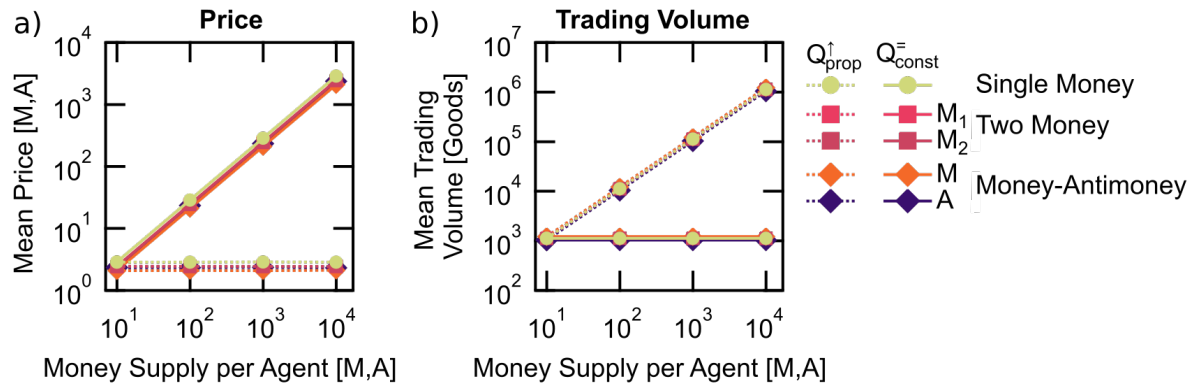
Figure 3.4: The money–antimoney system satisfies quantity theory similar to prevailing monetary systems. (a) Shows the mean price and (b) the trading volume dependence on the initial money supply. For constant trading volume $Q^=$ the mean prices rose linearly with an increased money supply for the single money, the two money and the money–antimoney system under the above introduced antimoney boundary conditions. For a proportional trading volume $Q^\uparrow$ the prices stayed at a constant level. The velocity of money circulation V was constant, resulting from a constant trading frequency of the agents and thus quantity theory $M \cdot V_M = GDP_M = \sum_i p_{M,i} \cdot q_{M,i}$ held for all monetary systems, especially indicating the functionality of a money–antimoney system. Figure reproduced from[1].

the prices stayed at their initial level – while the antimoney limit the agents, the harvest, the good supply in the markets and d_{max}, were set proportional to the money supply M_0. These findings suggest that quantity theory, as stated in Eqn.1.8 holds in equilibrated money and antimoney markets, respectively.

The similar outcome of the different monetary systems indicated the respective application of quantity theory. The application of quantity theory may serve as an indicator for a principal functionality of the time-homogeneous money–antimoney system, as macroeconomic variables behave similarly to those known in literature. However, the rather simple approach could also be seen as an calibration of the supply and demand to reasonable prices that scale with the holding limitations.

3.1.4 Production shocks and booms

To compare the systems' response and recovery capability from external production booms and shocks, scenarios were conducted for a single money, a two money and a money–antimoney system. During production shocks, see Sec.2.3, the trading volume immediately decreased – as programmed– see Fig.3.5b), and the prices rose, see Fig.3.5a). When the harvest returned to its initial value after three rounds, the prices and trading volumes quickly returned to their pre-shock levels. During booms, the increased harvest led to an increased supply and the trading volume rose, and the prices dropped. When the boom ended, the prices and trading volumes quickly returned to their pre-shock levels.
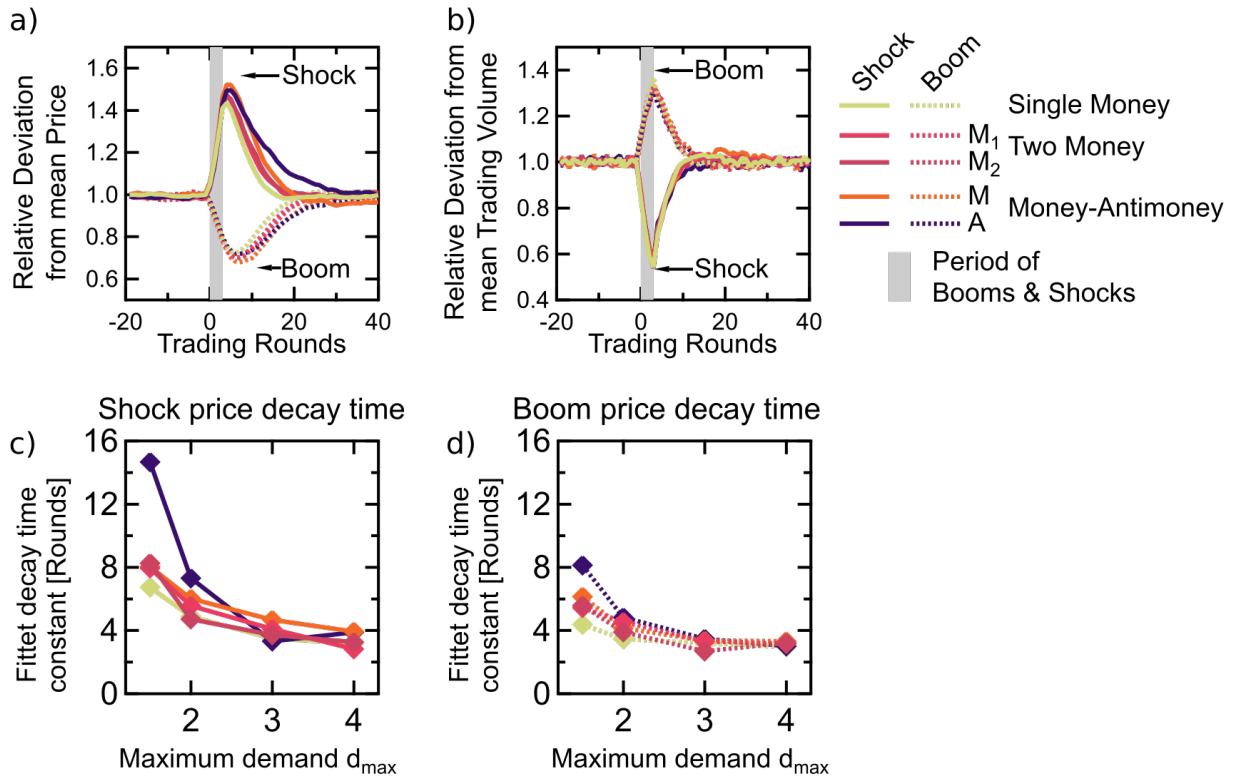
Figure 3.5: Production shocks and booms affect the money–antimoney system similar to the prevailing monetary system. The boom and shock scenarios were simulated for the single money, the two money and the money–antimoney system. After the systems were equilibrated for 90 rounds they experienced a shock (solid lines) or boom (dashed lines) for three rounds (gray area) during which the harvest increased (boom) or decreased (shock) by 50% and then returned to its initial level. Due to the shock, the supply curve declined within the order book (not shown) and (a) the prices increased along with (b) a decrease of the trading volumes. After the shock, the prices dropped and the trading volumes increased, both reaching their pre-shock level. The antimoney price within the money–antimoney system needed slightly more time to equilibrate. (b) In a boom the trading volume increased due to the increased supply curve in the order book (not shown) and (a) the prices dropped. The prices and trading volumes had a smaller amplitude due to the boom than to the shock. The mean decay times for the prices are shown for (c) shocks and (d) booms. For increasing demands, the decay times decreased and converged, indicating that the money–antimoney systems dynamic response to external shocks (booms) is similar to the prevailing monetary system. Figure reproduced from[1].

The prices and trading volumes for a single money, two money and money–antimoney system responded similar for both, economic shock and boom scenarios. The relative deviation from the mean price and trading volume was more pronounced for a shock than for a boom. This may result from the excess demand, possibly being more sensitive to a supply shock, which exacerbates the gap between supply and demand more than a supply boom relaxes the situation. The present study was focused on the comparison of the systems and less on a boom-shock asymmetry, which was not further investigated.

To compare the systems' resilience, it was desirable to quantify the recovery time constants of all monetary systems for the simulated booms and shocks. The recovery time was an indicator how fast and if at all the systems returned to equilibrium after the shock/boom. For the shock scenario, the money time constants were similar, see Fig.3.5c,d): The antimoney markets needed slightly more time to recover and for large excess demand, all systems similarly responded to a shock or boom. This finding indicates the fundamental similarity of the money–antimoney system and the prevailing monetary system, as both systems showed a similar dynamic price and trade volume response on exogenous production shocks.

3.1.5 Credit shocks

Moving now to the systems' responses to credit shocks, a tight good market was used for all three systems by setting an excessive demand $d_{max} = 4$ which reflects a tense market situation. Studying credit shocks in tense market situations is beneficial in comparison to loose markets, as the markets are pushed stronger out of their equilibrium state. The expected response signal of the market prices and trade volumes is assumed to be stronger pronounced. Fig.3.6 shows a) the price deviation from the mean price, b) the utility gain deviation from its mean value and c) the trading volume deviation from the mean trade volume for the single money (yellow), the two-money (red) and the money–antimoney system (violet).

During the credit shock, the amplitude of the antimoney price deviation from equilibrium was larger than the amplitude of the single money and the two-money prices, see Fig.3.6a). For the two-money system, only the price in the increased currency M_2 increased, while the other M_1 money currency's price M_1 stayed almost constant. The utility gain deviation during the shock was smaller in the two-money market than in the single money system, see Fig.3.6b). The money–antimoney system digested the shock better than the single money system, as the utility gain dip during the bubble crash was not as large as in the single money system.

The aggregate trading volumes (solid lines) peaked in the immediate round after the shock for the markets of the currencies, see Fig.3.6c). This was caused by the increased liquidity, as agents had more money to spend and agents could hoard more antimoney units, as also the antimoney limit was increased. The trade volume relaxed between round two and five after the shock started. Because price and trade volumes decreased in this phase this could be interpreted as the burst of a financial bubble, which corrects the
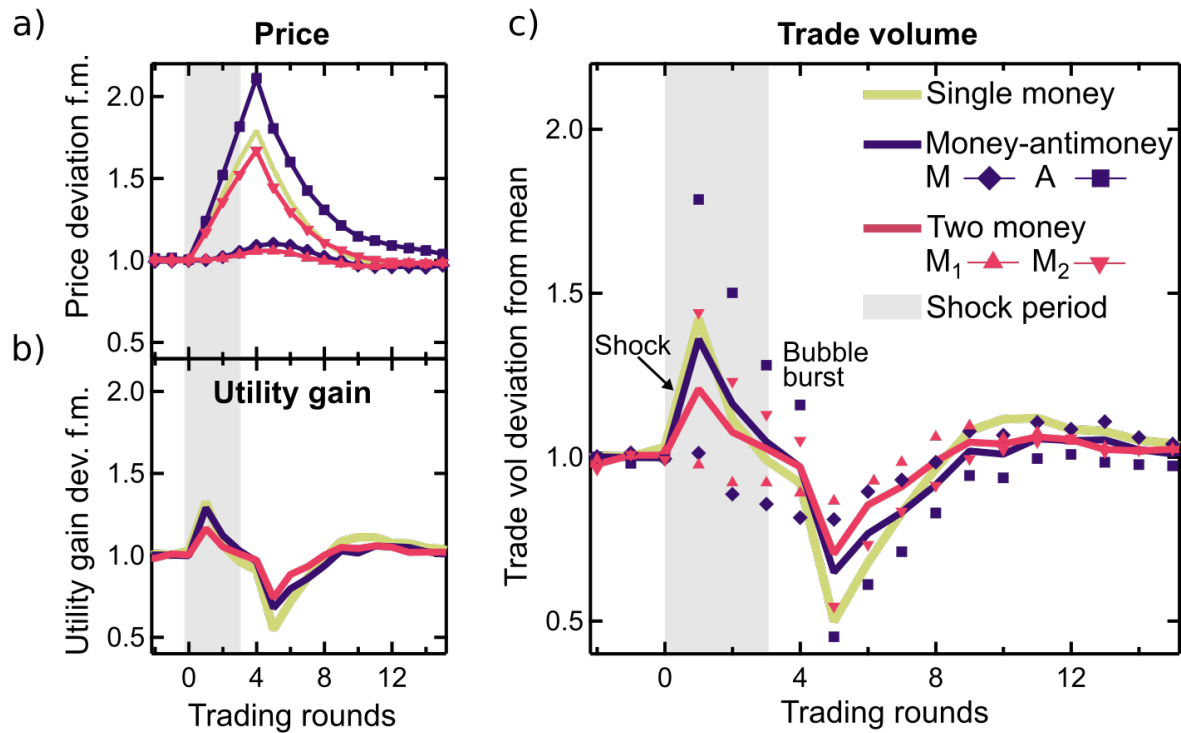
Figure 3.6: Credit shocks affect the moneyantimoney system similar to a two money system. Credit shock scenarios were simulated for a single money system (yellow), a two money system (red) and a money–antimoney system (violet). After the system was equilibrated for 90 rounds, the credit shock temporarily affects the systems for three rounds (gray area). During the shock, all agents additionally received the initial money, initial M_2 and initial antimoney endowments for the single money, two-money and money–antimoney system, respectively. For the money–antimoney system, the agents' antimoney-limits were increased by the factor two during the shock. After the shock, each agents' holdings – which were increased before – were halved. (a) During the shocks, all prices increased and then returned to the pre-shock equilibrium. (b) The utility gain temporarily increased and then undershot before it returned to the equilibrium level. (c) The aggregated trade volumes (solid lines) increased for all markets. Interestingly, for the two-money and the money–antimoney system, the markets which currency experienced the shock (M_2 and A) had a temporarily increasing and then sharply decreasing trade volume, while the opposite markets had the contrary development. When the credit bubbles burst, that is when prices and trade volumes crashed, the money–antimoney and two-money systems' responses were more robust in the sense that the deviations from the mean trade volume and utility gain were not as large as in the single money system. These results may suggest an increased capability of the moneyantimoney system to digest credit shocks. Figure reproduced from [1].

overvalued prices by falling prices and trade volumes.[154] The aggregate trading volumes sharply dropped below their equilibrium value, slowly reached their pre-shock value from below again. Interestingly, the trading volumes in the money-good market of the money–antimoney system and the M_1 market in the two-money system changed oppositely to the antimoney and M_2 market during the shock, respectively. In round five after the shock, the trade volume in the non-shocked markets surmounted the trade volume of the shocked markets. During the burst of the bubble, the trade volumes in the non-shocked markets declined, but their amplitudes of the deviations from the mean were much smaller than for the shocked markets. This may be an indicator for an increased absorbing ability of the money–antimoney system for credit shocks. The swapping of the trading volume to the shocked markets and at the same time a relatively constant non-affected market could serve as a mechanism to buffer debt-sided shocks.

Studying the monetary distributions for selected time points, before, during and after the shock for the respective systems, yields for deeper insight into the shock mechanism and the digestion of the shocks. See Fig.3.7a–c) for the single money system, the two-money system and the money–antimoney system, respectively. The money distributions for all equilibrated (round -1, dark violet) states were similar to each other and to the reported distributions for random exchange models.[83] However, an exponential distribution, which could be expected due to random exchange was not obtained, for neither the money nor the antimoney distribution. Instead, the money distribution had a nearly symmetric form around the initial money endowments $M_0 = 10$. This possibly stems from artifacts from the setup of good harvest and stochastic market selling.

The shape of the antimoney distribution can be explained as follows: The peak in the antimoney markets for zero antimoney is caused by the resizing order book, which leaves many agents with zero antimoney after successful selling at higher prices than they submitted in their order. This mechanism 'depleted' the states of small and moderate antimoney holdings and caused the a peak at zero antimoney holdings. The constraint that no agent was allowed to possess at maximum 56 antimoney (see below) cut the distribution at this value.

When the credit shock hit the monetary systems, all agents were endowed 10 additional units (single money, M_2 and antimoney, respectively) and the respective distributions change quickly and got broader (dark green). In the money–antimoney system, see Fig.3.7c), agents accumulated as much as possible antimoney ($56 = 2.8 \cdot A_{0,shock} = 2.8 \cdot 20$) within just two rounds. A doubling of the antimoney prices supported the quick redistribution. Only two rounds after the shock ended (light green), the distributions quickly returned to their pre-shock shape. The distributions for the currencies, which were not hit by a shock – M_1 in the two-money system and money in the money–antimoney system – were not affected and remained their shape throughout the shock. This may be associated with the little price changes during the shock for the M_1 and money markets.
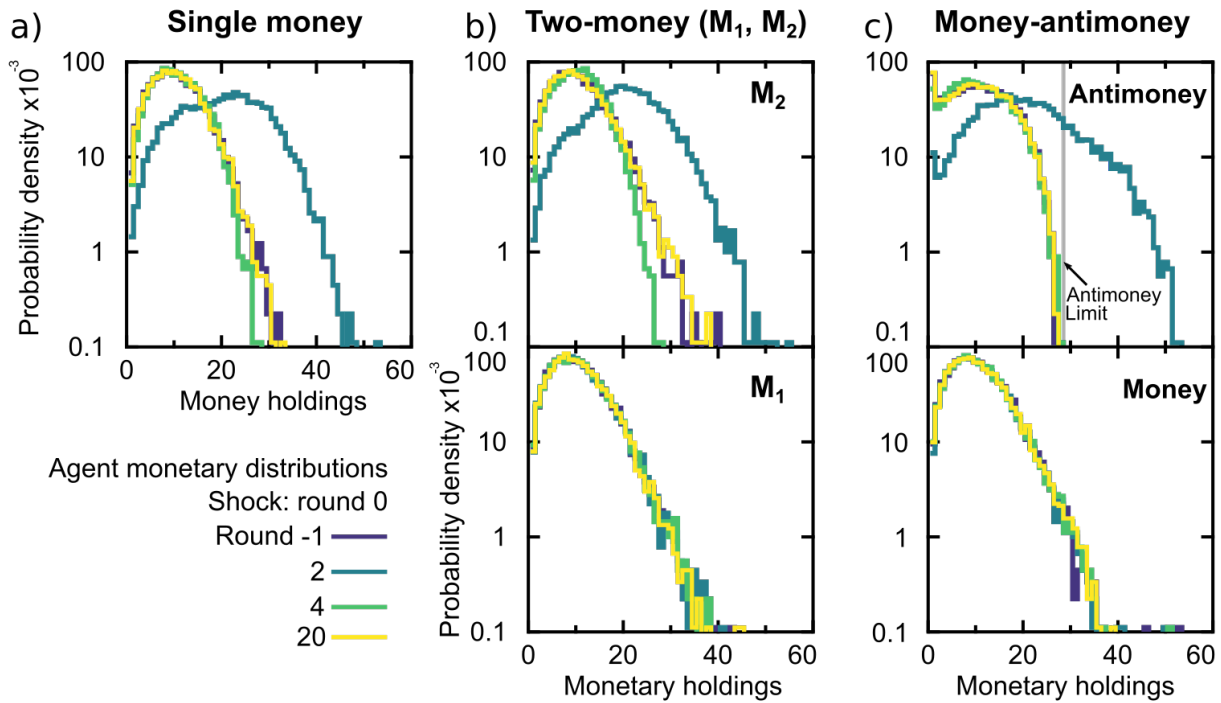
Figure 3.7: Money and antimoney distributions before, during and after a credit shock. The money and antimoney distributions for (a) a single money system, (b) a two-money system and (c) a money–antimoney system before (dark violet), during (dark green) and after (light green and yellow) the shock. The equilibrated money distributions for all systems were similar to known random exchange distributions. The antimoney distribution had a sharp peak at zero due to the order book clearing mechanism. The shock hit the system after it was equilibrated for 90 rounds and the agents were endowed 10 additional money, M_1 and antimoney holdings in the respective systems. In the last round of the credit shock, the agents holdings were halved for the formerly increased currencies. During the shock, the distributions for the currencies which were hit by the shock got broader due to the increased amount of currency holdings in circulation. Interestingly, the distributions for the non-affected currencies (M_1 in the two-money system and money in the money antimoney system) did not change during the shock. The constant money distribution in the money–antimoney system during the shock suggests that the money–antimoney system may digest credit shocks in a more robust way than the current (single) money system. Figure reproduced from[1].
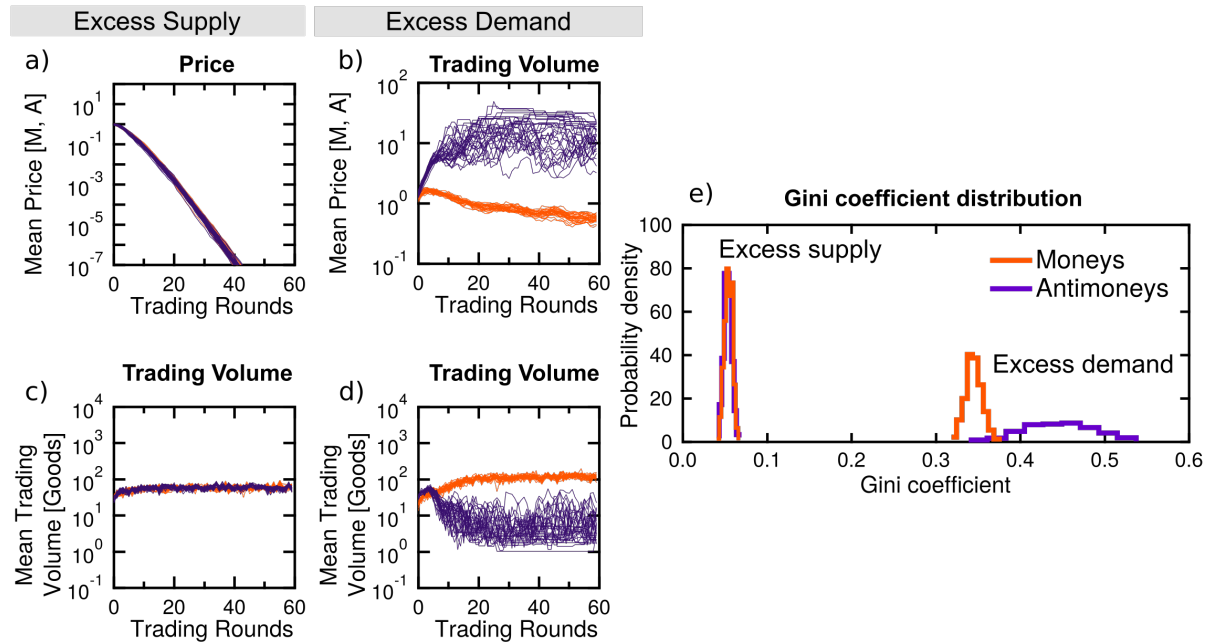
Figure 3.8: Multi-flavor money and antimoney systems exhibit similar behavior like non-constrained money–antimoney system a) For excess supply $d_{max} = 0.5$, flavor money and anti-money prices drop towards zero and c) trade volumes equilibrate at constant values. b) For excess demand $d_{max} = 5$ the antimoney prices explode and d) the antimoney trade volumes decrease towards zero. Trade is shifting to the good-money markets which equilibrate quickly. e) For excess supply, the distribution of the Gini-coefficients of the moneys and antimoneys is narrowly focused around small values. This means that moneys and antimoneys are equally distributed along the agents, due to all agents starting with $M_{0,i} = A_{0,i} = 10$ and small prices, which do not lead to large exchanges of monetary units. For excess demand, the moneys are still relatively narrowly distributed but the antimoneys are broadly distributed around higher Gini-coefficients. Large Gini-coefficients are an indicator for the malfunction of unconstrained antimoney markets, where high prices and antimoney distribution inequalities freeze the markets.

3.2 Multi-flavor money-antimoney system

The individual limitation of antimoney holdings equilibrated the markets in the money–antimoney system. In a multi-flavor money-antimoney system, it could be expected that symmetric behavior of the agents could lead to different output than in a single money–antimoney system. Arguing with entropy, that would distribute the delta-like antimoney distribution more broadly with multiple flavor moneys and antimoneys and thus may stabilize the antimoneys distributions.

Simulations of a multi-flavor money-antimoney system were conducted with $N = 500$ agents for an excess supply scenario $d_{max} = 1$ and an excess demand scenario $d_{max} = 5$, $f = 4$, $h = 2$ $M_{0,i} = 10$, $A_{0,i} = 10$ and no antimoney holding limitations, each flavor market exhibits the same results as for the money–antimoney system, see Fig.3.8. To measure the inequality of distributions, the Gini-coefficient is used. It is a measure, how

strong a distribution deviates from a uniform distribution and assigns a value between 0 (uniform distribution) and 1 (delta distribution) to the studied distribution.

For excess supply, the distribution of the Gini-coefficients of the moneys and anti-moneys is narrowly focused around small values. This means that moneys and antimoneys are equally distributed along the agents, due to all agents starting with $M_{0,i} = A_{0,i} = 10$ and small prices, which do not lead to large exchanges of monetary units. For excess demand, the moneys are still relatively narrowly distributed but the antimoneys are broadly distributed around higher Gini-coefficients. Large Gini-coefficients are an indicator for the malfunction of unconstrained antimoney markets, where high prices and antimoney distribution inequalities freeze the markets.

Chapter 4

Discussion & Conclusion

The global financial crisis of 2008 not only exemplified various deficits of the prevailing monetary system due to credit creation[15,24,155,156] but also motivated advancing regulations on financial markets and spurred the exploration of alternative monetary systems. The flourishing field of econophysics thereby might help to approach macroeconomic problems from a different perspective by beneficial contributions to economic research and may even allow an improved policy setting.[157] Currently, the communication between the fields faces challenges on the fundamentals of macroeconomic theory, such as the application of rationality and the representative agent in economic modeling.[95,98,129]

A step towards a possibly more neutral and more stable monetary system is made by the physics motivated time–homogeneous system of money and antimoney. The previously studied analytical properties of the system show promising results, indicating a general functionality of the system which benefits from the time-homogeneity property and liquidity market mechanism.[39,68,69,72,73] The time-homogeneity property in principle mitigates connected problems of information loss[24] and non-local shifts of purchasing power.[39]

The presented simulation results of the money–antimoney system show that price and trade volume equilibria do not emerge naturally from simple random trading strategies. The inability of the simple random strategy to equilibrate an antimoney market stems from the lack of an intrinsic antimoney budget constraint. Yet, a constraint-free antimoney market that mitigates credit crises was one of the motivations of the money–antimoney system. The conclusion that additional boundary conditions are needed to equilibrate the antimoney market, comparable to regulatory requirements for credit markets, is an important step in understanding this kind of monetary systems and more generally the debt-side of monetary systems.[79,84] The introduction of multi-flavor moneys and antimoneys did not entropically solve the problem. The explicit antimoney budget constraints led to symmetric equilibration of the antimoney market and the money market. The implemented local antimoney holding limitations were similar to real conditions of granting a credit in which individuals are not allowed to accumulate excessive debts. The findings may be interpreted as an indicator that setting a monetary system's boundary conditions may not be enough to stabilize it. The force of the markets to push the systems away from equilibrium may fundamentally be stronger than the boundary conditions. The relation between market

forces and monetary boundary conditions could yield valuable insights: Under which monetary boundary conditions can markets drive systems out of equilibrium by their inherent construction and what role do various trading strategies play?

Studying the impact of structural changes of production and credit granting provided access to testing the stability of the equilibria.[90] External shocks were modeled as bubbles that formed from external stimulus and subsequent burst.[154] For the production shocks, the results let conclude that the single money, two money and money–antimoney system show qualitative and quantitative similar price-, trade volume- and utility-responses. The response of the money–antimoney system after being hit by a credit shock suggests similar if not increased robustness in comparison to a single money system with smaller deviations in the utility gain during the shock. Although a two-money system digested the credit shock similarly to the money–antimoney system, the two-money system did not benefit or suffer from the conceptual advantages of the money–antimoney system. These findings strengthen the claim that a money–antimoney system is similar in many respects to a single money currency system, while at the same time the time-homogeneous money–antimoney system prevents non-local shifts of monetary wealth and conserves economic information. Specifically, the work of this thesis showed that the money–antimoney system is compatible with a market mechanism.

The central question of individual bankruptcy still needs further investigation. When an agent leaves the system the agent's initial money–antimoney pair must be annihilated. Yet, the question remains open how an algorithm should annihilate an agent's balance if it is not equal to the initial endowments. In this way, the negative consequences of the Cantillon Effect are mitigated. This is a major improvement to the prevailing monetary system, in which two credit partners (commercial bank and creditworthy client) can influence all other market participants without their consent[39] within the limits of the monetary boundary conditions.

Future works could aim for an incorporation of the liquidity market, which trades money against antimoney, to study the money–antimoney stability under a credit market. How does a credit market influence the digestion of booms and shocks? Are equilibria stable when hazardous subpopulations (that try to drive prices out of equilibrium) enter the system? Could informed traders insure against shocks, e.g. by obtaining credit before a shock? Structural future research beyond this could aim for empirical studies on how humans act in a money–antimoney system. Therefore, on the basis of the presented simulations a game with interacting humans would be suitable. From a large scale view, human interaction would be best studied with a real-world issuance of a digital money–antimoney currency to pursue one of the fundamental challenges of mankind: The search of a stable monetary system.

Conclusion

Stability of monetary systems has played a fundamental role in human societies for 5000 years of civilization and credit creation has been shown to be one of the driving sources of

instability. Inspired by the Noether theorem, energy conservation is applied on money and debt, like on matter-antimatter, yielding for the time-homogeneous bi-currency system of money and antimoney. To test the stability of the system, limit order-book market simulations with stochastic agent trading strategies were performed in an agent-based economy. Simulations of a system without limits on individual antimoney holdings reveal a freezing of the good-antimoney market. Imposing limits on agent antimoney holdings leads to vital money and antimoney markets with symmetric prices and trade volumes. Results from single money, two money and money–antimoney systems show that quantity theory is satisfied. A comparison of the monetary systems' responses from deviations from equilibrated states due to external production and credit shocks shows similar behavior. The findings indicate an overall functionality and compatibility of market mechanisms in the framework of the money–antimoney system under individual debt-limiting boundary conditions.

Part II

Kinetic Microscale Thermophoresis

Chapter 5

Introduction & Theory

In this part of the thesis, the novel measurement method Kinetic Microscale Thermophoresis (KMST) is presented. It offers an immobilization-free measurement method of kinetic on-rates and off-rates of biological ligand-binder systems in free solution. DNA hybridization rates were measured for complementary DNA oligomers and the findings are discussed and compared to other kinetic measurement methods.[1].

5.1 Binding processes in life sciences

A chemical reaction is a process that results in the interconversion of chemical species.[159] This process is governed by the structure of the reactants, the thermodynamic equilibria determining the direction of the reaction and the energy landscape together with the kinetic rates that determine the speed of the reaction.[160] In the biological context, molecular interactions of proteins, carbohydrates, nucleic acids, lipids and other biomolecules can be described by their respective reaction properties. One central type of biological molecular interaction is the molecular binding process, in which a biological molecule called *ligand* can bind reversibly to a biological target molecule called *binder*, forming a reversible ligand-binder complex.

   The formation, stability and dissociation of biological ligand-binder systems play a fundamental role in nearly all aspects of living matter: Receptor-ligand interactions in *homeostatic pathways*,[161] multivalent binding in the cellular *organization*,[162] fatty-acid binding in *metabolic pathways*,[163] processes of cell growth,[164] cellular *response* to external stimuli,[165] *evolution*[166] and *reproduction*.[167] As essential as molecular binding processes are for life, they also play a central role in pathogenesis: microbial pathogens binding to host cells during *infections*,[168] gene expression regulation in inflammatory processes[169] and receptor binding in signaling pathways of cancer[170] and tissue breakdown.[171] In order to cure diseases, their pharmacological treatment largely targets the interaction of proteins

---

[1]Parts, Tables and Figures of this (5), the methods & materials (6), results (7), discussion (8) and in the appendix (9) section contain works of me that were previously published in[158] and are reproduced under CC BY license

with cell surface receptors, enzymes and ion channels.[172] Lately, evidence is consolidating that the efficacy of therapeutics is significantly determined by their kinetics.[173]

Apparently, the in-depth study of molecular binding processes can contribute to a far-reaching understanding of various fields of life sciences. This requires a thorough study of the structure of the involved molecules, the binding equilibrium and the binding rates for each interaction. Whereas the theoretical characterization of binding processes has been established over a century ago[174] and subsequently expanded and developed up to the description of complex reaction networks,[175] empirical knowledge expanded rather recently upon the application of high-throughput screening methods[176–178]. Currently, the molecular structures of several hundred thousand biomolecules are known[179] as well as the respective binding equilibria.[180]

5.2   Challenges of kinetic rate determination

The experimental determination of kinetic binding rates faces analytical and experimental challenges. The analytical description of binding processes of more complex than simple ligand-binder system becomes 'difficult or impossible'.[181] The nature of the binding rates, which describe the transition between equilibrium states, can be experimentally measured by observing the transition from the bound to the unbound state (or vice versa), which is experimentally significantly more demanding.[182] In addition, the determination of the time-resolved active concentration, that is the concentration of unbound ligands and binder which can participate in the binding reaction, is experimentally difficult to determine.[183] Lastly, e.g. for DNA-DNA and DNA-RNA hybridization, controllability and reproducibility of results across different experimental devices has not been achieved yet.[184] These circumstances make the comparison of the obtained results even more difficult.

The established experimental methods aim for immobilization and/or labeling of the reactant(s). Immobilizing methods rely on the immobilization of one of the reactants, which is then exposed to the diluted ligand and subsequent binding is recorded.[185–187] Methods that rely on immobilization of the target share the problems that the target's physical properties can change upon binding which influences the measured rates.[188] Methods that use fluorescent labeling of the reactants aim to detect fluorescence intensity changes upon binding.[189,190] The labeling of the reactants could possibly change the way the binder interacts with the ligand.[191] Recently, immobilization-free and label-free methods provide access to kinetic rates.[192] However, inconsistent measurement results of kinetic rates[193] and limited comparability between them remain a central challenge.

To target the challenges of the field of kinetic binding rates, this part of the thesis describes the novel experimental method of Kinetic Microscale Thermophoresis (KMST)[158] with which the rates of DNA hybridization reactions, one of the most central reactions of life sciences, were systematically determined. Kinetic Microscale Thermophoresis bases on the established method of Microscale Thermophoresis (MST)[194–199] with which equilibrium binding constants can be successfully determined. In MST experiments a microscale temperature gradient is induced by an infrared laser and the temperature-related fluo-

rescence change can be used to determine binding equilibrium constants. By increasing the thermal coupling of the sample with the environment by placing the sample capillary on silicon and immersing with oil, KMST provides access to the kinetic rates during the transition from unbound to bound state.

The work is structured as follows: First, the theoretical basis of relaxation kinetics and the predominant probing methods are briefly presented. Second, the experimental setup of KMST, the analysis of the fluorescence data and the sample preparation are described in detail. Third, the experimental results on DNA hybridization are presented. Fourth, the KMST technique's challenges and the found exponential off-rate dependence and weak on-rate dependence of DNA on salt, strand length and temperature are discussed.

5.3 Kinetic binding theory

5.3.1 Equilibrium binding

The chemical reaction for a simple ligand-binder process reads

$$L + B^* \underset{k_{off}}{\overset{k_{on}}{\rightleftharpoons}} LB^* \tag{5.1}$$

with the ligand species L, the fluorescent binder species B^*, the bound complex LB^*, the on-rate k_{on} and the off-rate k_{off}. The reaction can take place in aqueous solution or on the surface of membranes. Therefore, in the following the concentrations L, B^* and LB^* (in Molar) denote the concentrations of the species in the buffer solution, respectively. The off-rate has the unit $[\text{s}^{-1}]$ and the on-rate $[\text{M}^{-1}\,\text{s}^{-1}]$.

In the following kinetic description, the kinetic on-rate and off-rate are identified as the rates with which the reaction takes place. In equilibrium, for a simple ligand-binder process, the amount of molecules that unbind equals the amount of molecules that bind in a defined period and it holds

$$k_{off} \cdot LB^* = k_{on} \cdot L \cdot B^* \Leftrightarrow K_d \equiv \frac{k_{off}}{k_{on}} = \frac{L \cdot B^*}{LB^*}. \tag{5.2}$$

K_d is the dissociation constant (also binding constant and inverse equilibrium constant $K_{eq} = \frac{1}{K_d}$) and has unit Molar [M]. Eqn.5.2 is valid for single binder-ligand systems which do not have multiple binding sites. For multiple binding sites, the Hill-equation applies.[200]

In experiments, commonly only the total concentration of ligand $L_{tot} = L + LB^*$ and binder $B_{tot}^* = B^* + LB^*$ are known or accessible. The fraction bound $f_b = LB^*/B_{tot}^*$ expresses the fraction of bound complex over total binder and can be expressed by L_{tot} and B_{tot} by

$$f_b = \frac{LB^*}{B_{tot}^*} = \frac{L_{tot} + B_{tot}^* + K_d - \sqrt{(L_{tot} + B_{tot}^* + K_d)^2 - 4L_{tot}B_{tot}^*}}{2B_{tot}^*} \tag{5.3}$$

Plotting f_b over the total ligand concentration yields for the typical binding curve, see Fig6.4**a**. Microscale Thermophoresis uses the fluorescence signal to determine the fraction bound and fit K_d to the binding curve with known L_{tot} and B^*_{tot}.[197] For systems in equilibrium, the dissociation constant is a suitable quantity to characterize the affinity of a ligand-binder system. For systems, in which different ligands which bind to the same binder, assessment of the respective K_d allows for quantification of the strength of the affinities.

However, the characterization of a ligand-bindersystem by K_d is limited. First, consider a system in which two different ligand species bind to the same binder and exhibit the same K_d, but dissimilar kinetic properties, they can not be distinguished by the measurement of K_d. Simply consider $K_d = k_{off}/k_{on}$ where various sets of k_{off} and k_{on} result in the same K_d. Second, if a change of a parameter in a ligand-binder system results in the change of K_d, it requires the knowledge of the kinetic rates to assess if the formation or dissociation of the complex was affected.

5.3.2   Kinetic relaxation

The kinetic on-rate and off-rates ultimately define the timescale on which biological processes are triggered.[201] Therefore, they are accessed experimentally by a deflection of the ligand-binder system from equilibrium and a subsequent analysis of the relaxation process. The corresponding rate equations for free ligand concentration L, free binder concentration B^* and bound complex concentration LB^* describe the evolution of the concentrations of the species over time

$$
\begin{aligned}
\frac{\partial LB^*}{\partial t} &= \ -k_{off} \cdot LB^* + k_{on} \cdot L \cdot B^* \\[6pt]
\frac{\partial B^*}{\partial t} &= \ \ \ k_{off} \cdot LB^* - k_{on} \cdot L \cdot B^* \\[6pt]
\frac{\partial L}{\partial t} &= \ \ \ k_{off} \cdot LB^* - k_{on} \cdot L \cdot B^*
\end{aligned}
\tag{5.4}
$$

for an ideal 0D system. In equilibrium, the time derivatives of the concentration become $0 = \frac{\partial LB^*}{\partial t} = \frac{\partial B^*}{\partial t} = \frac{\partial L}{\partial t}$ and the binding equilibrium constant K_d is derived, see above.

The system can be deflected from equilibrium by a change of temperature, pressure, reactant concentration, pH and buffer conditions.[202] The rate equations govern the time evolution from the former equilibrium to the new equilibrium. A change of reactant concentrations, e.g. addition of free ligand, will shift the fraction bound accordingly. A change of external parameters can affect the on-rate and off-rate and shift the reaction equilibrium.

When the system is subjected to a temperature jump, it relaxes from an initial equilibrium to a final equilibrium. In the latter, the temperature jumps from hot to cold and is assumed to be instantaneous on the timescale of the following relaxation. For small changes in the fraction bound between the initial hot state and the final cold state, the

concentrations L, B^* and LB^* follow an exponential relaxation with time constant $\tau_{kinetic}$

$$\tau_{kinetic}^{-1} = k_{on}(L + B^*) + k_{off} \qquad (5.5)$$

where L and B^* are the free concentrations of the final state.[202] Substituting L and B^* by Eq.5.2 and Eq.5.3 yields for the kinetic relaxation time constant which then only depends on quantities that are accessible with a Kinetic Microscale Thermophoresis setup.[158] With the assumption that the the process relaxes homogeneously in the detected volume, the on-rate k_{on} can be fitted to a ligand assay with constant B_{tot}^* and K_d determined from the binding curve:

$$\tau_{kinetic}^{-1} = k_{on}\sqrt{(L_{tot} + B_{tot}^* + K_d)^2 - 4L_{tot}B_{tot}^*}. \qquad (5.6)$$

Measurement of a ligand assay with various L_{tot} increases the robustness of the k_{on}-fit.

5.4 Thermodynamics of ligand-binder systems

5.4.1 Van't Hoff analysis

On the molecular level, binding is the result of a successful collision of the reactant molecules with appropriate orientation and sufficient energy. For an ensemble of molecules, many processes take place in solution and consequently a thermodynamic description is suitable. The ligand, binder, solvent and buffer ions form a thermodynamic system which exhibits complex interactions and heat exchange. The Gibbs free energy is a thermodynamic potential and quantifies the the maximum reversible work of the system at constant temperature and pressure. Fig.5.1 shows a schematic Gibbs free energy landscape of a simple ligand(orange)-binder(purple) process with the unbound state, the transition state (during collision) and the bound state.

In equilibrium, the Gibbs free energy can be thermodynamically described by the difference of the Gibbs free energy of the unbound and bound state ΔG which is independent of the pathway between these states. At standard temperature $295\,\mathrm{K}$ and pressure $1\,\mathrm{atm}$ the standard free Gibbs energy is defined as ΔG^0. Spontaneous processes and thus binding occurs when ΔG is negative. The magnitude of ΔG is a measure for the stability of the bound complex. For large negative ΔG, the bound state is strongly favored. By utilizing the definition of the standard chemical potential, the partial molar Gibbs energy and the reaction quotient, the standard Gibbs energy change can be related to the binding affinity K_d with

$$\Delta G^0 = RT \ln \frac{K_d}{c^0} \qquad (5.7)$$

with R the universal gas constant $1.987\,\mathrm{cal\,K^{-1}\,mol^{-1}}$, T the temperature and c^0 the standard concentration $1\,\mathrm{M}$.

The Gibbs free energy can be expressed by its enthalpic and entropic contributions by Legendre transformation

$$\Delta G = \Delta H - T\Delta S \qquad (5.8)$$
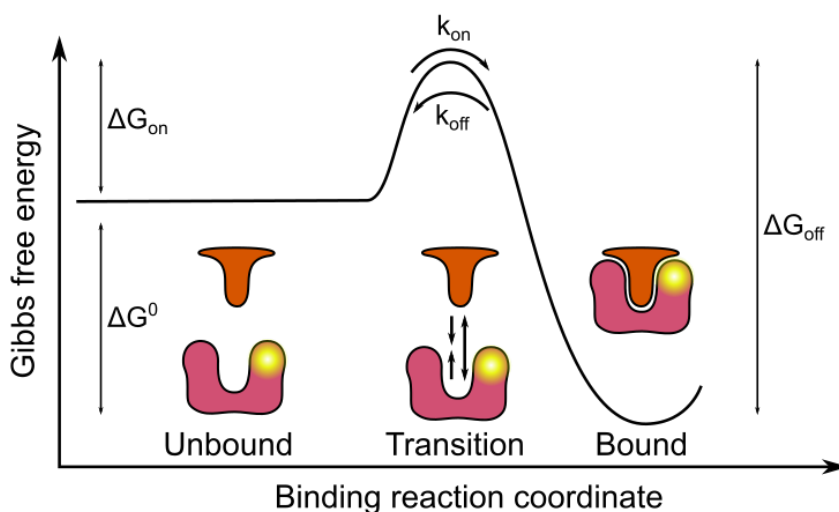
Figure 5.1: The Gibbs free energy for the unbound state, the transition state and the bound state. For spontaneous processes $\Delta G^0 < 0$. The transition between bound and unbound state depends on the energy barrier ΔG_{on} and ΔG_{off}. If the reaction coordinate is properly defined – which is the case only for elementar binding processes – the transition between the bound and unbound state can be related to the kinetic on-rate and off-rate.

The associated enthalpy change ΔH upon binding is a measure of the total internal energy change of the system by the absorbance $\Delta H > 0$ or release $\Delta H < 0$ of heat due to the formation or disruption of noncovalent interactions, i.e. van der Waals contacts, hydrogen bonds, ion pairs and other polar and apolar interactions.[203] The change of entropy ΔS is a measure of the disorder of the system, including the ligand, the binder and the solvent. The Van't Hoff equation connects the binding affinity K_d with the standard change of enthalpy $\Delta H^\ominus$ and entropy $\Delta S^\ominus$

$$\frac{d\ln(K_d/c^0)}{dT} = \frac{\Delta H^\ominus}{RT^2} \tag{5.9}$$

and in the integrated form

$$\ln\frac{K_d}{c^0} = \frac{\Delta H^\ominus}{RT} - \frac{\Delta S^\ominus}{R} \tag{5.10}$$

at standard concentration $1\,\mathrm{M}$, assuming $\Delta H^\ominus$ and $\Delta S^\ominus$ are constant and the temperature interval is small. The *Van't Hoff* equation was widely used in literature to characterize the thermodynamic quantities of chemical dynamics and awarded the first Nobel prices in chemistry in 1901.[204,205]

5.4.2 Connection of kinetic and thermodynamic quantities

Whereas the characterization of the ligand-binder system in equilibrium has been established by Van't Hoff over one hundred years ago, the thermodynamic treatment of the

transition between the bound and unbound state is much more difficult and subject of ongoing debate.[206–209] The Arrhenius analysis and Eyring-Polanyi identification of the temperature-dependence of the kinetic on-rate and off-rate provide two frameworks to connect the experimentally-accessible kinetic data of KMST with thermodynamic quantities.

The Arrhenius equation states that the temperature dependence of the rate constant k of a reaction is

$$k = A \cdot \exp\left(\frac{-E_A}{RT}\right) \tag{5.11}$$

with k the on-rate or off-rate of the ligand-binder system, A the so called exponential pre-factor (also frequency factor) and the temperature-independent activation energy E_A. The pre-factor A can be identified as the highest achievable magnitude of the rate constant k. The exponential term defines the fraction of molecules that has enough energy to react. E_A represents a barrier to reactivity, which has passed for each reaction direction. The Arrhenius equation describes the empirically determined rates for a broad spectrum of biological and chemical systems.[210,211] For enzyme-catalyzed reactions, also non-linear Arrhenius plots with two straight-line segments have been found. These could be explained by changes of the solvent with temperature and the parallel presence of successive reactions with different E_A.[212]

The Eyring-Polanyi equation bases on the framework of transition state theory (TST) which was developed to describe elementary chemical reaction steps.[209] TST states that a quasi-equilibrium *transition state* is formed between the unbound and bound ligand-binder complex, between which the complex can convert at the kinetic on-rate and off-rate, see Fig.5.1. For the special case of DNA hybridization, the on-rate and off-rate can be expressed each by the Eyring-Polanyi equation

$$k = k^0 \nu \cdot \exp\left(\frac{-\Delta G^{\ddagger}}{RT}\right) = k^0 \nu \cdot \exp\left(\frac{-\Delta H^{\ddagger}}{RT} + \frac{\Delta S^{\ddagger}}{R}\right) \tag{5.12}$$

with k^0 unity for the off-rate and [M] for the on-rate, ν the attempt frequency, $\Delta G^{\ddagger}$, $\Delta H^{\ddagger}$ and $\Delta S^{\ddagger}$ the change of Gibbs free energy, enthalpy and entropy.[207,213,214] Knowledge of $\Delta G^{\ddagger}$, $\Delta H^{\ddagger}$ and $\Delta S^{\ddagger}$ allows for the determination of the Gibbs free energy, enthalpy and entropy landscapes of the free state, transition state and bound state along a reaction coordinate. The reaction coordinate measures the progress of the reaction along the re-action pathway in the one dimensional energy function of the system. The energy barrier between the bound and unbound state can be shifted by changes of the environment, e.g. salt concentration, temperature or pressure.

Importantly, the application of the Eyring-Polanyi equation for the analysis of ligand-binder systems bases on the assumptions that the binding process can be assumed to proceed along one reaction coordinate. Binding only involves the ligand and the binder molecules in a single step binding event with the only reaction rates defined by the on-rate and off-rate.

The attempt frequency ν can be estimated by the diffusion-limited on-rate k_{diff}. It is the upper limit for the collision of ligand and binder that leads to the forming of the bound complex by

$$\nu = k_{diff} \cdot B_{tot}^* = 4\pi \cdot R \cdot D \cdot N_A \cdot B_{tot}^* \tag{5.13}$$

with $B_{tot}^* = 2\,\text{nM}$ the total binder concentration, R the collision radius of the ligand and binder, D the temperature-dependent diffusion coefficient of the ligand and binder and $N_A = 6.02 \times 10^{23}\,\text{mol}^{-1}$. For oligomer DNA strands, it was calculated to be $\nu = 2 \cdot 10^9 \cdot B_{tot}^*$ $\text{M}^{-1}\,\text{s}^{-1} = 4\,\text{s}^{-1}$.[158,207]

Both approaches of Arrhenius and Eyring-Polanyi have their advantages: The Arrhenius analysis has been successfully applied to a broad range of studied systems since the beginning of the 20th century and is well-accepted to characterize empirical data. The Eyring-Polanyi equation provides a more fundamental characterization of the thermodynamic quantities of a ligand-binder process. However, results of thermodynamic values from an Eyring-Polanyi fit, that is plotting $\ln k/(\nu k^0)$ over $1/T$ and fitting Eq.5.12, have to be treated with caution, which was already recognized by Eyring.[215] The underlying assumptions, when applying the Eyring-Polany equation to ligan-binder systems, are based on considerable simplifications, which suggest to emphasize the qualitative nature of its analysis. Nevertheless, the comparison of ligand-binder systems is possible and yields for valuable insights.[207]

However, the connection of kinetic parameters with thermodynamic quantities is challenging, especially the assumption of single step ligand-binder processes. Morrison et al.[216] point out that the difference of activation energies $E_{A,on}$ and $E_{A,off}$ for DNA hybridization from Arrhenius plots (kinetic approach) only match to a limited extend with experimental values of ΔH^0 obtained from melting curve experiments (thermodynamic perspective). Assumably, the DNA-zippering can only described to a limited extend as a single step process. The matching also depends on the experimental methods and recent literature encourages the use of Eyring-Polanyi analysis for thermodynamic characterization.[206,207,213,214,217]

5.5   Established kinetic methods

The experimental determination of kinetic rates commonly relies on the measurement of the time-resolved response signal from unbound to bound state or vice versa. Therefore, the established experimental methods aim for immobilization and/or labeling of the reactant(s). This section provides a brief overview of established methods, subdivided in label-free and immobilization-free applications and their limitations, respectively.

5.5.1   Label-free methods

Surface Plasmon Resonance (SPR)   is one of the predominant techniques to measure kinetic on-rates and off-rates of many biomolecular interactions.[185,218,219] In SPR measurements, the change of the refractive index on the back of a thin (gold) surface, which is

coated with binder molecules, is measured upon binding when exposed to ligands. In an SPR assay, one of the reactants (binder) is immobilized on the sensor surface and at a defined point it is exposed to a starting flow containing the buffer and the ligand. The ligand can bind to the immobilized binder and an association curve is recorded in real-time. After saturation, pure buffer is flushed and the bound complexes unbind; a dissociation curve is recorded. The kinetic on-rate and off-rate are fitted to the association and dissociation curves and for an assay of various ligand concentrations K_d is obtained by the absolute response plateaus.

On-rates in the range of 10^3–$10^9\,\mathrm{s^{-1}\,M^{-1}}$ and off-rates in the range of 5×10^{-6} –$10^{-1}\,\mathrm{s^{-1}}$ can be measured.[218,220] The measurement of high on-rates may face mass transport limitation, that is when the diffusion from the bulk to the surface is slower than the association rate.[221] Although SPR is highly sensitive, the measurement signal is prone to changes of the refractive index due to the solvent flowing over the surface.[222]

With SPR measurements, a wide range of interactions was studied: protein-protein,[223] protein-DNA,[224] enzyme-substrate,[225] drug-target,[226] lipid membrane-protein,[227] cell-protein[228] and other interactions. Modified SPR methods also allow for DNA aptamer characterization via linker sequences.[229]

Biolayer interferometry (BLI) is an optical technique to analyze the interference pattern of white light in an optical fibre tip which is reflected from a reference layer and an optical surface. On the back of the optical surface, ligands are immobilized and when the tip is brought into contact with the binder-containing solution, the molecules bind to the surface-attached binders. Upon binding, the optical thickness increases and the interference pattern changes. This allows for real-time studies of protein-protein interaction,[230,231] affinity[232] and kinetics.[186,233] BLI can potentially measure on-rates in the range of 10^1–$10^7\,\mathrm{s^{-1}\,M^{-1}}$ and off-rates in the range of 10^{-6}–$10^{-1}\,\mathrm{s^{-1}}$.[234]

Free molecules in solution, and changes of the refractive index upon binding do not change the interference pattern significantly and enable for studies of even crude lysates.[233] The dependence of the interference signal on a sufficient change of the optical thickness infers an analyte mass dependence of the measurements.[186,235]

Kinetic Isothermal Titration Calorimetry (kinITC) provides immobilization- and label-free access to kinetic on and off-rates as well as the thermodynamic quantities of standard enthalpy changeΔH^0, standard entropy change ΔS^0, standard Gibbs free energy change ΔG^0 and K_d.[192,206] In a kinITC experiment, a reference cell and a sample cell are surrounded by an adiabatic jacket and each connected to a heat power supply and sensitive thermometer. The sample cell contains the binder in buffer solution. With a syringe, the ligand is injected into the sample cell in subsequent titration steps. The heat change of the sample cell is observed and the power supply of the sample cell maintains isothermal conditions. Integrating the peak power against time yields for ΔH^0 and plotting ΔH^0 against the ligand concentration yields for the binding curve. Kinetic data is obtained by careful analysis of the equilibration time of the heat power of the measurement cell during

successive injections. So far, kinetic on-rates in the range of $3 \times 10^3 - 8 \times 10^6 \, s^{-1} \, M^{-1}$ and off-rates in the range of $5 \times 10^{-4} - 10^{-1} \, s^{-1}$ have been measured.[236]

The applicability of the results obtained by the kinITC method is limited, as the experiments require very high sample concentrations (mM) to detect the heat changes upon reactant mixing. The high concentrations could shift the thermodynamic quantities and as molecular processes also take place at sub-mM concentrations,[237] the kinITC results have to be interpreted carefully.

5.5.2   Immobilization-free methods

Stopped-flow fluorescence anisotropy   developed from chemical rapid-mixing kinetic techniques and now is one of the most frequently used techniques to determine kinetics in solution.[238] In a stopped-flow experiment, the binder and ligand in solution are initially separated and brought together via motor-driven syringes in a mixing cell. The ligand-binder solution is then transferred into an observation cell and the liquid flow is stopped. The mixing and transfer can be experimentally accomplished within a few milliseconds, which makes Stopped-flow methods capable of measuring rapid association processes.[238] The kinetic change of concentrations is monitored by an optical signal.[239] For fluorescently-labeled species, the emission is proportional to its molar concentrations and thus the optical signal provides access to the labeled species' concentration.[240]

In Fluorescence Anisotropy (FA) measurements, the sample is illuminated with polarized light and (typically smaller) fluorescently-labeled reactants are excited when their dipole is oriented accordingly. The orientation of the excited fluorophore (and dipole) changes due to rotational diffusion and, less pronounced, energy resonance transfer[241] and is detected in parallel and perpendicular polarization planes. The ratio of parallel polarized light to total light intensity is called anisotropy. The anisotropy depends on the fluorophore's vibration, the excited state lifetime and intrinsic anisotropy of the molecule species, being smaller for small molecules than large molecules. Time-resolved anisotropy measurement upon mixing allows for determination of kinetic rates of protein-DNA,[242] drug-target,[243] protein-membrane interactions[190] and more.[240]

Fluorescence correlation spectroscopy FCS   uses the fluorescence fluctuation intensity in a small sample volume to determine kinetic and thermodynamic parameters.[244] Typically, a laser focuses into a sample volume with very dilute (nm to pm) concentrations on a small spot so that only very few fluorophores are excited. When a fluorophore enters the focal spot, it fluoresces and the emission photon is collected by a photo detector, which measures the intensity versus time signal. Although it is not possible to extract kinetic rates or transport parameters from a single fluctuation, the rates with which the single molecules dissipate are in average governed by the same rates of the macroscopic dynamic processes.[244,245]

In contrast all of the formerly presented methods, FCS measurements are made in equilibrium. To extract the kinetic rates, the fluctuation are analyzed statistically. With FCS,

DNA-hairpin opening and closing rates,[246] protonation kinetics,[247] membrane receptor-antibody dissociation kinetics,[248] RNA- and DNA-hybridization rates,[189] drug discovery[249] and more. FCS can be extended to Fluorescence Cross-Correlation Spectroscopy (FCCS)[189] where differentially labeled molecules allow for quantification of localization, diffusion and changing composition of protein complexes in cells, recently also in high-throughput applications.[250] FCS allows for measurement of very high kinetic on-rates in the range of 10^6–$10^{10}\,\mathrm{s}^{-1}\,\mathrm{M}^{-1}$ (near the diffusion limit) and off-rates up to $5 \times 10^4\,\mathrm{s}^{-1}$.[193] The capability to measure high rates stems from the fact that FCS can effectively resolve small timescales.

5.5.3   Comparison of kinetic measurement methods

Each measurement method has advantages and disadvantages. Methods that rely on immobilization of the target share the following problems: First, the target's physical properties and stability could be changed upon immobilization.[188] Conformational changes can influence the binding behaviour,[251] e.g. slow the speed of the reaction in comparison with free solution.[217] Second, binding events could be inhibited due to random orientation.[252] Third, the strength of the binding could be overestimated due to erroneous treatment of the off-rate.[183] Fourth, mass transport limitation has to be considered, when the mass transfer from bulk solution to the surface is limited.[221] Fifth, surface immobilization is prone to extreme salt concentrations and binding to nonspecific surface sites can influence the binding signal.[221]

For fluorescent labeling methods, the way the binder interacts with the ligand possibly changes the binding process.[191] The labeling of the reactants may be difficult and for radiolabeling the signal strength needs to be high enough above the background.[253] For all types of FCS measurements, particularly, the assumptions in the theoretical models underlying the autocorrelation analysis and many free parameters in the fitting procedures possibly cause discrepancies.[193] The advantages and drawbacks need to be considered for each studied system and may point to a preferred method.

5.6   DNA hybridization

The applicability of Kinetic Microscale Thermophoresis is tested by probing the extensively studied system of asociation and dissociation of complementary DNA strands.[216,251,254,255] *Hybridization* is the forming of a duplex through non-covalent, sequence-specific interactions of two nucleic acid single strands. In this view, one of the strands is called the ligand and the other (fluorescently labeled) strand is called the binder – both could be interchanged, but KMST requires the labeled strand to be constant through the array, see below. Single strands of DNA have a sugar-phosphate backbone to which bases – adenosine *A*, thymine *T*, guanine *G* or cytosine *C* – can attach in regular intervals.[256] The formation of hydrogen bonds between A-T and G-C of and stacking of adjacent bases results in a helical duplex structure for complementary sequences.[257] Knowledge of

the molecular mechanism, the thermodynamics and the kinetics of DNA hybridization are fundamental for the understanding of non-encymatic replication in early evolution,[258] DNA replication,[259] transcription and denaturation,[260] translation, regulation of intracellurar proceesses (also with RNA),[261] analytical biotechnologies,[262] DNA-guided drug delivery[263] and other processes.

The two complementary DNA sequences that hybridize can be two single stranded DNA strands (ssDNA) or one DNA strand, forming a hairpin loop. The formation of the hairpin is not static but fluctuates between the folded and unfolded conformation.[246] The dynamics of hairpin formation (folding) could be subdivided into a fast intrachain collision, followed by a slower base-stacking process.[264] The unfolding follows a first-order process. DNA hybridization of two single strands can be described by a three state model:[264] First, in a nucleation step, two random-coiled ssDNA are brought together to form an intermediate state, in which a few base pairs have have formed. Then, the intermediate state proceeds further to form the fully hybridized double strand by zippering or slithering pathways of the base-pairs.[256] Recent molecular dynamics (MD) simulations suggest that during zippering/slithering multiple metastable intermediates exist along the pathways, calling for a more confined description.[265]

The hybridization process is governed by the complex energy landscape of the hybridizing strands.[256] Unfortunately, experimental access to the energy landscape is limited, in particular the acquisition of data points along a reaction coordinate.[266] The energy landscape $\Delta G = \Delta H - T\Delta S$ is shaped by ΔH the enthalpic and ΔS the entropic changes, which can be accessed experimentally.[267–269] The formation of a hybridized double strand is associated with negative ΔH and ΔS: The enthalpy change ΔH is negative due to the formation of hydrogen bonds during base stacking. The entropy change ΔS is negative due to a decrease of the elastic torsional, bending and acoustic vibration contributions.[270] Hybridization is dominated by the entalpic contribution for temperatures well below the duplex melting temperature, and by the entropic contribution for higher temperatures.[217] Assuming that the three state model of DNA hybridization can be approximately described by the Eyring-Polanyi equation, the energy barriers by between the unbound and bound state in the energy landscape can be quantified by the measurement of $\Delta H_{on}^{\ddagger}$, $\Delta H_{off}^{\ddagger}$, $\Delta S_{on}^{\ddagger}$ and $\Delta S_{off}^{\ddagger}$.[207,213,214] However, the results are limited due because the process is more complex than the three state model assumed by the Eyring-Polanyi equation.

For a thorough understanding of the hybridization process, the dependence of the energy barrier on salt, strand length, sequence and temperature is necessary. The on-rates have been reported to increase with salt.[271] This can be explained by a reduced retention of the phosphate backbones for increased ionic strength, lowering the energy barrier and facilitating hybridization. The dependence of the on-rates on strand length is not yet conclusive: Independent[216] and decreasing behavior[272] have been reported. The dependence of the on-rates on temperatures has been reported contrarily to be increasing,[216] decreasing[273] and non-monotonic.[271] The off-rate showed exponentially decreasing behavior for increasing strand length,[216,271,273] salt concentration[271] and temperature .[216,254,271] Ultimately, a precise understanding how the kinetic rates of hybridization and dehybridization

together with the thermodynamic quantities of Gibbs free energy, enthalpy and entropy change depend on sequence, buffer conditions and temperature is pursued.

Furthermore, the solution environment affects diffusion, conformation and reactivity of reaction processes.[274] The role of crowding and excluded volume effects is debated.[275] It is experimentally difficult to access kinetic rates in crowded solutions and fluorescence-based methods have shown to be suitable.[276] For DNA, the solution environment ranges from pure buffer solutions in biotechnological applications to physiological intracellular crowded solutions that can contain up to 30% of large polymers and small constitues.[277] Binding kinetics of DNA hybrdization have been reported to accelerate and decelerate in vivo compared with identical solutions in vitro.[278] The open and closing rates of DNA hairpins have been reported to slightly decrease and strongly increase for increasing polyethylene glycol (PEG) 8000 concentrations.[279] However, systematic studies of DNA hybridization kinetics and thermodynamics in solutions ranging from in vivo environments like the highlgy crowded cell nucleus[280] to in vitro DNA diagnostics biotechnological of applications.[281] To yield for comparable results, the measurement technique has to be capable to measure samples in the various environments. Kinetic Microscale Thermophoresis showed to allow for an appropriate characterization of DNA hybridization kinetics and thermodynamics for various fluids.[158]

Chapter 6

Methods & Materials

6.1 Kinetic Microscale Thermophoresis Setup

6.1.1 Experimental setup

Kinetic Microscale Thermophoresis (KMST) measurements were carried out with a Nanotemper Monotlith NT.115 Pico with a modified capillary sample holder. An infrared laser at a wavelength of 1480 nm and minimal beam waist smaller than 25 µm focused on the sample-containing capillary and created a local temperature gradient of about 10 K in average, for a defined time period. During the whole measurement, the sample was illuminated with red LED light of $605 - 645$ nm and the emitted photons ($660 - 710$ nm) from the fluorohpore passed a dichroic mirror to be detected by a photodiode which collected the fluorescence signal over time[195,196,269], see Fig.6.1. The used fluorophore attached to the binder was required to absorb near or in the LED emission wavelength spectrum. Ambient temperature was held constant and could be set between 283 K and 301 K.

The detected fluorescence signal depended on molecular interaction processes, see Fig.6.1**a**: First, binding of the ligand and binder changed the quantum yield and decreased the absolute fluorescence intensity and increased bleaching. Second, the fluorophore bleached upon LED illumination. Third, during the laser was switched on, the fluorophore's quantum yield decreased due to higher temperature and convection and thermophoresis changed the amount of fluorophores in the illuminated region. The placement of the capillary on silicon and immersing with oil decreased the heating and cooling times upon laser switching on or off, see Fig.6.1**b** and below.

A KMST experiment consisted of a serial dilution of 16 samples with ligand-binder serial solution. The binder was kept constant to obtain comparable fluorescence levels and the ligand was diluted typically 1:1 between the capillaries. To dissect the convection/thermophoresis influence on the fluorescence signal, two zero-ligand measurements were made. Each sample capillary was measured with the same protocol, see Fig.6.2: For the first 50 s, the sample's bleaching was recorded in the *pre-heat phase*. During the following *heating-phase*, the laser was switched on and locally heated the sample and the
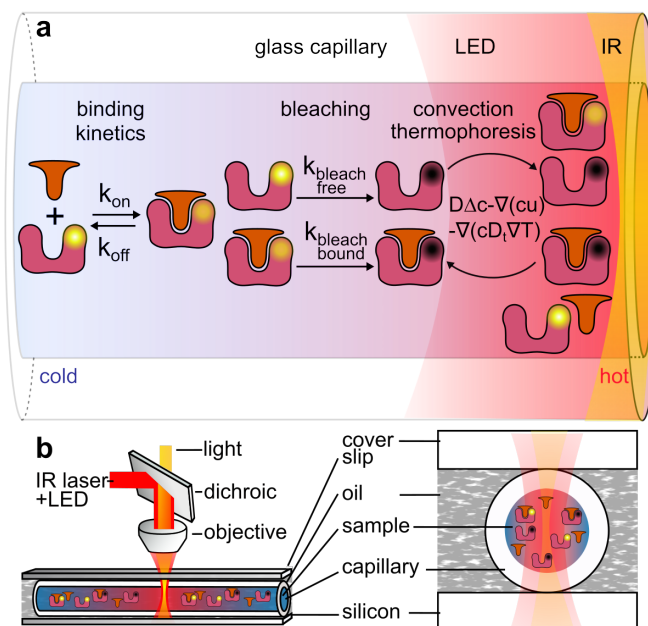
Figure 6.1: Kinetic Microscale Thermophoresis setup **a** Molecular interaction processes that change the detected fluorescence of the sample. Binding kinetics: ligand and binder associate with k_{on} and dissociate with k_{off}. Photobleaching: the illumination with LED light bleaches the fluorescent dye. Convection and thermophoresis: the temperature gradient of 10 K induced by the IR-laser leads to convective and thermophoretic movement of the fluorescent binder and ligand in and out of the detection volume. **b** To obtain a strong thermal coupling, the sample solution inside a capillary is placed between a temperature-controlled silicon wafer and a glass cover slip, surrounded with immersion oil and locally heated with an IR-laser. Through the same objective, fluorescence emission and excitation LED light is detected by a photodiode. Figure reproduced from [158].

fluorescence changed due to the temperature jump and the molecular processes described above. After heating, the laser was switched off and the temperature jumped back to ambient temperature. In the *post-heat phase*, the fluorescence trace was used to extract the kinetic parameters from the relaxation of the system towards equilibrium. The quick temperature change upon switching the laser on/off was necessary for the applicability of Eqn.5.6 in the analysis.

6.1.2   Rapid sample heating and cooling

The rapid heating and cooling was obtained by a strong thermal coupling of the sample with its environment. The basic idea was to make the heated volume smaller and increase the heat flux of the sample to its environment. Therefore, four changes in comparison with a conventional Nanotemper NTT.115 measurement were made. First, capillaries with smaller size were used (CM Scientific). The inner diameter was 300 µm and the outer diameter was 400 µm instead of the conventional ID 500 µm and OD 1000 µm. The
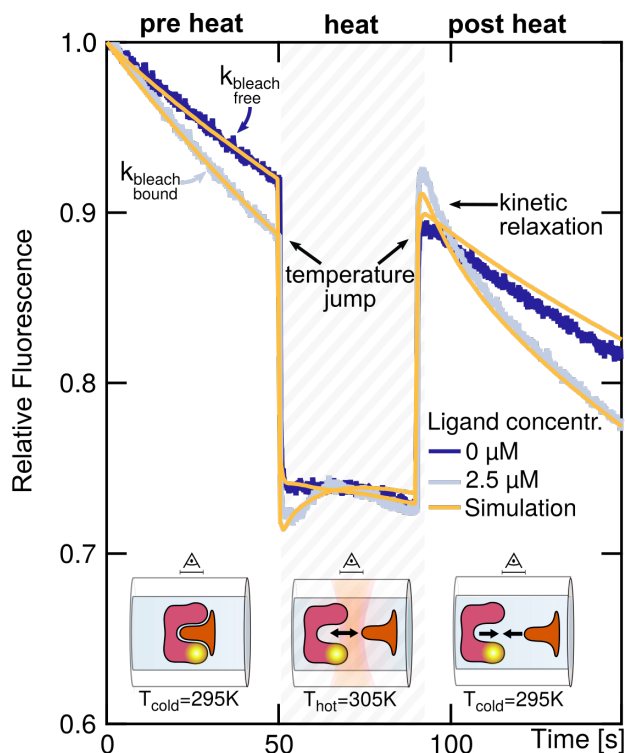
Figure 6.2: Fluorescence traces unravel kinetics In the pre heating phase, the sample is in equilibrium at ambient temperature and the fluorophore bleaches due to LED illumination. The bleach rate is higher for the bound complex than for free binders. When the IR laser is switched on during the heating phase, the fluorescence quickly changes upon the temperature jump within several hundreds of milliseconds. Then, the fluorescence change stems from unbinding of bound complexes, convection and thermophoretic movement. After the laser is switched off in the post heating phase, the sample quickly returns to ambient temperature. The fluorescence jumps back and shortly thereafter is governed by kinetic relaxation from unbound state towards the bound state. Fluorescence differences of the bound state and unbound state allow for an analysis of the kinetic fingerprint. Fluorescence traces are shown for 0 and 2.5M of 12mer DNA strands (dark and light blue) at 19C with 2 nM complementary labeled binder strand and COMSOL simulations (yellow), respectively. Figure reproduced from [158].

absolute fluorescence counts were reduced but were still sufficiently high to extract valid traces (10,000 to 3,000 counts instead of 20,000 to 10,000 for the larger capillaries). Second, the capillaries were placed on a silicon wafer instead of freely-lying in air to increase the thermal conductivity of the sample. Third, the capillaries on the silicon were immersed with oil (Zeiss Immersion Oil 518 F) and fourth, a thin glass cover slip (Carl Roth) was put on top of the capillaries, see Fig.6.3**d**. The coverslip and immersion with oil yielded for homogeneous fluorescence counts for all capillaries; which was not the case for absent coverslip measurements where possibly inhomogeneities on the oil-air interface at each capillary randomly influenced the optical signal.
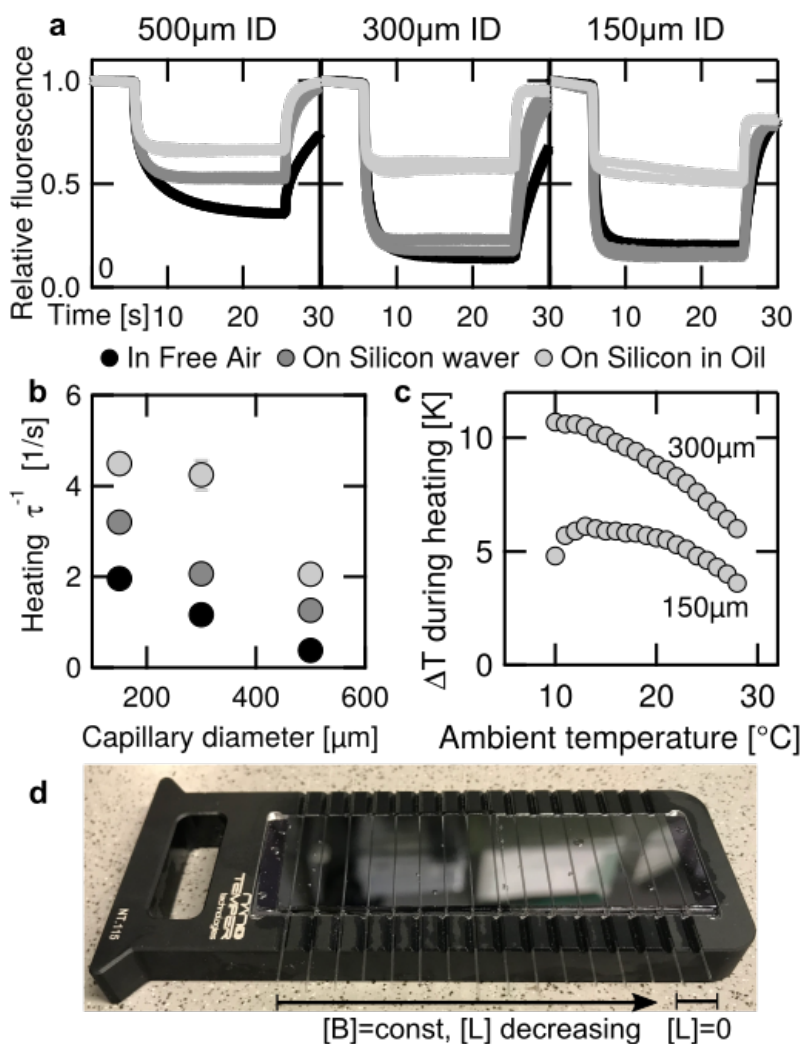
Figure 6.3: Sample heating characteristics **a** Relative fluorescence over time of Cy-5 in 1xPBS solution during heating for various capillary sizes (500 µm, 300 µm and 150 µm inner diameter) and sample holder specifications. **b** The strong heat-coupling of the sample to the Silicon-Oil-Coverslip holder (SOC) enables for short high inverse heating times. **c** the temperature jump during the hot time is about 10 K for capillaries with inner diameter 300 µm. **d** The SOC sample holder with capillaries filled with constant binder and decreasing ligand concentrations - from left to right. Figure reproduced from [158].

As a result, the strong thermal coupling enabled for heating times ten fold faster than with a conventional sample holder, see Fig.6.3**a**,**b**. The heating time was measured by the inverse time constant τ^{-1} of an exponential fit of the fluorescence traces during the hot phase of Fig.6.3**a** and plotted over the inner diameter in Fig.6.3**b**. For the following measurements, the 300 µm ID capillaries were chosen as they provided reasonably fast heating, easy handling at sample filling and sufficient absolute fluorescence counts. Notably, the smaller capillaries also reduced the effects of thermophoresis and convection

due to smaller temperature gradients. This improves the data analysis as the respective correction is smaller and less prone to systematical errors, such as underestimating back-diffusion of fluorescent molecules in the post-heat phase back into the illuminated region (which were displaced during the hot phase.

The absolute temperature jump during the hot phase is important to know for simulation modeling, see below. Therefore, the absolute fluorescence levels of Cy-5 fluorophore-only samples (biomers, Ulm) in 0.1xPBS buffer (Ambion) in the pre-heating phase and during the heating phase were measured. The absolute fluorescence levels in the pre-heat phase was linearly dependent on temperature (now shown) in the range of 283–301 K. The amplitude of the temperature jump was measured by the absolute fluorescence level during the hot phase and this value was related to the corresponding pre-heat level. The respective temperature of the pre-heat level is assumed to be the averaged temperature during the hot phase. The temperature difference between heating phase and pre-heating phase was plotted against the initial temperature, see Fig.6.3**c**, concluding that the temperature jump was $\Delta T \approx 10$ K in average for the observed spot. The absolute values of the pre-heat time had to be linearly estimated due to lack of measurements with ambient temperature higher than 303 K. As a remark, the heating and cooling time scales were one order smaller than the detected relaxation time constant, compare heating τ^{-1} of Fig.6.3**b** with $\tau_{kinetic}^{-1}$ of Fig.6.4**c**.

6.2 Kinetic binding analysis

6.2.1 K_d and binding curve analysis via bleaching rates

The dissociation constant K_d was obtained by the analysis of the bleaching rates in the pre-heat phase. Similar to the standard analysis of fluorescence levels[269], the bleaching rates were used to fit Eqn.5.3 with

$$f_b = \frac{LB^*}{B_{tot}^*} = \frac{k_{bleach} - k_{bleach,bound}}{k_{bleach,free} - k_{bleach,bound}}. \tag{6.1}$$

Where k_{bleach} was the experimentally determined bleaching rate and $k_{bleach,bound}$ and $k_{bleach,free}$ were the bleaching rates for the fully bound and free state, respectively. The experimental bleaching rates were determined by fitting an exponential function $F_{preheat}(t) = A \cdot \exp\left(-t/\tau_{bleach}\right)$ to the normalized fluorescence curves (through division of the initial fluorescence) and $k_{bleach} = A/\tau_{bleach}$. The binding curve was obtained by fitting K_d, $k_{bleach,bound}$ and $k_{bleach,free}$ to Eqn.5.3, see Fig.6.4**a**. Importantly, the K_d fit was sensitive to the total binder concentration B_{tot}^*, which needed to be smaller than K_d to obtain meaningful K_d fits and binding curves.

6.2.2 Reaction kinetics from fluorescence traces

Choice of post heat phase In principle, the kinetic rates could have been determined in the heating phase and in the post-heating phase. However, the heating phase was not
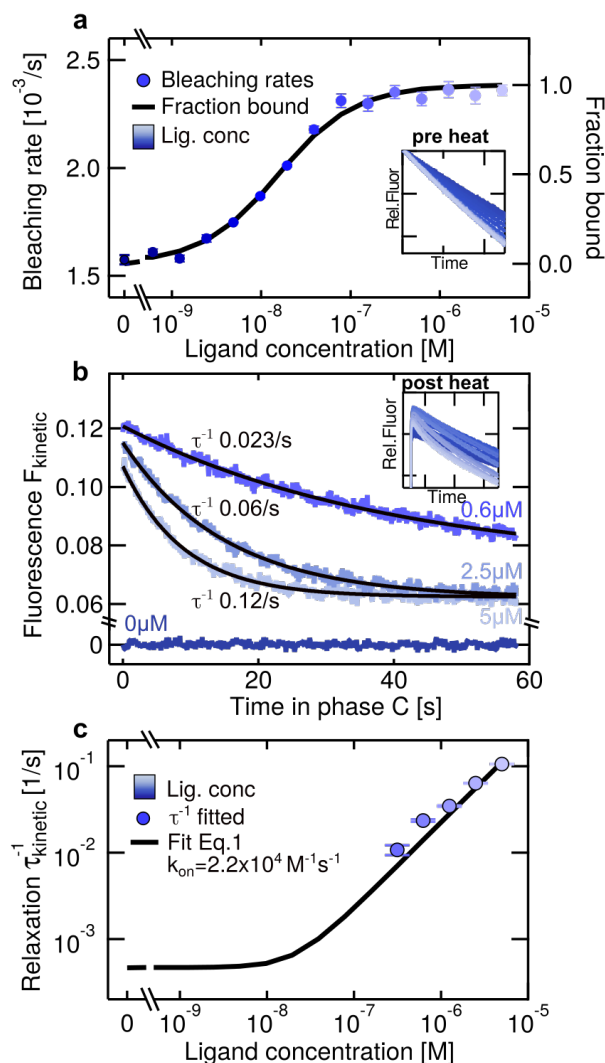
Figure 6.4: Kinetic data extraction **a** The binding curve and K_d were obtained by plotting the bleaching rate in the pre heat phase against the ligand concentration. **b** Kinetic relaxation traces were obtained by analyzing the fluorescence traces in the post heat phase. Exponential fitting of the kinetic traces yielded for the inverse kinetic time constant $\tau_{kinetic}^{-1}$. The insets show all measured fluorescence curves of one dilution series. **c** $\tau_{kinetic}^{-1}$ were plotted over the ligand concentration to fit k_{on} according to Eqn.5.6, for fully-complementary 12mer in 0.1xPBS buffer at 295 K, $k_{on} = 2.2 \times 10^4 \, \mathrm{M}^{-1} \, \mathrm{s}^{-1}$. Figure reproduced from [158].

suitable for kinetic rates determination for two reasons. First, the determination of the kinetic rates according to Eqn.5.6 would only be valid for systems with homogeneous temperature. The temperature gradient induced by the heating laser during the hot phase did not allow the application of Eqn.5.6. In addition, K_d would have been needed to be determined during the hot phase, which was difficult due to non-stationarity of the high-ligand concentration traces during the hot phase, see light blue trace in Fig.6.2. Second, convec-

tive and thermophoretic movement had a strong influence on the fluorescence traces that it was difficult if not impossible to extract the kinetic fingerprint from them. Both arguments strongly support extraction of the kinetic rates in the post-heat phase, in which the system is almost instantly at thermal equilibrium and bleaching and convection/thermophoretic movement can be accounted for reasonably well.

Extraction of kinetic rates To extract the kinetic fingerprint from the fluorescence traces in the post-heat phase, the following simple model was applied. The detected fluorescence signal $F(t)$ [emitted photons / second] per time interval Δt was assumed to be the integral over the illuminated detection volume dV of the time and spacial-dependent free $B^*(t, \vec{x})[mol/m^3]$ and bound $LB^*(t, \vec{x})[mol/m^3]$

$$F(t) = \int dV \left(B^*(t, \vec{x}) \cdot \left(F_{Free} + \frac{\partial F_{Free}}{\partial T} \cdot \Delta T \right) + LB^*(t, \vec{x}) \cdot \left(F_{Bound} + \frac{\partial F_{Bound}}{\partial T} \cdot \Delta T \right) \right)$$
(6.2)

With $F_i \left[\frac{\# \text{ emitted photons}}{second \cdot mol} \right]$ the fluorescence quantum efficiencies of bound and free binder states, $\partial F_i/\partial T$ the respective temperature dependence, $\Delta T = T - T_0$ the temperature change compared to the equilibrium (ambient) temperature T_0.

The concentrations of ligand L, free B^* and bound LB^* (bleached B, LB) binder depended on kinetics, diffusive/convective movement and bleaching, see Fig.6.1**a**. For any point $\vec{x}$ and the time dependent concentrations c_i and their partial time derivatives $\dot{c_i}$ of the species the following rate equations applied

$$\dot{L} = +k_{off} \cdot LB^* - k_{on} \cdot L \cdot B^* + \quad D\Delta L - \nabla \left(L \cdot (\vec{u} - D_T \nabla T) \right)$$

$$\dot{B^*} = +k_{off} \cdot LB^* - k_{on} \cdot L \cdot B^* + \quad D\Delta B^* - \nabla \left(B^* \cdot (\vec{u} - D_T \nabla T) \right) \quad -k_{Bleach,free} \cdot B^*$$

$$\dot{LB^*} = -k_{off} \cdot LB^* + k_{on} \cdot L \cdot B^* + \quad D\Delta LB^* - \nabla \left(LB^* \cdot (\vec{u} - D_T \nabla T) \right) \quad -k_{Bleach,bound} \cdot LB^*$$

$$\dot{B} = +k_{off} \cdot LB - k_{on} \cdot L \cdot B + \quad D\Delta B - \nabla \left(B \cdot (\vec{u} - D_T \nabla T) \right) \quad +k_{Bleach,free} \cdot B^*$$

$$\dot{LB} = -k_{off} \cdot LB + k_{on} \cdot L \cdot B + \quad D\Delta LB - \nabla \left(LB \cdot (\vec{u} - D_T \nabla T) \right) \quad +k_{Bleach,bound} \cdot LB^*$$
(6.3)

With $k_{Bleach,i}$ the bleaching rates of free and bound state, $D\Delta LB - \nabla \left(LB \cdot (\vec{u} - D_{T,i} \nabla T) \right)$ the diffusive, advective and thermophoretic contributions with the diffusion constant D, the thermal diffusion constant D_T and $\vec{u}$ the velocity field for the respective concentration c_i. D, D_T and $\vec{u}$ were assumed to be approximately equal for all species[282]. In the following, the motion term is abbreviated with $D(t)$ and approximated to be the same for B^* and LB^*.

The kinetic relaxation constant was extracted from the fluorescent traces in the post heating phase. The solution of the rate equation system was approximated to be of the form $B^*(t) = B^*_{tot} \cdot B_{kinetic}(t) \cdot B_{bleach}(t) \cdot B_{diffusion}(t)$ and similarly for LB^*. It is a product of the kinetic, bleaching and convective solution. B^* and LB^* were expressed by the total concentration of labeled binder $B^*_{tot} = B^* + LB^*$ and the fraction bound $LB^* = f_b \cdot B^*_{tot}$, see Eqn.5.3. The kinetic solution after a quick temperature jump is a second order exponential

relaxation and was expressed with the fraction bound in hot time and equilibrium

$$B_{kinetic}(t) = 1 - f_b = 1 - (f_{b,eq} - (f_{b,eq} - f_{b,hot}) \cdot \exp(-t/\tau_{kinetic})) \tag{6.4}$$

with the fraction bound in equilibrium $f_{b,eq}$, the fraction bound in the hot phase $f_{b,hot}$ and the kinetic relaxation constant $\tau_{kinetic}^{-1}$ from Eq.5.6. The bleaching term was extracted from the pre heating phase for free binder $B_{bleach}(t) = \exp(-t \cdot k_{Bleach,free})$ and the respective bleaching term for bound binder $LB_{bleach}(t) = \exp(-t \cdot k_{Bleach,bound})$. The diffusion term $B_{diffusion}(t)$ was obtained by the zero ligand trace, see below. With $\hat{F}_i = (F_i + \frac{\partial F_i}{\partial T} \cdot \Delta T) \cdot B_{tot}^*$ the fluorescence in the post heat phase read

$$F(t) = \int dV \cdot D(t) \cdot (\ \hat{F}_{Bound}(f_{b,eq} - (f_{b,eq} - f_{b,hot}) \cdot \exp(-t/\tau_{kinetic})) \cdot \exp(-t/\tau_{Bleach,bound})$$

$$+ \qquad\qquad \hat{F}_{Free}(1 - (f_{b,eq} - (f_{b,eq} - f_{b,hot}) \cdot \exp(-t/\tau_{kinetic}))) \cdot \exp(-t/\tau_{Bleach,free}) \ ).$$
$$\tag{6.5}$$

To access the time-dependent kinetic relaxation, the bleaching and diffusion contributions needed to be treated appropriately. The idea was to reduce the complexity of the equation system Eq.6.3 in order that the Eq.5.6 solved the reduced Eq.5.4. The measured data was normalized to its initial value $F_m = F(t)/F(t = 0)$, then, according to Eq.6.5, F_m was divided by the exponential bleaching and diffusion contributions. The remaining kinetic term was fitted to an exponential.

Therefore, the effective bleaching rate k_{bleach}, effective as an approximate for the underlying free and bound bleaching rates were obtained from equilibrium by fitting $F_{eq} \approx F_0 \cdot \exp(-t \cdot k_{Bleach})$ to the pre heat phase. Notably, the fit for this exponential bleaching did not have an offset, as it was assumed that the bleached fluorescence signal converged to 0 for $t \to \inf$.

To eliminate artifacts from the temperature jump, the first 2.1 seconds after the detection of the second temperature jump were cut out. The diffusion term $D(t)$ was obtained from the zero-ligand fluorescence trace in the post heat phase $F_{Ligand=0}(t) = \int dV \cdot D(t) \cdot \hat{F}_{Free} \cdot \exp(-t \cdot k_{Bleach,free})$. Yet, only $D(t) \cdot \hat{F}_{Free} \approx F_{Ligand=0}/\exp(-t \cdot k_{Bleach,free})$ could be determined which was sufficient for further analysis. Dividing $F(t)$ in the post heat phase by the effective bleaching contribution $\exp(-t \cdot k_{Bleach})$ and $D(t) \cdot \hat{F}_{Free}$ and yielded for the kinetic fluorescence term

$$F_{kinteic}(t) = \int dV \cdot \left(1 - f_{b,eq} + \frac{\hat{F}_{bound}}{\hat{F}_{Free}} \cdot f_{b,eq} + \frac{\hat{F}_{Free} - \hat{F}_{Bound}}{\hat{F}_{Free}} (f_{b,eq} - f_{b,hot}) \cdot \exp(-t/\tau_{kinetic}) \right)$$
$$\tag{6.6}$$

The right hand side of the equation has a single time-dependent term $\exp(-t/\tau_{kinetic})$, which is the kinetic relaxation term. From the right hand side of of Eq.6.6 first 1 was subtracted and an exponential function of the form $F_{kinetic}(t) = F_{kin,offset} + F_{kin,amplit} \cdot \exp(-t/\tau_{kinetic})$ was fitted to obtain $\tau_{kinetic}$, see Fig.6.4b. For all fitting routines, a Levenberg-Marquart algorithm was used in Labview. The subtraction of 1 yielded for better converging fits but is in general not necessary. $F_{kin,offset}$ was not further investigated as it carries no information of interest of the kinetic relaxation. The error of the fit

is obtained by multiplication of the the root mean squared error and the variance of the the fitted $\tau_{kinetic}$.

Error analysis With $\tau_{kinetic}$ at hand, the on-rate is fitted according to Eq.5.6 for all ligand concentrations L_{tot} which yielded for a valid (converging) $\tau_{kinetic}$ fit with known K_d and B_{tot}^*, see Fig.6.4**c**. For some ligand assays, only a few valid $\tau_{kinetic}$ contributed to the on-rate fitting. Therefore, the fitting-weights ω were used. For each data point in the on-rate fit, the fitting weights are the inverse quadratic relative errors $\omega = (\Delta\tau_{kinetic}^{-2}/\sum\tau_{kinetic}^{-2})^{-1}$, with the fitting errors $\Delta\tau_{kinetic}^{-1}$. If a fluorescence trace did not show kinetic behavior, the fitted relative error $\Delta\tau_{kinetic}^{-1}/\tau_{kinetic}^{-1}$ was comparably large (> 0.15). Those traces were excluded from the on-rate fit. The off-rate was calculated by $k_{off} = K_D \cdot k_{on}$ and the error of the off-rate is obtained by Gaussian error propagation from K_d and k_{on} fits.

6.3 Finite elements simulation

Finite element simulations of the experiment were conducted with COMSOL Multiphysics. The geometry was modeled according to the capillary lying on the silicon sample holder, see Fig.6.5**a** and the heating, laminar flow, bleaching and kinetic rates were simulated according to the rate equation Eq.6.3. In order to compare the simulated concentrations B, L, LB, B^* and LB^* the concentrations were converted into a fluorescence signal according to Eq.6.2. The simulation allowed a more detailed insight into the spacial- and time-dependent concentration distribution, see Fig.6.5**b**.

The kinetic input parameters were the experimentally-determined kinetic rates and fluorescence parameters for the 12mer in 0.1xPBS solution at 19 °C. The simulation input parameters are shown in Tab.6.1. The resulting fluorescence traces matched the measured experiment traces for 0 M and 2.5 µM and their analysis yielded for kinetic rates $k_{off,simulation} = 0.0016\,\mathrm{s}^{-1}$ and $k_{on,simulation} = 3.45 \times 10^4\,\mathrm{M}^{-1}\,\mathrm{s}^{-1}$ that are in very good agreement with the experimental data, see Fig.6.4 and Tab.9.1–9.3.

6.4 Influence of diffusion on fluorescence analysis

To test the accuracy of the analysis of the kinetic rates on the deconvolution of the diffusion contribution, the traces for 12mer at 19 °C with and without diffusion correction were compared, see Fig.6.6. This corresponds to the scenario that the ligand is diffusing but the labeled binder would not diffuse. When the correction for backdiffusion was dropped, the resulting rates changed by a factor less than two. With regard to the orders of magnitude, by which the measured kinetic rates differ within literature, the factor smaller two is comparably small. This finding indicates that the analysis method shows robust results regarding differences of diffusion properties of the binder and ligand.

Next, the 3D-Comsol simulations were used to test, how the fluorescence traces would look and the kinetic rates would be fitted, if one of the reactants exhibited strongly different
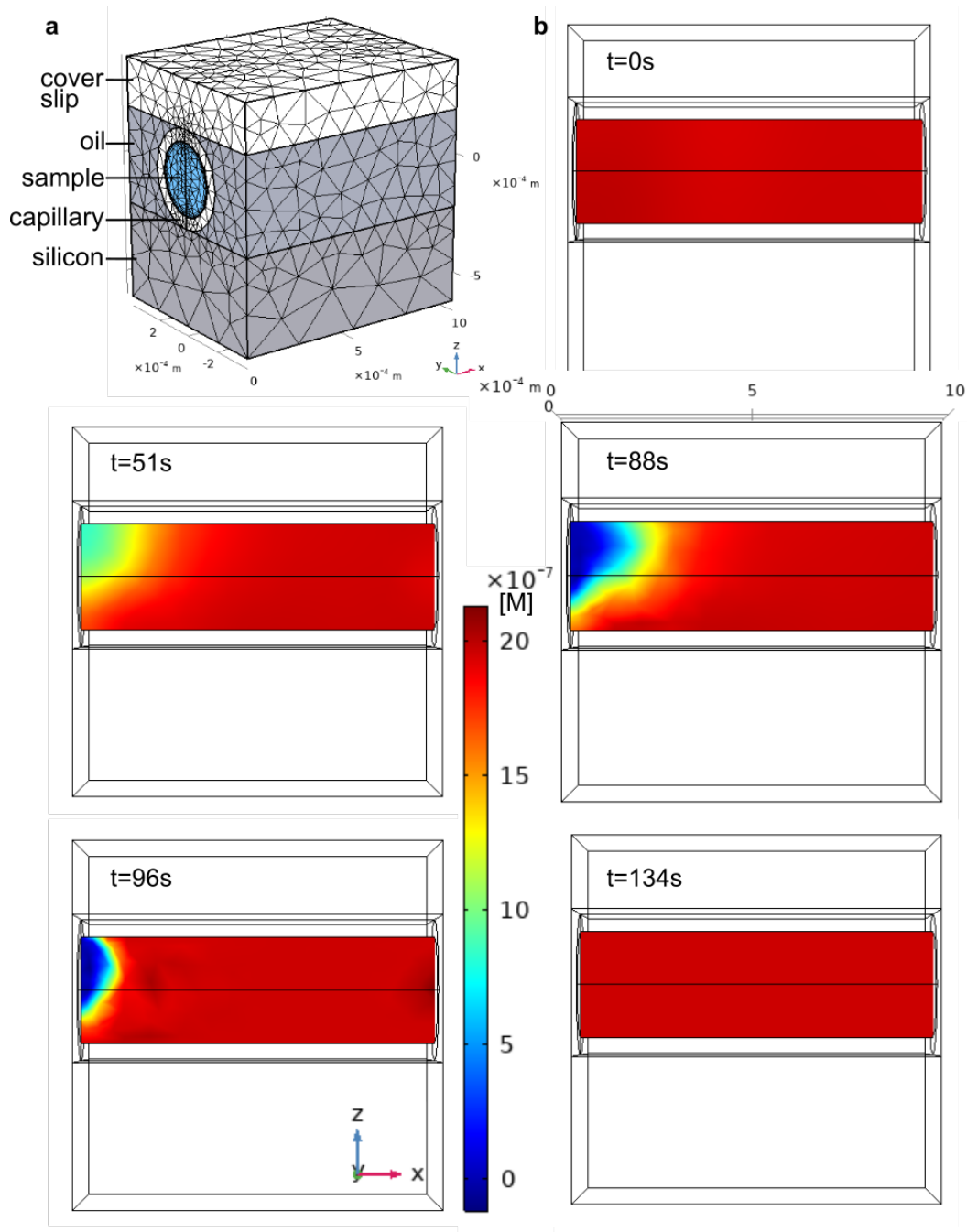
Figure 6.5: a Finite element simulation model and **b** bound concentration $LB + LB^*$ of the $z - x$ plane for selected times. The laser heated centrally at the left end, according to Fig.6.1**a**. For t=0 the system is in equilibrium (pre heat phase). Shortly (51 s) and long (88 s) after the laser heating was switched on, the concentration at the heated spot depleted. Immediately (96 s) after the laser was switched off (post heat phase), kinetic relaxation governed the rebinding. The first 200 µm along the x-axis were simulated to be homogeneously illuminated and used to detect the fluorescence signal. The corresponding fluoresence curve is 2.5 µM in Fig.6.4

Table 6.1: Finite element simulation input parameters

Fluorescence parameter	Value	Comment
F_{Free}	1	Set as reference
F_{Bound}	0.9	Estimated from initial F_{Free}
$\partial F_{Free}/\partial T$	$-0.026\,\mathrm{K}$	Measured with initial absolute fluorescence
$\partial F_{Bound}/\partial T$	$-0.026\,\mathrm{K}$	Similar to $\partial F_{Free}/\partial T$
$k_{Bleach,free}$	$0.0021\,\mathrm{s}^{-1}$	From binding curve fit
$k_{Bleach,bound}$	$0.0029\,\mathrm{s}^{-1}$	From binding curve fit
Kinetic parameter	**Value**	**Comment**
B_{tot}^{*}	$2\,\mathrm{nM}$	Total labeled binder
L_{tot}	$0\,\mathrm{\mu M}$, $2.5\,\mathrm{\mu M}$	Total ligand
D	$1.5 \times 10^{-10}\,\mathrm{m^2\,s^{-1}}$	Estimated from [283]
D_T	$1.8 \times 10^{-12}\,\mathrm{m^2\,s^{-1}\,K^{-1}}$	Estimated from [283]
$k_{off,offset}$	117.89	From k_{off} data
$k_{off,slope}$	$-3.631\,34 \times 10^4\,\mathrm{K}$	From k_{off} data
$k_{off}(T)$	$\exp\left(k_{off,offset} + k_{off,slope}/T\right)\mathrm{s}^{-1}$	Exponential off-rate dependence
k_{on}	$3.5 \times 10^4\,\mathrm{M^{-1}\,s^{-1}}$	From k_{on} data
Setup parameter	**Value**	**Comment**
l, ID, OD	$2\,\mathrm{mm}$, $300\,\mathrm{\mu m}$, $400\,\mathrm{\mu m}$	Capillary length, inner and outer diameter
$d_{silicon}$, $d_{coverslip}$	$400\,\mathrm{\mu m}$, $200\,\mathrm{\mu m}$	Thickness of silicon wafer and coverslip
w_0, NA, W, λ	$12\,\mathrm{\mu m}$, 0.12, $100\,\mathrm{W\,m^{-1}}$, $400\,\mathrm{\mu m}$	IR laser minimal beam waist, numeric aperture, power density, attenuation length
b_{LED}	$400\,\mathrm{\mu m}$	LED illumination length
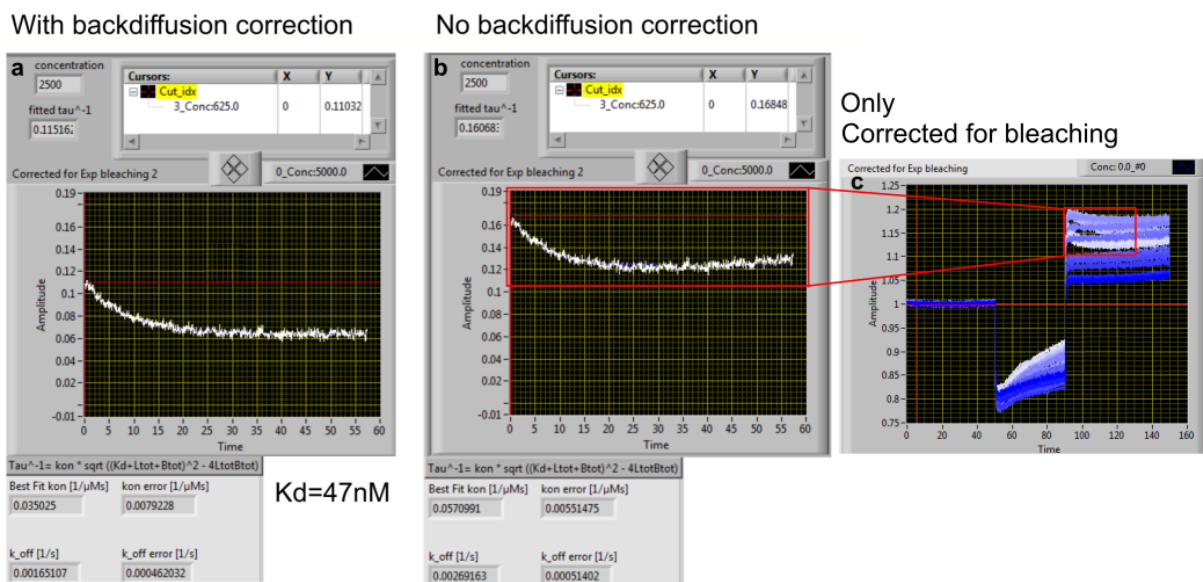
Figure 6.6: Backdiffusion contribution to kinetic analysis **a** Bleaching- and diffusion-corrected fluorescence trace of 12mer at 19 °C for 2.5 µM ligand and 2 nM binder with resulting on- and off-rate as described in Sec.6.4. **b** Analysis of the same trace without backdiffusion correction, that is the division by the averaged zero-ligand trace and resulting kinetic relaxation time constant and rates. **c** Fluorescence traces with only bleaching correction but no diffusion correction. Figure reproduced from[158].

diffusion coefficient, while the on-rate and off-rate did not change. Therefore, two cases were simulated: In the first, the ligand had tenfold increased diffusion coefficient $D_L = D_{LB^*} = 10 \times D_B^*$, i.e. because the non-labeled ligand was much larger than the labeled binder. In the second case, the labeled binder had tenfold increased $D_B^* = D_{LB^*} = 10 \times D_L$. In both cases, it is assumed that the diffusion coefficient was the same for bound ligand LB and the respective larger free L or B^*, which had the higher diffusion coefficient. The diffusion behavior of the larger reactant would not change, when bound to the much smaller reactant.

For the first case, the fluorescence trace for high ligand concentration $L_{tot} = 2.5$ µM (over 1000-fold excess of binder $B_{tot}^* = 2$ nM) looked significantly different for the hot phase (50-90 seconds), see purple traces Fig.6.7. The deviation of the simulated detected fluorescence at the beginning of the hot phase, compare Fig.6.8 **a** and **e**, could be explained by the concentrations of free L, free B^* and bound LB^*: During the heating time, the absolute fluorescence initially dropped due to the quick temperature change. Shortly after the temperature change, within about 10 seconds, bound complexes diffused quickly ($D_{LB^*} = 10 \times D_{B^*}$) from the cold non-illuminated region (where $c_{LB^*} > c_{B^*}$) back into the top center of the capillary (heated area, illuminated), see Fig.6.8 **b** and **f**, and the absolute fluorescence increased quickly again. In the hot center, the bound complexes unbound, see Fig.6.8 **c** and **g**, the fast diffusing unbound ligand molecules moved away from the top
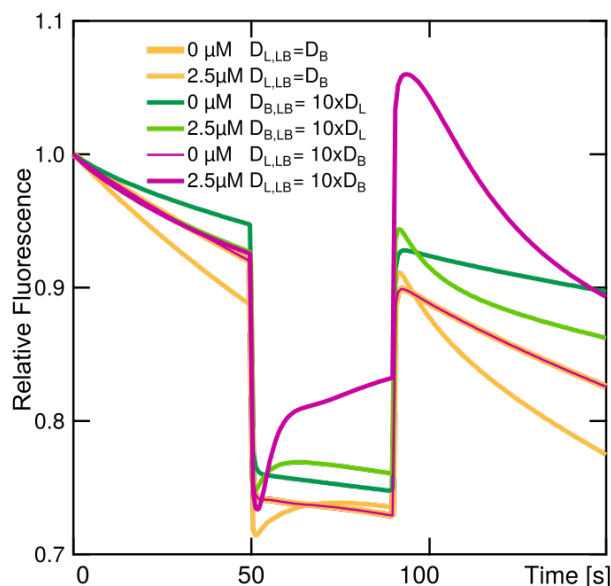
Figure 6.7: Simulated fluorescence traces for various diffusion behavior. Simluated fluorescence traces for similar diffusion behavior (yellow), larger fluorescent binder (green) and larger fluorescent ligand (purple) for 0 nM and 2.5 μM ligand concentration with the rates of 12mer at 19 °C. The traces of the larger fluorescent binder simulations are similar to the results of equal diffusion behavior, with similar kinetic rates. For the larger ligand simulations, the labeled binder accumulates in the top center of the capillary, see Fig.SIMCONC g and fluorescence restores quickly. The analyzed kinetic rates differ by a factor of 5 in comparison with the similar diffusion behavior simulations. Reproduced from[158].

center of the capillary, see Fig.6.8 **d** and **h**, whereas the slowly diffusing labeled binder molecules got stuck at the top center. This left an excess of unbound labeled binder molecules in the top center of the capillary, see Fig.6.8 **c**, and explained the increased absolute fluorescence (purple) in the hot phase.

When the laser was switched off, the initial absolute fluorescence level was higher due to accumulated free labeled binders in the top center capillary, see Fig.6.7 purple line at 90 seconds and Fig.6.8 **i** and **m**. The kinetic relaxation of rebinding free labeled binder, see Fig.6.8 **k**, and free ligand see Fig.6.8 **l**, yielded for slower kinetics. The analysis of the traces yielded for an on-rate $7 \times 10^3 \, \text{M}^{-1} \, \text{s}^{-1}$, which was about one fifth of the input rate $3.5 \times 10^4 \, \text{M}^{-1} \, \text{s}^{-1}$. The analysis of the off-rate yielded for $3.3 \times 10^{-4} \, \text{s}^{-1}$ which was also about one fifth smaller than the input rate. This deviation of the analyzed kinetics from the simulations with equal diffusion behavior can be explained by the reduced homogeneously distributed free binders. In the analysis, a similarly homogeneously distributed binder and ligand in the detected volume were assumed, see Sec.6.2.2. But due to non-homogeneous accumulation of labeled binder in the top center, the assumption of homogeneity was not as valid as in the similar diffusion behavior simulations, see Fig.6.8 **k** and **l**, which are less homogeneously distributed than Fig.6.8 **o** and **p**. In the second case, the fluorescent
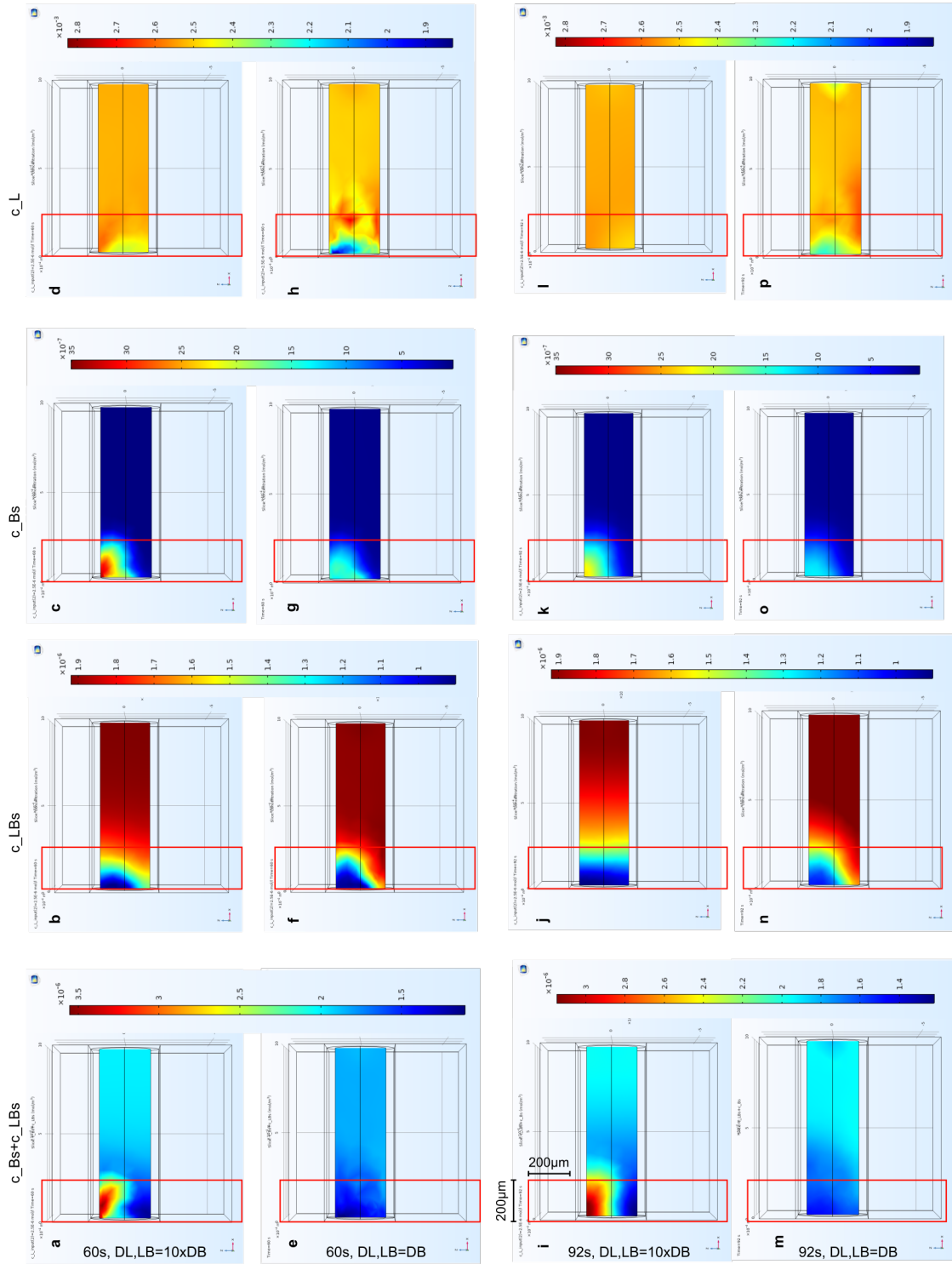
Figure 6.8: Simulated concentrations of free L, free B^* and bound LB^* **a-h** at 60 s during the hot phase and **i-p** at 92 s shortly after the rebinding start for L_{tot} =2.5 µM and B^*_{tot} =2 nM. **a-d** and **i-l** show the concentrations for tenfold increased ligand diffusion coefficient $D_{LB^*} = D_L = 10 \times D_{B^*}$. **e-h** and **m-p** show the concentrations for equal ligand and binder diffusion coefficient. The illuminated region (200 µm width) is shown by the red rectangle and shows the symmetrical half of the simulated capillary. The laser focus is on the left edge of each plot. Reproduced from[158].

binder had tenfold increased diffusion coefficient, e.g. a small compound that binds to a larger (labeled) protein. The simulated fluorescence trace showed less bleaching and similar behavior during the heating period and post-heating period, resulting with an on-rate of $5.6 \times 10^4\,\mathrm{M^{-1}\,s^{-1}}$ and off-rate of $2.7 \times 10^{-3}\,\mathrm{s^{-1}}$. The on-rate was a factor of 1.6 higher and the off-rate a factor of 1.6 smaller than the input parameters, which is very close to the input parameters. K_d stayed the same, as only the diffusion behavior was varied and not the binding behavior.

The analysis method is robust against different sizes of ligand and binder. Simulations of systems with significant size differences between ligand and binder yield for kinetic rates that differ by a factor less than five. Compared to the orders of magnitude, the kinetic rates differ in literature,[184,216,271,272] the variations within the KMST simulations are rather small. The effect is minimized, if the larger reactant is labeled.

6.5   DNA sequences & preparation

The DNA strands used for hybridization kinetics determination were purchased at biomers (Ulm, Germany). The fluorescent labeled binder was a 16mer with sequence Cy5-5'CCT CAT CCA TAG TTG C3'. The ligand strands are shown in Tab.6.2. The ligand strands bind the binder at the Cy-5-End to obtain a strong binding-dependent fluorescence signal. All used strands were factory HPLC purified before purchase. The stock concentration for all strands was $100\,\mathrm{\mu M}$ and all were dissolved in water (nuclease-free H_2O, Ambion). The fluorophore is located next to the binding nucleotides and the fluorescence becomes binding-dependent[269,272]. Importantly, the bleaching rates become binding dependent. Both strands are not self-complementary and no side reactions are expected. The DNA strands were dissolved in 0.75x, 0.5x, 0.25x and 0.1x PBS buffer (stock: 10xPBS invitrogen ThermoFisher, diluted in nuclease-free water H_2O, Ambion). To avoid sticking of material to the capillary walls, 0.05% (wt/vol) Tween 20 (NanoTemper) was added to all used buffers.

All dilution series were conducted as follows: first the labeled strand was diluted in $200\,\mathrm{\mu L}$ buffer to $2\,\mathrm{nM}$ and $10\,\mathrm{\mu L}$ were filled into vial 2-16 of the dilution series, each. The highest concentration of binder was diluted in the first vial of the dilution series with buffer and labeled binder. Then $10\,\mathrm{\mu L}$ were diluted 1:1 from vial 1 to 14. Vial 15 and 16 remained with zero ligand, only labeled binder. After the dilution series was completed, all vials incubated for $20\,\mathrm{min}$ to make sure equilibrium has established and then filled in the capillaries and were measured with the Silicon-Oil-immersed sample holder in the Nanotemper NT.115 Monolith.

The experiment ambient temperatures were chosen to be below the melting temperature T_m of the fully complementary strand to obtain a high change of fraction bound due to the temperature change. Fig.6.9 **a** shows the raw fluorescence units of the melting curve of 12mer in 0.1xPBS (orange), an empty vial (background, blue) and fluorescent binder and Eva green dye only (green). The concentration of binder and ligand were $10\,\mathrm{\mu M}$ each for the melting curve and $10\,\mathrm{\mu M}$ for the dye and binder only curve. To correct for the tem-

Sequence length	Sequence (5' to 3')
10	a tgg atg agg
12	cta tgg atg agg
12 far end	gca act atg gat
14	aa cta tgg atg agg
16	g caa cta tgg atg agg
16-labeled	Cy5 − cct cat cca tag ttg c

Table 6.2: Probed DNA sequences of 10-16mer, and complementary Cy5-labeled 16mer. Reproduced from [158]

Salt concentration (x PBS)	0.1				0.25	0.5	0.75
Strand length	10	12	14	16	12	12	12
Oligo Calc nearest neighbor [284]	-2.1	8.1	16.2	25.9	14.9	19.9	22.8
Oligo Calc salt adjusted [284]	20.3	26.3	28.3	38.4	33.3	38.2	41.2
NUPACK [285]	-	-	-	-	-	23.5	25

Table 6.3: Calculated melting temperature T_m (°C) for strand lengths and salt concentrations. Reproduced from [158]

perature dependence of the dye, the background was subtracted from the melting curve and the dye and binder-only curve, respectively, and then divided the melting curve by the dye and binder-only curve to obtain the fraction bound, see Fig.6.9 **b**. The melting curve was recorded with a Biorad Thermocycler C 1000 between 5 °C and 80 °C. From the curve, T_m=43 °C and it was concluded that the strands were bound in the pre heat and post heat phase and heating the sample with the infrared laser melted the hybridized DNA strands. When the laser was switched off, the DNA strands hybridized and kinetics were detected. Simulations of the 12mer (10 µM like melting curve) with NUPACK (0.05 M Na$^+$) yielded for $T_m = 38$ °C. Simulation of T_m for the used strands (2 nM binder) under the respective PBS buffer Na$^+$ conditions were rather inconclusive for low salt concentrations and short strands. The simulation of melting temperature with Oligo Calc [284] (salt adjusted and nearest neighbor mode) and NUPACK [285] are shown in Tab.6.3.
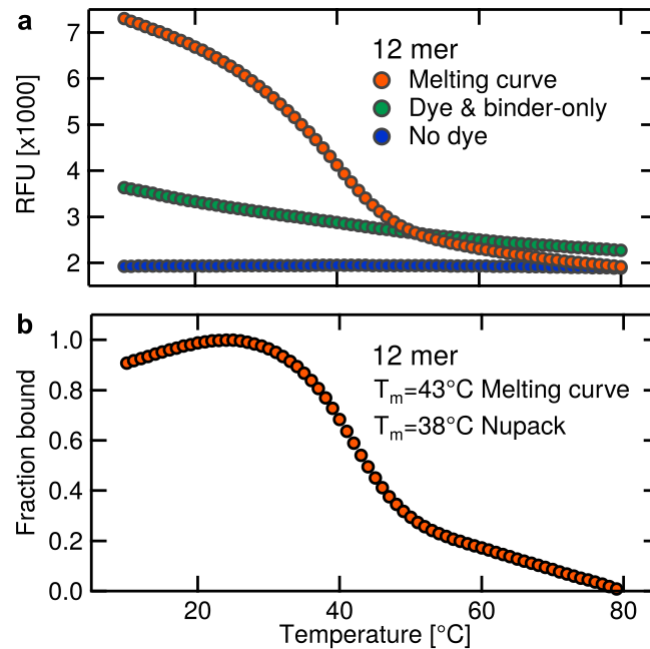
Figure 6.9: Melting curve and fraction bound **a** shows the raw fluorescence units of 1xEva Green intercalating dye obtained with a Biorad Thermocycler of the complementary 12mer in 0.1xPBS (orange), binder and dye only (green) and background (blue). The concentration of the strands were $10\,\mu$M for the melting curve, each, and $10\,\mu$M for the binder-only curve. **b** shows the fraction bound f_b, which was obtained by temperature correction of the dye. Therefore, the background was subtracted from the melting curve and the binder-only curve, respectively, and then the melting curve was divided by the binder-only curve. The fraction bound was normalized to one. T_m was $43\,°$C. Reproduced from [158].

Chapter 7

Results

7.1 DNA hybridization kinetics

The hybridization kinetics of complementary DNA strands with sequences between 10 and 16 base pairs were measured under 0.1, 0.25, 0.5 and 0.7xPBS buffer between $10\,°C$ and $28\,°C$. All measured rates are summarized in Fig.7.1, Fig.7.2 and Tab.9.1-9.3. The measured on-rates showed weak if no dependence on strand length and increased linearly with salt concentration $(1.9 \pm 0.2) \times \dfrac{10^6 \text{ M}^{-1} \cdot \text{s}^{-1}}{\text{x PBS}}$, see Fig.7.1**a** & **b**. The measured off-rates showed exponential dependence on strand length (characteristic length 0.81[bp]) and salt concentration (characteristic length 0.19[xPBS]) see Fig.7.1**c** & **d**. The resulting equilibrium constant K_d showed exponential dependence on strand length (characteristic length 0.72[bp]) due to its off-rate dependence and $K_d \propto \exp(-c_{PBS})/c_{PBS}$ dependence on salt-concentration, see Fig.7.1**e** & **f**.

7.2 DNA hybridization thermodynamics

The measurements of the binding affinity and the kinetic rates for various temperatures allowed for thermodynamic analysis. The Van't Hoff plot was obtained according to fitting the measured K_d values to Eq.5.10, see Fig.7.2 **e** & **f** and and Tab.9.4 under $K_d^0 = 1\,\text{M}$ standard conditions at 295 K. ΔG^0 and $T\Delta S^0$ were calculated. For increasing temperature, the bound state destabilizes and K_d increases. The negative slope and positive intercept of the Van't Hoff fits yield for $\Delta H^0 \approx -60\,\text{kcal}\,\text{mol}^{-1}$ and ΔS^0 between -170 and $-270\,\text{cal}\,\text{K}^{-1}\,\text{mol}^{-1}$.

To compare the obtained thermodynamic data from KMST experiments with the data obtained from the melting curve, K_d over $1/T$ was plotted in a single graph, see Fig.7.3. K_d over $1/T$ from the linear regime of the melting curve (between 3.05 and $3.3 \times 10^{-3}\,\text{K}^{-1}$) was obtained by applying the fraction of bound complex $f_{b,eq} = LB^*/B_{tot}^*$ and Eq.5.2 $K_d = L \cdot B^*/LB^*$. Fig.7.3 shows the K_d values and Van't Hoff fits for the KMST data and the K_d obtained from the melting curve. The thermodynamic values from the Van't
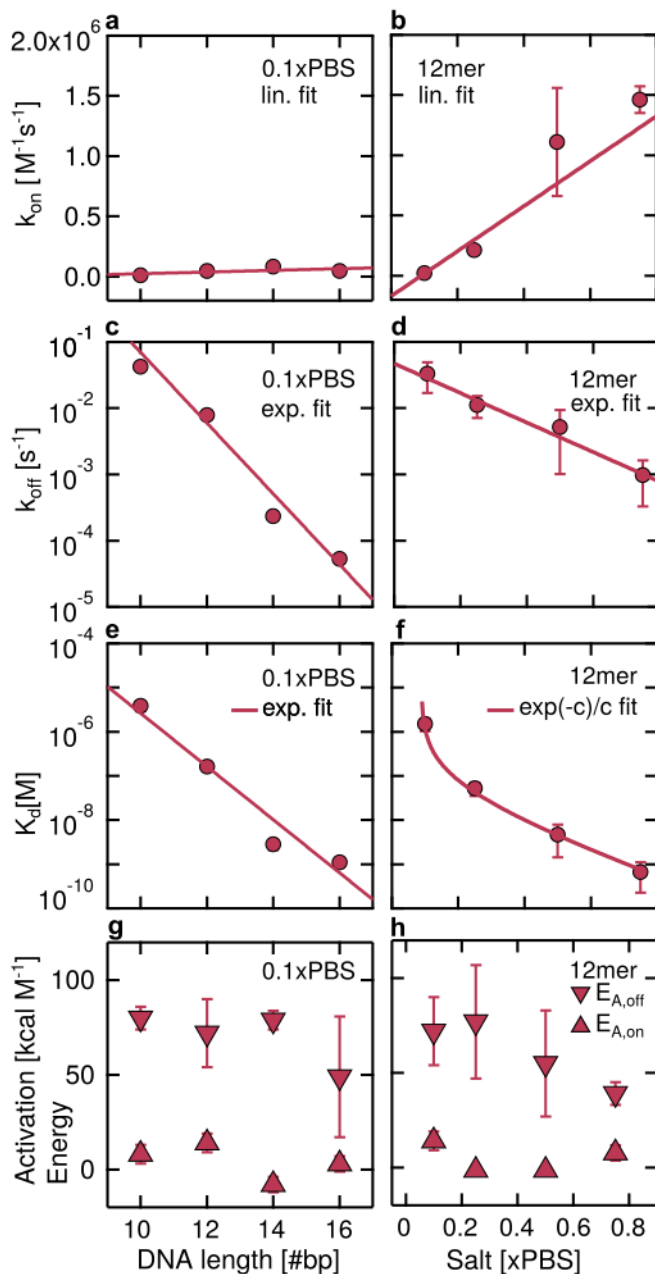
Figure 7.1: Strand length and salt dependence of k_{on}, k_{off} and K_d **a** The on-rate did not show strand length dependence and **b** it showed linear salt dependence for constant strand length. **c** The off-rate decreased exponentially with strand length and **d** salt concentration. **e** The resulting equilibrium constant $K_d = k_{off}/k_{on}$ decreased exponentially for increasing strand length and **f** according to $K_d \propto \exp(-c_{PBS})/c_{PBS}$ for increasing PBS concentration. Length dependence was measured at $22\,°C$ and salt dependence at $25\,°C$. Figure reproduced from [158].
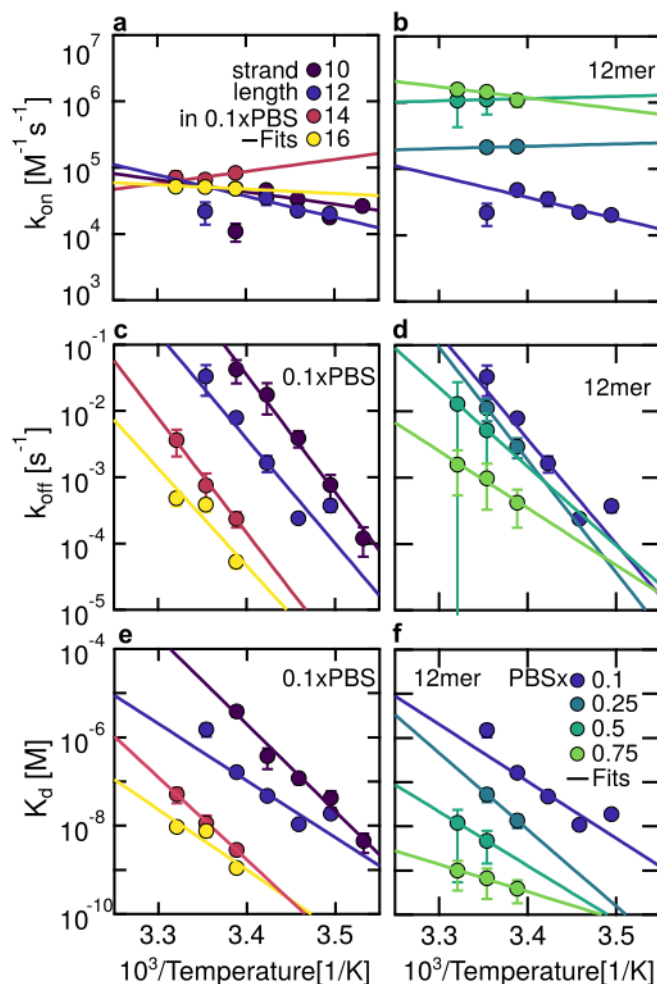
Figure 7.2: Temperature dependence of K_d, k_{off} and k_{on} of fully-complementary DNA strands **a-d** Eyring plots of transition state theory of on-rates and off-rates. **a & b** On-rates show no strong temperature or strand length dependence. **c & d** the corresponding off-rates decrease with $1/T$ **e & f** Van't Hoff plot for various lengths in 0.1xPBS and b salt conditions for 12mer. Kd decreases exponentially with $1/T$ and decrease for increasing high salt concentrations and strand length. Figure reproduced from[158].
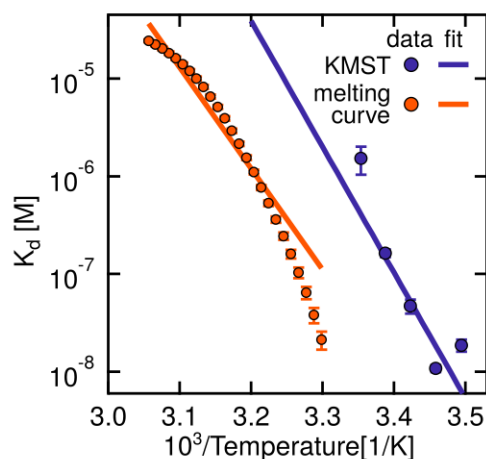
Figure 7.3: Comparison of Van't Hoff fits from melting curve and KMST experiments K_d and Van't Hoff fits of a complementary 12mer in 0.1xPBS which was obtained by melting curve with Eva Green dye (orange, from Fig.6.9**b**) and KMST measurements (purple, from Fig.7.2**e**). Both curves show similar slopes $\Delta H^0 = (-47 \pm 1)\,\mathrm{kcal\,mol^{-1}}$ (melting curve) and $\Delta H^0 = (-58 \pm 16)\,\mathrm{kcal\,mol^{-1}}$ (KMST) but dissimilar $\Delta S^0 = (-117 \pm 1)\,\mathrm{kcal\,K^{-1}\,mol^{-1}}$ (melting curve) and $\Delta S^0 = (-168 \pm 56)\,\mathrm{kcal\,K^{-1}\,mol^{-1}}$ (KMST). The shift of the measured K_d may stem from interferences of the intercalation dye with the probe. Furthermore, the applicability of melting curves to obtain K_d values well below T_m is limited. Figure reproduced from [158].

Hoff plot of the K_d from the melting curve yielded for $\Delta H^0 = (-47 \pm 1)\,\mathrm{kcal\,mol^{-1}}$ and $\Delta S^0 = (-117 \pm 1)\,\mathrm{kcal\,K^{-1}\,mol^{-1}}$. The temperature dependence was similar for both measurement methods: KMST $\Delta H^0 = (-58 \pm 16)\,\mathrm{kcal\,mol^{-1}}$ but the entropies deviated KMST $\Delta S^0 = (-168 \pm 56)\,\mathrm{kcal\,K^{-1}\,mol^{-1}}$.

The measured temperature dependence of the on-rates and off-rates was analyzed with an Arrhenius plot according to Eq.5.11. The activation energies $E_{A,on}$ and $E_{A,off}$ are shown in Fig.7.1 **g** & **h** and corresponding Arrhenius plots are shown in Fig.7.2**a**-**d**. All values are summarized in Tab.9.4–9.6. Note that E_A are approximately $\Delta H^{\ddagger}$ for the on-rate and off-rate, respectively, due to the applied analysis method. The on-rates showed no if slight increase with temperature, see Fig.7.2**a** & **b**, corresponding to small positive $E_{A,on} \approx 0\,\mathrm{kcal\,M^{-1}}$. $E_{A,on}$ did not show significant dependence on strand length or salt concentration, see in Fig.7.1**g** & **h**. The off-rates showed expected exponential dependence on inverse temperature,[216] see Fig.7.2**c** & **d**. The measured $E_{A,off}$ became smaller for increasing strand lengths and salt concentrations, see Fig.7.1**g** & **h**.

In order to compare the thermodynamic quantities' dependencies on salt concentrations and lengths, the enthalpy and entropy changes for the free, transition and bound state were plotted in Fig.7.4. All changes have been referenced to the bound state. Ideally, $\Delta G^{\ddagger}_{on}$ and $\Delta G^{\ddagger}_{off}$ could be plotted to characterize the DNA hybridization energy landscape as a spontaneous process. Unfortunately, the error of $\Delta G^{\ddagger}$ is too large for a concluding remark. The data suggests, that increasing salt concentration and increasing oligomer length favor
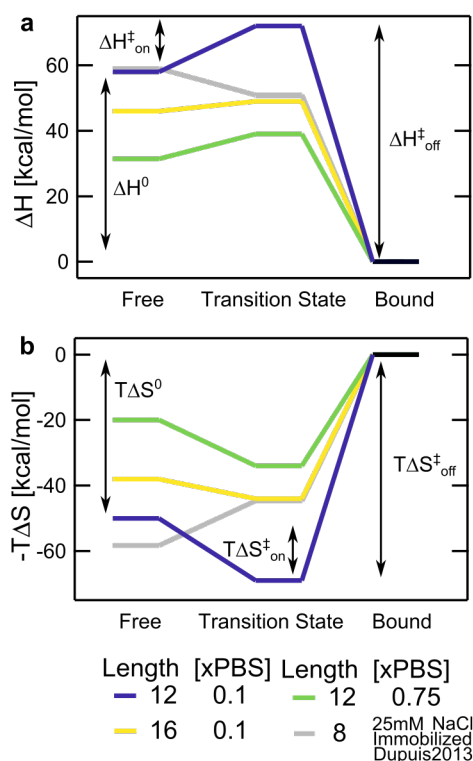
Figure 7.4: Thermodynamic quantities of DNA hybridization for various oligomer length and salt conditions. **a** the enthalpy and **b** the entropy for free, transition and bound state. Grey data from Dupuis et al.[207] Figure reproduced from[158].

the annealing reaction and reduce the enthalpy barrier and the entropy barrier from free to bound state.

7.3   DNA hybridization kinetics in crowded solutions

Lastly, the capability of KMST to measure kinetic rates in various fluids with minor loss of accuracy is shown. DNA hybridization takes place in more crowded fluids than pure buffer solutions, but the measurement in more complex solutions is typically experimentally more demanding. Polyethylene glycol PEG 8000 can be used to simulate the effect of molecular crowding.[278,279] The results shed light into the behavior of DNA hybridization rates in free solution at low ionic salt concentrations, see Fig.7.5 and Tab.9.8: Small concentrations of PEG < 5% (v/w) facilitated binding and yielded for stronger affinities due to decreased off-rates, possibly due to excluded volume effects. But increasing PEG concentrations from 5 to 10 (v/w) led to increasing off-rates, resulting in reduced affinities. The on-rates showed weak if no dependence on PEG concentration.
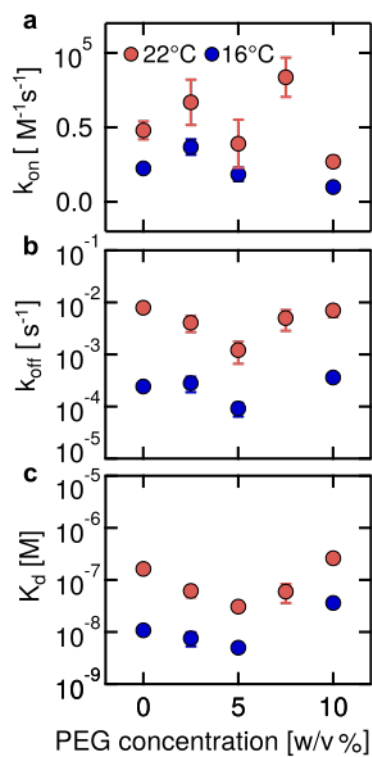
Figure 7.5: Hybridization rates k_{on}, k_{off} and K_d of fully-complementary 12mer DNA strands in crowded solutions with PEG 8000 **a** The on-rates do not show significant dependence on PEG concentrations **b** Off-rates show decreasing ($<5\%$ PEG) and increasing (5-10% PEG) behavior **c** The resulting K_d are dominated by the off-rate dependence on PEG. All measurements were conducted in 0.1xPBS with 0.05% Tween. Figure reproduced from [158].

Chapter 8

Discussion & Conclusion

8.1 Reaction kinetics in a KMST device

Kinetic Microscale Thermophoresis extends the applicability of Microscale Thermophoresis of probing ligand-binder interactions in equilibrium to the measurement of the associated binding kinetics. Thereby, KMST inherits all of the advantages of Microscale Thermophoresis: Rate determination is purely optical and in free solution (Sec.6.1.1) and is accomplished with an experimental setup that provides robust (Sec.6.4), reliable (Sec.6.3, low-cost and reproducible kinetic rate measurements.[194–199,269] Data analysis is robust against single capillary uncertainties as the rates are determined with multiple concentrations of the dilution series. Preparation of the dilution series – except sample pipetting –, that is filling and placement of the sample capillaries and immersing with oil does not require high-precision adjustments or handling. Sample consumption is low: less than 5 µL and only nM concentrations of labeled binder and up to µM concentrations of ligand. The costs per experiment are only several Euro per dilution series for consumables. Similar to MST applications,[269] KMST should be capable of high-throughput measurements by parallelization and automation of the sample handling, capillary filling, fluorescence measurement and fluorescence analysis.

The rather subtle experimental modification of increasing the thermal coupling of the heated sample to its environment by placing the sample capillaries on a silicon wafer and immersing with oil yield for about ten-fold faster heating and cooling times. The fast thermal relaxation allows for extraction of the kinetic fingerprint from the fluorescence signal immediately after the temperature jump. Appropriate treatment of convection/thermophoresis and bleaching contributions of the fluorescence signal is possible through equilibrium state and zero-ligand fluorescence trace analysis.

The fluorescence relaxation traces in all measurements confirmed that incubation of 20 min was sufficient to reach equilibrium at the beginning of each experiment. Four major limiting factors can be identified: First, the detection of small K_d <1 nM is difficult due to a weak fluorescence signal. For correct determination of the binding curve with Eq.5.3, the B^* must be smaller than K_d and B^* <1 nM is at the lower reliable detection limit of

the Nanotemper machine. Increasing the LED illumination does not solve the problem as then bleaching gets too strong and flaws repetitive measurements needed for binding curve determination.

Second, detection of fast relaxation processes with $\tau^{-1} > 1\,\mathrm{s}^{-1}$ is difficult for two reasons. First, the kinetic relaxation time scale is similar to the thermal relaxation time scale and the assumption of exponential kinetic relaxation becomes invalid – which assumes rapid thermal relaxation. Extension of the analysis to non-instantaneous thermal relaxation would be more complex and thus difficult. Second, the fluorescence signal change due to heating and kinetic relaxation becomes difficult to disentangle.

Third, the temperature jump relaxation method is dependent on ligand-binder systems with significant enthalpic contribution ΔH^0. During heating, the ligand-binder system must unbind, at least partially, to detect rebinding in the post-heat phase. Measurements of p38α MAP-Kinase with BIRB, SB203580, SB239063 and ATP did not show kinetic fingerprints in kinetic traces, possibly due to a small enthalpic contribution.

Fourth, the free and bound state need to show an absolute change of fluorescence in order to detect the transition from free to bound state in the post heat phase. In the analysis, $F_{kin,amplit} > 0.05$ allowed for reasonable fitting. The origin of the binding-dependent fluorescence intensity may play a minor role. It may stem from a change in conformation upon binding,[269] thus the fluorophore does not necessarily need to be in close proximity to the binding site, which reduces the label influence on binding characteristics.

Importantly, a KMST measurement only requires one of the reactants to be fluorescently-labeled (instead of both) which facilitates sample preparation and ultimately minimizes label-related interferences within the binding process. In all measurements, the fluorescent label was attached to the end of the strand at which the (shorter) complementary DNA strand bound to. I measured similar kinetic rates of a fully complementary strand with distantly attached label. A complementary 12mer strand hybridized starting at the 3' end of the Cy5-5'-16mer-3' strand, leaving a distance of 4 single strand bases between the Cy5 label (which is at the 5'end) and the hybridized strand. The measured K_d and kinetic rates of this hybridized strand with an increased distance of the label to the hybridized based pairs were similar to the results of the close label, see Tab.9.7. I conjecture that a confirmation change upon binding, that leads to different fluorescence levels of the bound and unbound state, is sufficient to detect kinetic rates.

The range of measurable on-rates and off-rates is comparable to label-free methods, like SPR.[185] With KMST, on-rate in the range of $10^2\,\mathrm{s}^{-1}\,\mathrm{M}^{-1}$ to $10^6\,\mathrm{s}^{-1}\,\mathrm{M}^{-1}$ and off rates in the range of of $10^{-5}\,\mathrm{s}^{-1}$ to $1\,\mathrm{s}^{-1}$ can be measured. In comparison with other kinetic measurement methods, the limitations of measurable on-rates and off-rates for KMST are the speed of the temperature jump and fluorescence detection for low labeled binder concentrations. FC(C)S measurements provide more suitable experimental approach for fast kinetics.[193] KMST does not face the limitation of SPR-measurements associated mass transportation and molecular mass.[221] With respect ot buffer conditions, KMST is applicable to a wide range of salt concentrations, which may be limited for surface-related kinetic measurement method's sensor responses.[184]

To validate the analysis of the kinetic rates from the fluorescence traces, 3D finite element simulations of the experiments with input parameters from the experimental results were performed. The simulated rate equations governed the convection/thermophoresis of the reacting species, bleaching and kinetics. The resulting simulated fluorescence curves were analyzed with the same procedure as the experimental results. The simulation results yielded for on-rates and off-rates very similar to the experimental rates. The author suggests that the coherency of experimental results with 3D rate equation simulations is a strong indicator for validity of kinetic rate determination with KMST devices.

To validate the measurement technique, the measured thermodynamic values were compared with values obtained from a melting curve experiment. The deviation of the K_d values from the melting curve and KMST could be explained as follows: First, the Eva Green intercalating dye may be interfering with the Cy5-label of the binder in a way that the melting curve signal and thus did not properly report the fraction of bound complexes. Second, the quantification of K_d by the melting curve is most suitable for temperatures around $T_m = 43\,°\mathrm{C}$. The extraction of K_d data from the melting curve well below T_m is difficult because the intercalation fluorescence signal does not change significantly at $T \ll T_m$, as almost all strands are hybridized. As all KMST measurements were carried out at $T \ll T_m$, direct comparison is difficult. Third, to obtain a good signal from melting curves, the concentration of both strands needed to be in the µM range. This range was 1000-fold higher than for the KMST measurements ($2\,\mathrm{nM}$). The high concentration of strands may also shift the melting temperature signal to higher temperatures.

I also performed experiments with a Dynamic Light Scattering instrument (DynaPro NanoStar, Wyatt) to measure K_d and kinetic rates but could not detect the probes (0.1xPBS, 12mer of $10\,\mathrm{µM}$ sample concentration). Due to the small size and low concentration, the correlation function of the labeled binder could not be distinguished from the buffer-only correlation function. This illustrates the advantage of KMST to determine kinetic rates of probes at low nM concentrations, which are not accessible by other kinetic methods.

8.2 DNA hybridization kinetics

The comparison of the absolute values of the measured rates with literature is difficult due to the many different measurement methods and sequences used. For high salt concentrations (1xPBS), Surface Plasmon Fluorescence measurements report $10^4\,\mathrm{M^{-1}\,s^{-1}}$[286] which is an order of magnitude smaller than my measurement. FRET measurements for 9mers reported on-rates in the low $10^6\,\mathrm{M^{-1}\,s^{-1}}$ range[207] (with 50mM HEPES), similar to my findings. Measurements with TOOL[278] reported on-rates in the order of 10^6–$10^7\,\mathrm{M^{-1}\,s^{-1}}$ for 12mer and 16mer complementary DNA strands, which is an order of magnitude larger than my findings. For low salt concentrations (< 0.1xPBS) FRET measurements found on-rates of 10mers to be about $10^4\,\mathrm{M^{-1}\,s^{-1}}$[272] in free solution buffer, also found in works with Quartz Crystal Microbalance[271] of immobilized 10mers, similar to my results. Multi-channel graphene bionsensors[184] report $10^5\,\mathrm{M^{-1}\,s^{-1}}$ for immobilized target strands, which

is an order of magnitude higher than my findings. The results suggests on-rates for low salt concentrations to be in the range of 10^4–$10^5\,\mathrm{M^{-1}\,s^{-1}}$ linearly increasing with salt concentration up to $10^6\,\mathrm{M^{-1}\,s^{-1}}$ for 0.75xPBS, see Fig.7.1, similarly reported earlier.[287]

The observed on-rates showed no dependence on strand length, see Fig.7.1 **a**, similarly reported earlier.[216] But literature also reported contrarily dependence.[271,272,278]. Bielec et al[272] argue that the higher total charge of the longer strands pose a higher energetic barrier for hybridization, especially for low ionic salt environments. My findings are limited to a strand length difference of 6 by a total length of 16, which may be too short to observe strand-dependent on-rates. The comparison of our rates with the results presented by Okahata et al[271] is limited due to the immobilization of their used probes.

Literature reported both smaller and larger off-rates for low and high ionic salt conditions than my results suggest, respectively. For low salt concentrations (< 0.1xPBS), FRET measurements[272] reported off-rates two orders of magnitude smaller. Morrison and Stols[216] found higher off-rates at much higher salt concentrations of 10xPBS in temperature jump experiments. Tawa et al[286] measured smaller off-rates for longer strands in higher salt concentrations. The measured off-rates of this work show an exponential decrease with salt concentration, see Fig.7.1 **d**, also reported by Okahata et al[271] and qualitatively supporting findings of Braunlin et al.[287] The exponential decrease of the off-rates with strand length, see Fig.7.1 **c**, was in agreement with literature.[216,271,273]

8.3   DNA hybridization thermodynamics

The measured VantHoff plot provide support of $\Delta H^0 \approx -60\,\mathrm{kcal\,mol^{-1}}$ and ΔS^0 between -170 and $-270\,\mathrm{cal\,K^{-1}\,mol^{-1}}$ are in agreement with reported surface-tethered FRET measurements[207] and slightly above previously reported values of 8mers measurements with NMR.[287] At room temperature, both contributions cancel out and yield for rather small negative ΔG^0, supporting the view that DNA hybridization is a spontaneous process:[206,207] the formation of hydrogen bonds and base stacking lead to the exothermic release of heat and the decrease in entropy results from reduced conformational flexibility in the bound state.[214,288]. The findings contribute to the understanding that increased cationic strength increases ΔH^0 and ΔS^0, both becoming less negative. Although ΔH^0 increases with cationic strength, $T\Delta S^0$ increases stronger, resulting in a net more negative ΔG^0 thus favoring the bound. However, the meaningfulness of allows only for limited conclusions, due to large errors. For increasing strand length, ΔH^0 and ΔS^0 increase, resulting in a decrease of favoring the hybridized state, also reported earlier.[207].

The findings of $E_{A,on} \approx 0\,\mathrm{kcal\,mol^{-1}}$ contribute insofar, as the determined $E_{A,on}$ slightly above and below zero can not be used to exclude one of the proposed hypotheses of increasing, decreasing or other non-monotonic on-rate dependence on temperature.[216,271,273] The decreasing $E_{A,off}$ decreasing with length and salt concentration is in line with the view that the electrostatic repulsion between the anionic chains of the DNA strands decreases for high ionic salt concentrations and in result stabilize the hybridized bonds.[271]. Similar behavior was also found for DNA hairpins.[246]

The thermodynamic analysis of the measured data with the Eyring-Polanyi equation allowed for a connection of kinetic quantities with thermodynamic quantities,[206,207], but in general involves conceptual difficulties.[209]. The enthalpy and entropy landscapes of free state, transition state and bound state are in line with the view increasing salt concentration favors the hybridized state. The conclusion that may be drawn from the rather speculative enthalpy and entropy landscapes is that the reduction of the enthalpic and entropic barrier may contribute to the favoring of the bound state.

8.4   DNA hybridization in crowded solutions

The results of DNA hybridization in crowded solutions with PEG 8000 highlight that at low ionic salt concentrations, crowding agents affect the DNA hybridization rates not only by excluding volume effects but also by destabilization of the hybridized complex. The increased off-rate for higher PEG concentrations may be explained by a destabilizing effect of the surrounding PEG molecules on the hybridized DNA. This result extends earlier studies with FRET measurements which found that kinetic relaxation time constants of DNA hybridization are weakly if not dependent on crowding agent concentrations for higher ionic salt concentrations for 1xPBS[278] and 1xPBS with 1mM Mg^{2+}.[289]

The results further underpin the versatile applicability of KMST to measure kinetic rates in crowded solutions. The applicability to measure kinetic rates in crowded solutions is important, as many biological processes take place in crowded solutions and the kinetics and thermodynamics are significantly shaped by the molecular environment.[275,280]

Conclusion

The combination of Microscale Thermophoresis with the temperature jump technique provides a novel method to determine kinetic rates together with binding affinities in a single experiment. By a straightforward hardware modification of a conventional MST setup increasing the thermal dissipation by placement of the sample-containing capillary on a silicon plate and immersion with oil kinetic relaxation could be extracted from the fluorescence traces. I systematically studied the dependency on salt concentration, strand length and temperature of on- and off-rates of DNA hybridization and also in crowded solutions. An exponential dependence of the off-rate on strand length, salt and temperature was found. The on-rate showed no if weak dependence on temperature and strand length and a linear dependence on salt concentration. The results shed light into the hybridization mechanism of DNA and summarized the determinants of DNA binding. The measurement method is compatible with a range of biological fluids, including crowded solutions, it needs very low sample quantities and it is a very easy-to-use and robust setup. While requiring the probed binding reaction to have a sufficient enthalpic contribution, no artifact-inducing processes, like molecule attachment to surface, are necessary. Because Microscale Thermophoresis is widely used, Kinetic Microscale Thermophoresis could be of

great interest for a broad audience including the numerous labs who have a MST device, and could open new possibilities for research in biophysical and medical sciences.

Chapter 9

Appendix

9.1 Kinetic & thermodynamic measurement values

Salt conc. (x PBS)		0.1				0.25	0.5	0.75
$\frac{1000}{T[K^{-1}]}$	T [°C]	10mer	12	14	16	12	12	12
3.53	10	4.5 ± 0.2						
3.49	13	43 ± 17	19 ± 3					
3.46	16	120 ± 32	11 ± 1					
3.42	19	380 ± 19	47 ± 8					
3.39	22	3900 ± 100	160 ± 15	2.8 ± 0.7	1.1 ± 0.2	14 ± 4		0.4 ± 0.2
3.35	25		1500 ± 490	11 ± 6	7 ± 2	53 ± 18	5 ± 3	0.7 ± 0.4
3.32	28			51 ± 19	9 ± 2		12 ± 11	1.0 ± 0.7

Table 9.1: Measured K_d in [nM] for various salt concentrations, DNA strand lengths and temperatures. Table reproduced from[158].

Salt conc. (x PBS)		0.1				0.25	0.5	0.75
$\frac{1000}{T[K^{-1}]}$	T [°C]	10mer	12	14	16	12	12	12
3.53	10	0.12 ± 0.06						
3.49	13	0.7 ± 0.3	0.37 ± 0.07					
3.46	16	4 ± 3	0.24 ± 0.03					
3.42	19	17 ± 8	1.7 ± 0.5					
3.39	22	42 ± 16	8 ± 1	0.23 ± 0.06	0.05 ± 0.01	2.9 ± 0.9		0.4 ± 0.2
3.35	25		33 ± 16	0.7 ± 0.4	0.39 ± 0.09	11 ± 4	5 ± 4	1.0 ± 0.7
3.32	28			4 ± 2	0.5 ± 0.1		13 ± 15	1.6 ± 0.9

Table 9.2: Measured k_{off} in $[10^{-3}\,\mathrm{s}^{-1}]$ for various salt concentrations, DNA strand lengths and temperatures. Table reproduced from [158].

Salt conc. (x PBS)		0.1				0.25	0.5	0.75
$\frac{1000}{T[K^{-1}]}$	T [°C]	10mer	12	14	16	12	12	12
3.53	10	26 ± 1						
3.49	13	18 ± 2	20 ± 3					
3.46	16	33 ± 1	22 ± 2					
3.42	19	46 ± 3	35 ± 8					
3.39	22	11 ± 3	48 ± 6	84 ± 3	48 ± 3	220 ± 11		1100 ± 300
3.35	25		22 ± 8	66 ± 9	51 ± 2	210 ± 30	1100 ± 500	1500 ± 100
3.32	28			70 ± 20	52 ± 7		1100 ± 700	1600 ± 200

Table 9.3: Measured k_{on} $[10^3\,\mathrm{M}^{-1}\,\mathrm{s}^{-1}]$ for various salt concentrations, DNA strand lengths and temperatures. Table reproduced from [158].

Salt conc. (x PBS)	0.1				0.25	0.5	0.75
	10mer	12	14	16	12	12	12
ΔG^0 [kcal mol^{-1}]	-6 ± 11	-8 ± 23	-11 ± 3	-11 ± 36	-10 ± 26	-12 ± 47	-12 ± 3
ΔH^0 [kcal mol^{-1}]	-86 ± 8	-58 ± 16	-85 ± 2	-49 ± 25	-80 ± 27	-55 ± 37	-27 ± 2
ΔS^0 [cal K^{-1} mol^{-1}]	-267 ± 30	-170 ± 60	-249 ± 6	-127 ± 85	-232 ± 81	-146 ± 99	-49 ± 6
$T\Delta S^0$ [kcal mol^{-1}]	-80	-50	-74	-38	-69	-44	-15

Table 9.4: The Van't Hoff parameters were obtained by fiting K_d (from Tab.9.1) to Eq.5.10. $T\Delta S^0$ was calculated. All values refer to standard $T_0 =298.15\,\mathrm{K}$. Table reproduced from [158].

Salt conc. (x PBS)	0.1				0.25	0.5	0.75
	10mer	12	14	16	12	12	12
$\Delta G^{\ddagger}_{on}$ [kcal mol^{-1}]	-6 ± 7	-6 ± 7	-6 ± 6	-5 ± 6	-6 ± 24	-7 ± 3	-7 ± 5
$\Delta H^{\ddagger}_{on}$ [kcal mol^{-1}]	8 ± 5	14 ± 5	-8 ± 4	3 ± 4	-1.5 ± 0.6	-1.5 ± 0.8^a	7 ± 4
$\Delta S^{\ddagger}_{on}$ [cal K^{-1} mol^{-1}]	47 ± 18	67 ± 17	-8 ± 14	28 ± 14	16 ± 81	19 ± 10^a	50 ± 14
$T\Delta S^{\ddagger}_{on}$ [kcal mol^{-1}]	14	20	-2	8	5	6	15

Table 9.5: Thermodynamic parameters for hybridization according to Eyring analysis (Eq.5.12) of the on-rates of Fig.7.2**a** & **b**. $\Delta G^{\ddagger}_{on}$ was calculated and its error was estimated by Gaussian error propagation. ^{a} estimated error of 50% due to lack of data. $T\Delta S$ is calculated for 298 K. Table reproduced from [158].

Salt conc. (x PBS)	0.1				0.25	0.5	0.75
	10mer	12	14	16	12	12	12
$\Delta G^{\ddagger}_{off}$ [kcal mol^{-1}]	1 ± 9	3 ± 26	5 ± 8	5 ± 45	3 ± 42	5 ± 38	5 ± 8
$\Delta H^{\ddagger}_{off}$ [kcal mol^{-1}]	80 ± 6	72 ± 18	79 ± 5	49 ± 32	77 ± 30	55 ± 28^a	39 ± 6
$\Delta S^{\ddagger}_{off}$ [cal K^{-1} mol^{-1}]	265 ± 20	231 ± 63	249 ± 19	148 ± 110	248 ± 100	169 ± 84^a	115 ± 19
$T\Delta S^{\ddagger}_{off}$ [kcal mol^{-1}]	79	69	74	44	74	50	34

Table 9.6: Thermodynamic parameters for DNA dissociation according to Eyring analysis (Eq.5.12) of the on-rates of Fig.7.2**c** & **d**. $\Delta G^{\ddagger}_{on}$ was calculated and its error was estimated by Gaussian error propagation. ^{a} estimated error of 50% due to lack of data. $T\Delta S$ is calculated for 298 K. Table reproduced from [158].

$\frac{1000}{T[K^{-1}]}$	T [°C]	K_d [nM]	k_{off} [s^{-1}]	k_{on} [M^{-1} s^{-1}]
3.46	16	12 ± 5	0.0003 ± 0.0002	$29\,000 \pm 9000$
3.39	22	176 ± 20	0.006 ± 0.001	$32\,000 \pm 5300$
3.35	25	1100 ± 300	0.03 ± 0.01	$35\,000 \pm 3000$

Table 9.7: Measured K_d, k_{off} and k_{on} of a 12mer which is distantly attached to the 16mer-labeled binder strand. The Cy5 fluorophore has a distance of 4 bp to the beginning hybridizing strand. Measurement was conducted under 0.1xPBS. Table reproduced from [158].

PEG (% v/w)	T [°C]	K_d [nM]	k_{off} [s^{-1}]	k_{on} [M^{-1} s^{-1}]
0	16	11 ± 1	0.00024 ± 0.00005	$22\,000 \pm 2000$
	22	163 ± 15	0.008 ± 0.001	$47\,933 \pm 6200$
2.5	16	8 ± 3	0.0003 ± 0.0001	$37\,000 \pm 6000$
	22	61 ± 15	0.004 ± 0.001	$66\,762 \pm 15\,400$
5	16	4.9 ± 0.8	0.00009 ± 0.00003	$18\,000 \pm 5000$
	22	31 ± 5	0.0012 ± 0.0005	$39\,000 \pm 16\,000$
7.5	16	-	-	-
	22	59 ± 23	0.005 ± 0.002	$84\,000 \pm 14\,000$
10	16	36 ± 4	0.00036 ± 0.00004	9900 ± 900
	22	263 ± 60	0.007 ± 0.002	$27\,000 \pm 4000$

Table 9.8: Measured K_d, k_{off} and k_{on} of a complementary 12mer in 0.1xPBS for increasing PEG 8000 concentrations. Table reproduced from [158].

Bibliography

[1] J. A. C. Stein and D. Braun. Stability of a time-homogeneous system of money and antimoney in an agent-based random economy. *Physica A*, 520(https://doi.org/10.1016/j.physa.2019.01.022): 232–249, 2019.

[2] J. A. C. Stein. *Agent-based Simulations in Random Economies In the Framework of a time-homogeneous System of Money and Antimoney.* Master's thesis, LMU München, 2016.

[3] D. Graeber. *Debt, the first 5000 years.* Melville House, 2010.

[4] J. Macdonald. *A Free Nation Deep in Debt: The Financial Roots of Democracy.* Princeton University Press, 2006.

[5] E. Samhaber. *Das Geld.* Keyser'sche Verlagsbuchhandlung München, 1964.

[6] N. Irwin. *The Alchemists: Three Central Bankers and a World on Fire.* Penguin Books, 2014.

[7] S. Quinn and W. Roberds. An Economic Explanation of the Early Bank of Amsterdam, Debasement, Bills of Exchange, and the Emergence of the First Central Bank. *Federal Reserve Bank of Atlanta working paper*, (September), 2006.

[8] Bank Charter Act. *Bank of England, http://www.legislation.gov.uk/ukpga/Vict/7-8/32/enacted (2021 - 01 -27)*, 1844.

[9] K. Galbraith. *The Great Crash 1929.* Mariner Books, 1955.

[10] J. M. Keynes. *The General Theory of Employment, Interest and Money.* Palgrave Macmillan, 1936.

[11] M. Friedman and A. Schwartz. *A Monetary History of the United States, 1867-1960.* University Press Group Ltd, 1971.

[12] D. Long and J. Bradford. "Liquidation" Cycles: Old Fashioned Real Business Cycle Theory and the Great Depression. *National Bureau of Economic Research Working Paper*, 3546, 1990.

[13] A. Kirman. The economic crisis is a crisis for economic theory. *CESifo Economic Studies*, 56(4): 498–535, 2010.

[14] C. Reinhart and K. Rogoff. A Decade of Debt. *National Bureau of Economic Research Working Paper*, 16827, 2011.

[15] M. Schularick and A. Taylor. Credit Booms Gone Bust: Monetary Policy, Leverage Cycles and Financial Crises. *American Economic Review Association*, 102(2):1029–61, 2012.

[16] J. B. Taylor and J. C. Williams. A black swan in the money market. *American Economic Journal: Macroeconomics*, 1(1):58–83, 2009.

[17] P. Temin. The Great Recession and the Great Depression. *National Bureau of Economic Research Working Paper*, 15645, 2010.

[18] S. Nakamoto. Bitcoin : A Peer-to-Peer Electronic Cash System. *www.bitcoin.org*, 2009.

[19] P. Tasca. Digital Currencies: Principles, Trends, Opportunities, and Risks. *ECUREX Research Working Paper*, September, 2015.

[20] J. Abraham, D. Higdon, J. Nelson, and J. Ibarra. Cryptocurrency Price Prediction Using Tweet Volumes and Sentiment Analysis Volumes and Sentiment Analysis. *SMU Data Science Review*, 1 (3), 2018.

[21] M. Friedman and A. Meltzer. Money. *Ecyclopedia Britannica Online (2019 - 10 - 29)*, 2019.

[22] M. Manning, E. Nier, and J. Schanz. *The Economics of Large-value Payments and Settlement: Theory and Policy Issues for Central Banks*. Oxford University Press, 2009.

[23] B. M. Mcleay, A. Radia, R. Thomas, and M. Analysis. Money in the modern economy: an introduction. (1):4–13, 2014.

[24] G. K. Ingham. The Nature of Money. *Cambridge: Polity Press*, 111(4):1227–1229, 2004.

[25] N. R. Kocherlakota. Money Is Memory. *Journal of Economic Theory*, 81(2):232–251, 1998.

[26] N. Kiyotaki and J. Moore. Evil Is the Root of All Money. *The American Economic Review*, 92(2), 2002.

[27] M. McLeay, A. Radia, and R. Thomas. Money creation in the modern economy. *Bank of England Quarterly Bulletin*, (Q1):1–14, 2014.

[28] M. King. Trusting in Money : From Kirkcaldy to the MPC. *Bank of England Speech*, (October): 1–15, 2006.

[29] C. Giannini. *The Age of Central Banks*. Edward Elgar Publishing, 2011.

[30] M. Rollins. *Money and Investments*. George Routledge & Sons, Ltd, 1917.

[31] C. E. Walsh. *Monetary Theory and Policy, Third Edition*. The MIT Press Cambridge Massachusetts, 2010.

[32] P. Mehrling. The Inherent Hierarchy of Money. In *Duncan Foley Festschrift Volume, and Conference April 20-21*, 2012.

[33] S. von der Becke and D. Sornette. Should Banks Be Banned From Creating Money? An Analysis From the Perspective of Hierarchical Money. *Journal of Economic Issues*, 51(4):1019–1032, 2017.

[34] M2 Monetary Aggregate. *European Central Bank, https://sdw.ecb.europa.eu/*, 2020.

[35] FRED Money Stock. *Federal Reserve Bank of St. Louis, https://fred.stlouisfed.org/series/M1NS#0 (2020-08-13)*, 2020.

[36] Monetary aggregates. *European Central Bank, https://www.ecb.europa.eu/stats/ money_credit_banking/monetary_aggregates/html/index.en.html*, 2019.

[37] Moneyterms. Repurchase Agreements. *https://moneyterms.co.uk/money-market-funds (2019-04-17)*, 2020.

[38] J. Zijlstra. Inflation and its impact on society. *De Economist*, 123(4):495–506, 1975.

[39] M. Schmitt, A. Schacker, and D. Braun. Statistical mechanics of a time-homogeneous system of money and antimoney. *New Journal of Physics*, 16(033024), 2014.

[40] R. A. Werner. Can banks individually create money out of nothing? - The theories and the empirical evidence. *International Review of Financial Analysis*, 36(C):1–19, 2014.

[41] R. Button, S. Pezzini, and N. Rossiter. Understanding the price of new lending to households. *Bank of England Quarterly Bulletin*, 50(3):172–182, 2010.

[42] N. Kaldor and J. Trevithick. A Keynesian perspective on money. *Lloyd's Bank review*, pages 1–19, 1981.

[43] D. Laidler. The Buffer Stock Notion in Monetary Economics. *The Economic Journal*, 94:17–34, 1984.

[44] S. Heffernan. *Modern Banking in Theory and Practice*. Chichester: John Wiley and Sons, 1996.

[45] L. Macfarlane, J. Ryan-Collins, O. Bjerg, and D. McCann. *Making Money from Making Money: Seigniorage in the Modern Economy*. The New Economics Foundation, 2017.

[46] A. Sahr. *Das Versprechen des Geldes: Eine Praxistheorie des Kredits*. Hamburger Edition HIS, 2017.

[47] R. Cantillon. Essai sur la Nature du Commerce en Général. *Auburn, L. von Mises Institute*, 2010.

[48] C. E. V. Borio and P. Disyatat. Global Imbalances and the Financial Crisis: Link or No Link? *Asian Economic Policy Review*, 5(2):198–216, 2010.

[49] C. Borio and P. Lowe. Asset prices, financial and monetary stability: exploring the nexus. *Bank for International Settlemen Working Paper*, 114, 2002.

[50] Z. Jakab and M. Kumhof. Banks are not intermediaries of loanable funds and why this matters. *Bank of England working papers*, 529, 2015.

[51] D. López-Salido, J. C. Stein, and E. Zakrajsek. Credit-Market Sentiment and the Business Cycle. *National Bureau of Economic Research Working Paper*, 21879, 2016.

[52] A. Mian. Household Leverage and the Recession of 2007 to 2009. *IMF Economic Review*, 58(1): 74–117, 2010.

[53] S. Claessens and M. A. Kose. Frontiers of macrofinancial linkages. *Bank for International Settlement Working Paper*, 95, 2018.

[54] A. Haldane. Why banks failed the stress test. In *Marcus-Evans Conference on Stress-Testing*, London, 2009. Bank of England.

[55] M. Baron and W. Xiong. Credit Expansion and Neglected Crash Risk. *Quarterly Journal of Economics*, 132(2):713–764, 2017.

[56] L. Bebchuk, A. Cohen, and H. Spamann. The Wages of Failure: Executive Compensation at Bear Stearns and Lehman 2000-2008. *Yale Journal on Regulation*, 257, 2010.

[57] J. C. Stein. Rational Capital Budgeting in an Irrational World. *The Journal of Business*, 69(4): 429–455, 1996.

[58] J. Bullard. Testing Long- Run Monetary Lessons from Propositions: Neutrality the Recent Research. *Federal Reserve Bank of St.Louis*, pages 57–78, 1999.

[59] R. M. Billi and G. A. Kahn. What Is the Optimal Inflation Rate? *Federal Reserve Bank of Kansas City*, 2008.

[60] S. Fischer. Why Are Central Banks Pursuing Long-Run Price Stability ? *Fed. Reserve Bank Kansas City Proc*, pages 7–34, 1996.

[61] J. Benhabib and M. M. Spiegel. Moderate inflation and the deflation-depression link. *Journal of Money, Credit and Banking*, 41(4):787–798, 2009.

[62] R. J. Barro. Inflation and economic growth. *Annals of Economics and Finance*, 14(1):85–109, 2013.

[63] M. Bruno, Easterly, and William. Inflation Crises and Long-Run Growth. *Policy Research Working Papers*, 1517:56, nov 1999.

[64] P. Ormerod, B. Rosewell, and P. Phelps. Inflation/unemployment regimes and the instability of the Phillips curve. *Applied Economics*, 45(12):1519–1531, apr 2013.

[65] G. A. Akerlof, W. T. Dickens, and G. L. Perry. The Macroeconomics of Low Inflation. *Brookings Papers on Economic Activity*, (1):1–48, 1996.

[66] F. A. Akinsola and N. M. Odhiambo. Inflation and Economic Growth: A Review of the International Literature. *Comparative Economic Research*, 20(3):41–56, 2017.

[67] O. Issing. *Einführung in die Geldtheorie*. Verlag Franz Vahlen München, 2011.

[68] D. Braun. Assets and liabilities are the momentum of particles and antiparticles displayed in Feynman-graphs. *Physica A, Elsevier*, 290:491–500, 2001.

[69] R. Fischer and D. Braun. Nontrivial bookkeeping: a mechanical perspective. *Physica A, Elsevier*, 324:266–271, 2003.

[70] W. Kniffin. *The practical work of a bank*. Wassen Publication Press, Cambrige Mass. USA, 9th edition, 1948.

[71] E. Noether. Invariante Variationsprobleme. *Nachrichten. d. K. Gesellsch. d. Wissenschaften zu Göttingen, Mathematisch-physikalische Klasse*, 235, 1918.

[72] R. Fischer and D. Braun. Transfer potentials shape and equilibrate monetary systems. *Physica A: Statistical Mechanics and its Applications*, 321(3-4):605–618, 2003.

[73] D. Braun. Nonequilibrium thermodynamics of wealth condensation. *Physica A: Statistical Mechanics and its Applications*, 369(2):714–722, 2006.

[74] I. Fisher. 100% Money and the Public Debt. *Economic Forum*, Spring Num:406–420, 1936.

[75] M. Kumhof and J. Benes. The Chicago Plan Revisited. *IMF Working Papers*, 12(202), 2012.

[76] R. Hall and M. Lieberman. *Macroeconomics: Principles and Applications*. South-Western College Pub, 6 edition, 2012.

[77] M. Friedman and M. D. Bordo. *The Optimum Quantity Of Money*. Transaction Publishers, 2005.

[78] G. Rule. Centre for Central Banking Studies: Understanding the central bank balance sheet. *Bank of England*, 2015.

[79] W. Xiong, H. Fu, and Y. Wang. Money creation and circulation in a credit economy. *Physica A: Statistical Mechanics and its Applications*, 465:425–437, 2017.

[80] M. Woodford. *Interest and Prices: Foundations of a Theory of Monetary Policy*. Princeton University Press, 2011.

[81] L. Gambetti and A. Musso. The macroeconomic impact of the ECB's expanded asset purchase programme (APP). *ECB Working Paper Series*, 2075(20):1–43, 2017.

[82] J. P. Bouchaud and M. Mézard. Wealth condensation in a simple model of economy. *Physica A: Statistical Mechanics and its Applications*, 282(3):536–545, 2000.

[83] V. Yakovenko and B. Rosser. Statistical mechanics of money, wealth, and income. *Reviews of Modern Physics*, 81:1703–1721, 2009.

[84] X. Xing, W. Xiong, L. Chen, J. Chen, Y. Wang, and H. E. Stanley. Money circulation and debt circulation: A restatement of quantity theory of money. Economics Discussion Papers 2018-1, Kiel, 2018.

[85] V. M. Yakovenko and A. Dragulescu. Statistical mechanics of money. *The European Physical Journal B*, 17:723–729, 2000.

[86] S. Chen, Y. Wang, K. Li, and J. Wu. Money creation process in a random redistribution model. *Physica A: Statistical Mechanics and its Applications*, 394:217–225, 2014.

[87] M. Adolfson, S. Laséen, J. Lindé, and M. Villani. Bayesian estimation of an open economy DSGE model with incomplete pass-through. *Journal of International Economics*, 72(2):481–511, 2007.

[88] S. An and F. Schorfheide. Bayesian analysis of DSGE models. *Econometric Reviews*, 26(2-4): 113–172, 2007.

[89] L. Christiano, M. Eichenbaum, and C. Evans. Nominal Rigidities and the Dynamic Effects of a Shock to Monetary Policy. *Journal of Political Economy*, 113(1):1–45, 2005.

[90] F. Smets and R. Wouters. An Estimated Stochastic Dynamic General Equilibrium Model Of The Euro Area. *Journal of the European economic association*, 1(171):1123–1175, 2003.

[91] J. F. Muth. Rational Expectations and the Theory of Price Movements. *Econometrica*, 29(3): 315–335, 1961.

[92] D. Colander, P. Howitt, A. Kirman, A. Leijonhufvud, and P. Mehrling. Beyond DSGE Models: Toward an Empirically Based Macroeconomics. *The American Economic Review*, 98(2):236–240, 2008.

[93] P. Krugman. How Did Economists Get It So Wrong? *New York Times Magazine*, 2009.

[94] P. Krugman. The Profession and the Crisis. *Eastern Economic Journal*, 37:307–312, 2011.

[95] J. E. Stiglitz. Rethinking macroeconomics: What failed, and to how repair it. *Journal of the European Economic Association*, 9(4):591–645, 2011.

[96] J. E. Stiglitz and M. Gallegati. Heterogeneous Interacting Agent Models for Understanding Monetary Economies. *Eastern Economic Journal*, 37(1):6–12, 2011.

[97] M. Lengnick. Agent-based macroeconomics: A baseline model. *Journal of Economic Behavior and Organization*, 86:102–120, 2013.

[98] G. Fagiolo and A. Roventini. Macroeconomic Policy in DSGE and Agent-Based Models. *Revue de l'OFCE*, 124(5):67, 2012.

[99] G. Akerlof. Behavioral Macroeconomics and Macroeconomic Behavior. *American Economic Review*, 92(3):411–433, 2002.

[100] P. De Grauwe. DSGE-Modelling: when agents are imperfectly informed. *ECB Working Paper*, (897), 2008.

[101] P. De Grauwe. The scientific foundation of dynamic stochastic general equilibrium (DSGE) models. *Public Choice*, 144(3):413–443, sep 2010.

[102] D. Massaro. Heterogeneous expectations in monetary DSGE models. *Journal of Economic Dynamics and Control*, 37(3):680–692, 2013.

[103] A. Kirman. Whom or What Does the Representative Individual Represent? *Journal of Economic Perspectives1*, 6(2):117–136, 1992.

[104] M. Gallegatti, S. Keen, T. Lux, and P. Ormerod. Worrying Trends in Econophysics. *EconoPhysics Forum*, 370:1–6, 2006.

[105] D. Colander. *Post Walrasian Macroeconomics: Beyond the Dynamic Stochastic General Equilibrium Model*. Cambridge University Press, 2006.

[106] J.-P. Fitoussi and F. Saraceno. Inequality and macroeconomic performance. *Documents de Travail de l'OFCE*, 13:0–18, 2010.

[107] J. Zietz. A clarifying note on converting to log-deviations from the steady state. *Economics Bulletin*, 3(50):1–15, 2008.

[108] A. Caiani and J. E. Stiglitz. Agent based-stock flow consistent macroeconomics: Towards a benchmark model. *Journal of Economic Dynamics & Control*, 69:375–408, 2016.

[109] J. Fernández-Villaverde and J. Rubio-Ramírez. Estimating dynamic equilibrium economies: linear versus nonlinear likelihood. *Journal of Applied Economics*, 20(7):891–910, 2004.

[110] W. B. Arthur. Out-of-Equilibrium Economics and Agent-Based Modeling. In *Handbook of Computational Economics,*, volume 2, pages 1551–1564. Elsevier, 2006.

[111] F. Ackerman. Still dead after all these years. *The Journal of Economic Methodology*, 9(2):119–139, 2002.

[112] A. Kirman. *Demand Theory and General Equilibrium: From Explanation to Introspection, a Journey down the Wrong Road*, volume 38. 2006.

[113] E. Gaffeo, D. Delli Gatti, S. Desiderio, and M. Gallegati. Adaptive Microfoundations for Emergent Macroeconomics. *Eastern Economic Journal*, 34(4):441–463, 2008.

[114] E. Gaffeo, M. Catalano, F. Clementi, D. Delli Gatti, M. Gallegati, and A. Russo. Reflections on modern macroeconomics: Can we travel along a safer road? *Physica A: Statistical Mechanics and its Applications*, 382(1):89–97, 2007.

[115] F. Canova and L. Sala. Back to square one: Identification issues in DSGE models. *Journal of Monetary Economics*, 56(4):431–449, 2009.

[116] F. Canova. How much Structure in Empirical Models? In *Palgrave Handbook of Economics, Vol. 2*. Palgrave Macmillan, 2008.

[117] G. Fagiolo, M. Napoletano, and A. Roventini. Are output growth-rate distributions fat-tailed? Some evidence from OECD coutries. *Journal of Applied Econometrics*, pages 639–669, 2008.

[118] C. Favero. Model Evaluation in Macroeconometrics: From early empirical macroeconomic models to DSGE models. *IGIER Working Paper Series*, (September), 2007.

[119] L. Christiano, M. Trabandt, and K. Walentin. Introducing financial frictions and unemployment into a small open economy model. *Journal of Economic Dynamics and Control*, 35(12):1999–2041, 2011.

[120] D. Delli Gatti, E. Gaffeo, and M. Gallegati. Complex agent-based macroeconomics: a research agenda for a new paradigm. *Journal of Economic Interaction and Coordination*, 5(2):111–135, 2010.

[121] C. A. E. Goodhart. The continuing muddles of monetary theory: A steadfast refusal to face facts. *Economica*, 76:821–830, 2009.

[122] H. E. Stanley. Anomalous fluctuations in the dynamics of complex systems: from DNA and physiology to econophysics. *Physica A: Statistical Mechanics and its Applications*, 224(1-2):302–321, 1996.

[123] R. N. Mantegna and H. E. Stanley. *An Introduction to Econophysics: Correlations and Complexity in Finance*, volume 53. Cambridge University Press, 2000.

[124] D. Rickles. Econophysics and the Complexity of Financial Markets. In *Handbook of the Philosophy of Science*, pages 1–32. Elsevier, 2008.

[125] V. Grimm. Pattern-Oriented Modeling of Agent-Based Complex Systems: Lessons from Ecology. *Science*, 310(5750):987–991, 2005.

[126] F. Black and M. Scholes. Pricing Options Black Scholes.pdf. *The Journal of Political Economy*, 81 (3):637–654, 1973.

[127] S. Galam. Sociophysics: A review of Galam models. *Int. J. Mod. Phys. C*, 19(3), 2008.

[128] E. Bonabeau. Agent-based modeling: methods and techniques for simulating human systems. *Proceedings of the National Academy of Sciences*, 99(suppl. 3):7280–7287, 2002.

[129] B. LeBaron and L. Tesfatsion. Modeling Macroeconomies as Open-Ended Dynamic Systems of Interacting Agent. *American Economic Review*, 98(2):246–250, 2008.

[130] R. Guesnerie. *L'economie de marché*. Editions le Pommier, 1996.

[131] M. Callon. Introduction: The Embeddedness of Economic Markets in Economics. *the Sociological Review*, 46(1):1–57, 1998.

[132] P. Bak, M. Paczuski, and M. Shubik. Price variations in a stock market with many agents. *Physica A*, 246:430–453, 1997.

[133] J. P. Bouchaud, J. D. Farmer, and F. Lillo. How Markets Slowly Digest Changes in Supply and Demand. *Handbook of Financial Markets: Dynamics and Evolution*, pages 57–160, 2009.

[134] R. Cont, S. Stoikov, and R. Talreja. A Stochastic Model for Order Book Dynamics. *Operations Research*, 58(3):549–563, 2008.

[135] S. S. Dhananjay K. Gode. Allocative Efficiency of Markets with Zero-Intelligence Traders: Market as a Partial Substitute for Individual Rationality. *Journal of Political Economy*, 101(1):119–137, 1993.

[136] D. Cliff. Minimal-intelligence agents for bargaining behaviors in market-based environments. *Technical Report HPL-97-91*, (September 1996):1–128, 1997.

[137] D. Cliff and J. Bruten. Shop 'Til You Drop I : Market Trading Interactions as Adaptive Behavior. *Hewlett Packard Laboratories*, 1998.

[138] D. Cliff and J. Bruten. Shop 'Til You Drop II: Collective Adaptive Behavior of Simple Autonomous Trading Agents in Simulated 'Retail' Markets. *Hewlett Packard Laboratories*, 1998.

[139] R. Das, J. E. Hanson, J. O. Kephart, and G. Tesauro. Agent-Human Interactions in the Continuous Double Auction. *The Proceedings of the International Joint Conferences on Artificial Intelligence IJCAI*, 2001.

[140] C. Schinckus. Econophysics and economics: Sister disciplines? *American Journal of Physics*, 78 (4):325–327, 2010.

[141] M. Blaug. *The Methodology of Economics: Or How Economists Explain.* Cambridge University Press, 1992.

[142] D. Keita. *Science, Rationality and Neoclassical Economics.* Associated University Press, 1992.

[143] C. Schinckus. Economic uncertainty and econophysics. *Physica A: Statistical Mechanics and its Applications*, 388(20):4415–4423, 2009.

[144] W. B. Arthur. Reasoning, Inductive Rationality, Bounded. *The American Economic Review*, 84(2): 406–411, 1994.

[145] D. Bourghelle, O. Brandouy, R. Gillet, and A. Orléan. Croyances, Représentations Collectives et Conventions en Finance. *Collection Recherche on Gestion*, pages 1–15, 2005.

[146] H. Föllmer. Random economies with many interacting agents. *Jounal of Mathematic Economics*, 1:51–62, 1974.

[147] J. Schewe, C. Otto, and K. Frieler. The role of storage dynamics in annual wheat prices. *Environmental Research Letters*, 12(5):054005, 2017.

[148] M. D. Gould. Limit order books. *Quantitative Finance*, 13(11):1709–1742, 2013.

[149] N. Xi, N. Ding, and Y. Wang. How required reserve ratio affects distribution and velocity of money. *Physica A: Statistical Mechanics and its Applications*, 357(3-4):543–555, 2005.

[150] V. M. Yakovenko. Monetary economics from econophysics perspective. *European Physical Journal: Special Topics*, 225(17-18):3313–3335, 2016.

[151] R. M. Navarro and H. Larralde. A detailed heterogeneous agent model for a single asset financial market with trading via an order book. *PLoS ONE*, 12(2):1–27, 2017.

[152] R. A. Rodríguez and J. J. Cáceres-Hernández. Information, entropy, value, and price formation: An econophysical perspective. *Physica A: Statistical Mechanics and its Applications*, 512:74–85, 2018.

[153] B. LeBaron. Agent-based Computational Finance. In *Handbook of Computational Economics*, volume 2, pages 1187–1233. Elsevier B.V., 2006.

[154] V. Smith, G. Suchanek, and A. Williams. Bubbles, Crashes, and Endogenous Expectations in Experimental Spot Asset Markets. *Econometrica*, 56(5):1119–1151, 1988.

[155] J. B. Taylor. Getting Back on Track : Macroeconomic Policy Lessons from the Financial Crisis. *Federal Reserve Bank of St Louis Review*, 92(3):165–176, 2010.

[156] F. S. Mishkin. Monetary Policy Strategy: Lessons from the Crisis. *National Bureau of Economic Research Working Paper*, 16755, 2011.

[157] D. Farmer and D. Foley. The economy needs agent-based modelling. *Nature*, 460(7256):685–686, 2009.

[158] J. A. C. Stein, A. Ianeselli, and D. Braun. Kinetic Microscale Thermophoresis for SimultaneousMeasurement of Binding Affinity and Kinetics. *Angewandte Chemie Internationale Edition*, (https://doi.org/10.1002/anie.202101261), 2021.

[159] A. D. McNaught and A. Wilkinson. Chemical Reaction. *IUPAC. Compendium of Chemical Terminology 2nd ed. (The 'Gold Book')*, 2015.

[160] K. A. Connors. *Chemical kinetics: the study of reaction rates in solution.* Wiley-VCH, 1990.

[161] R. W. Mahley and T. L. Innerarity. Lipoprotein Receptors and Cholesterol Homeostasis. *Biochimica et Biophysica Acta*, 737:197–222, 1983.

[162] C. Fasting, C. A. Schalley, M. Weber, O. Seitz, S. Hecht, B. Koksch, J. Dernedde, C. Graf, E.-W. Knapp, and R. Haag. Multivalency as a Chemical Organization and Action Principle. *Angewandte Chemie International Edition*, 51:10472–10498, 2012.

[163] M. Furuhashi and G. S. Hotamisligil. Fatty acid-binding proteins: role in metabolic diseases and potential as drug targets. *Nature reviews. Drug discovery*, 7(6):489, 2008.

[164] S. Firth and R. C. Baxter. Cellular Actions of the Insulin-Like Growth Factor. *Endocrine Reviews*, 23(6):824–854, 2002.

[165] A. Rev, C. Dev, B. Downloaded, A. B. Jaffe, and A. Hall. Rho GTPases : Biochemistry and Biology. *Annu. Rev. Cell Dev. Biol.*, 21:247–272, 2005.

[166] H. Escriva, R. Safi, C. Hänni, M. C. Langlois, P. Saumitou-Laprade, D. Stehelin, A. Capron, R. Pierce, and V. Laudet. Ligand binding was acquired during evolution of nuclear receptors. *Proceedings of the National Academy of Sciences of the United States of America*, 94(13):6803–6808, 1997.

[167] P. G. Knight and C. Glister. TGF-β superfamily members and ovarian follicle development. *Reproduction*, 132(2):191–206, 2006.

[168] J. Taubenberger and D. M. Morens. the Pathology of Influenza Virus Infections. *Annual Review of Pathology-mechanisms of Disease*, 3:67–97, 2008.

[169] T. H. Mogensen. Pathogen recognition and inflammatory signaling in innate immune defenses. *Clinical Microbiology Reviews*, 22(2):240–273, 2009.

[170] N. E. Hynes and H. A. Lane. ERBB receptors and cancer: The complexity of targeted inhibitors. *Nature Reviews Cancer*, 5(5):341–354, 2005.

[171] S. Elmore. Apoptosis: A Review of Programmed Cell Death. *Toxicologic Pathology*, 35(4):495–516, 2007.

[172] A. Christopoulos. Allosteric binding sites on cell-surface receptors: Novel targets for drug discovery. *Nature Reviews Drug Discovery*, 1(3):198–210, 2002.

[173] H. Lu and P. J. Tonge. Drugtarget residence time: critical information for lead optimization. *Current Opinion in Chemical Biology*, 14(4):467–474, 2010.

[174] J. H. Van't Hoft. *Studies in Chemical Dynamics*. F Muller & Co Amsterdam, 1896.

[175] A. N. Gorban and G. S. Yablonsky. Three Waves of Chemical Dynamics. *Mathematical Modelling of Natural Phenomena*, 10(5):1–5, 2015.

[176] R. MacArron, M. N. Banks, D. Bojanic, D. J. Burns, D. A. Cirovic, T. Garyantes, D. V. Green, R. P. Hertzberg, W. P. Janzen, J. W. Paslay, U. Schopfer, and G. S. Sittampalam. Impact of high-throughput screening in biomedical research. *Nature Reviews Drug Discovery*, 10(3):188–195, 2011.

[177] K. H. Bleicher, H. J. Böhm, K. Müller, and A. I. Alanine. Hit and lead generation: Beyond high-throughput screening. *Nature Reviews Drug Discovery*, 2(5):369–378, 2003.

[178] D. Cronk. High-throughput screening. In *Drug Discovery and Development: Technology in Transition*, pages 95–117. Elsevier Ltd, second edi edition, 2013.

[179] Protein Data Bank PDB. *www.rcsb.org (2020-07-21)*, 2020.

[180] The Binding Database. *https://www.bindingdb.org/bind/index.jsp (2020-07-21)*, 2020.

[181] T. A. Morton, D. G. Myszka, and I. M. Chaiken. Interpreting complex binding kinetics from optical biosensors: A comparison of analysis by linearization, the integrated rate equation, and numerical integration, 1995.

[182] M. M. Morelock, C. A. Pargellis, E. T. Graham, D. Lamarre, and G. Jung. Time-Resolved Ligand Exchange Reactions: Kinetic Models for Competitive Inhibitors for Recombinant Human Renine. *J. Med. Chem.*, pages 1751–1761, 1995.

[183] K. Sigmundsson, G. Másson, R. Rice, N. Beauchemin, and B. Öbrink. Determination of active concentrations and association and dissociation rate constants of interacting biomolecules: An analytical solution to the theory for kinetic and mass transport limitations in biosensor technology and its experimental verification. *Biochemistry*, 41(26):8263–8276, 2002.

[184] S. Xu, J. Zhan, B. Man, S. Jiang, W. Yue, S. Gao, C. Guo, H. Liu, Z. Li, J. Wang, and Y. Zhou. Real-time reliable determination of binding kinetics of DNA hybridization using a multi-channel graphene biosensor. *Nature Communications*, 8(14902), 2017.

[185] R. L. Rich and D. G. Myszka. Survey of the year 2007 commercial optical biosensor literature. *Journal of Molecular Recognition*, 2008(September):355–400, 2008.

[186] Y. Abdiche, D. Malashock, A. Pinkerton, and J. Pons. Determining kinetics and affinities of protein interactions using a parallel real-time label-free biosensor, the Octet. *Analytical Biochemistry*, 377 (2):209–217, 2008.

[187] J. Knezevic, A. Langer, P. A. Hampel, W. Kaiser, R. Strasser, and U. Rant. Quantitation of affinity, avidity, and binding kinetics of protein analytes with a dynamically switchable biosurface. *Journal of the American Chemical Society*, 134(37):15225–15228, 2012.

[188] N. R. Mohammad, N. H. C. Marzuki, and R. A. Wahab. Review; Agriculture and environmental biotechnology: An overview of technologies for immobilization of enzymes and surface analysis techniques for immobilized enzymes. *Biotechnology & Biotechnological Equipment*, 29(2):205–220, 2015.

[189] P. Schwille, J. Bieschke, and F. Oehlenschläger. Kinetic investigations by fluorescence correlation spectroscopy: The analytical and diagnostic potential of diffusion studies. *Biophysical Chemistry*, 66(2-3):211–228, 1997.

[190] K. N. Swonger and A. S. Robinson. Using Fluorescence Anisotropy for Ligand Binding Kinetics of Membrane Proteins. *Current Protocols in Protein Science*, 2018.

[191] M. Jerabek-Willemsen, C. J. Wienken, D. Braun, P. Baaske, and S. Duhr. Molecular Interaction Studies Using Microscale Thermophoresis. *ASSAY and Drug Development Technologies*, (August): 342–353, 2011.

[192] D. Burnouf, E. Ennifar, F. Disdier, M. Baltzinger, and P. Dumas. KinITC: A new method for obtaining joint thermodynamic and kinetic data by isothermal titration calorimetry. *Journal of the American Chemical Society*, 134(1):559–565, 2012.

[193] X. Zhang, A. Poniewierski, A. Jelińska, A. Zagozdzon, A. Wisniewska, S. Hou, and R. Hołyst. Determination of equilibrium and rate constants for complex formation by fluorescence correlation spectroscopy supplemented by dynamic light scattering and Taylor dispersion analysis. *Soft Matter*, 12(39):8186–8194, 2016.

[194] S. Duhr and D. Braun. Why molecules move along a temperature gradient. *Proceedings of the National Academy of Sciences of the United States of America*, 103(52):19678–19682, 2006.

[195] P. Baaske, C. J. Wienken, P. Reineck, S. Duhr, and D. Braun. Optical thermophoresis for quantifying the buffer dependence of aptamer binding. *Angewandte Chemie - International Edition*, 49(12): 2238–2241, 2010.

[196] C. J. Wienken, P. Baaske, U. Rothbauer, D. Braun, and S. Duhr. Protein-binding assays in biological liquids using microscale thermophoresis. *Nature Communications*, (May), 2010.

[197] C. J. Wienken, P. Baaske, S. Duhr, and D. Braun. Thermophoretic melting curves quantify the conformation and stability of RNA and DNA. *Nucleic Acids Research*, 39(8), 2011.

[198] S. A. Seidel, M. Jerabek-Willemsen, D. Braun, and S. Duhr. Microscale thermophoresis quantifies biomolecular interactions under previously challenging conditions. *Methods*, 59(3):301–315, 2013.

[199] S. A. I. Seidel, C. J. Wienken, M. Jerabek-Willemsen, S. Duhr, D. Braun, and P. Baaske. Label-Free Microscale Thermophoresis Discriminates Sites and Affinity of Protein Ligand Binding. *Angew. Chem. Int. Ed.*, pages 10656–10659, 2012.

[200] R. Gesztelyi, J. Zsuga, A. Kemeny-Beke, B. Varga, B. Juhasz, and A. Tosaki. The Hill equation and the origin of quantitative pharmacology. *Archive for History of Exact Sciences*, 66(4):427–438, 2012.

[201] R. A. Copeland. The drug-target residence time model: A 10-year retrospective. *Nature Reviews Drug Discovery*, 15(2):87–95, 2016.

[202] C. Bernasconi. *Relaxation Kinetics.* Academic Press Inc, 1976.

[203] X. Du, Y. Li, Y.-l. Xia, S.-m. Ai, J. Liang, P. Sang, and X.-l. Ji. Insights into Protein Ligand Interactions : Mechanisms , Models , and Methods. *International Journal of Molecular Sciences*, (i):1–34, 2016.

[204] J. I. Steinfeld, J. S. Francisco, and W. L. Hase. *Chemical kinetics and dynamics.* Prentice Hall, 1999.

[205] Z. Yang and K. N. Houk. The Dynamics of Chemical Reactions: Atomistic Visualizations of Organic Reactions, and Homage to van 't Hoff. *Chemistry - A European Journal*, 24(16):3916–3924, 2018.

[206] K. A. van der Meulen and S. E. Butcher. Characterization of the kinetic and thermodynamic landscape of RNA folding using a novel application of isothermal titration calorimetry. *Nucleic Acids Research*, 40(5):2140–2151, 2012.

[207] N. F. Dupuis, E. D. Holmstrom, and D. J. Nesbitt. Single-molecule kinetics reveal cation-promoted DNA duplex formation through ordering of single-stranded helices. *Biophysical Journal*, 105(3): 756–766, 2013.

[208] S. Khrapunov. for the Use of Some Basic Thermodynamic Equations. *Curr Protein Pept Sci.*, 19 (11):1088–1091, 2018.

[209] P. J. Doyle, A. Savara, and S. S. Raiman. Extracting meaningful standard enthalpies and entropies of activation for surface reactions from kinetic rates. *Reaction Kinetics, Mechanisms and Catalysis*, 129(2):551–581, 2020.

[210] S. Schilling-Bartetzko, F. Franceschi, H. Sternbach, and K. H. Nierhaus. Apparent association constants of tRNAs for the ribosomal A, P, and E sites. *Journal of Biological Chemistry*, 267(7): 4693–4702, 1992.

[211] B. Perez-Ramirez, K. E. Shearwin, and S. N. Timasheff. The Colchicine-Induced GTPase Activity of Tubulin: State of the Product. Activation by Microtubule-Promoting Cosolvents. *Biochemistry*, 33(20):6253–6261, 1994.

[212] D. L. Purich and R. D. Allison. *Handbook of Biochemical Kinetics: A Guide to Dynamic Processes in the Molecular Life Sciences*. Elsevier Science, 1999.

[213] E. D. Holmstrom, N. F. Dupuis, and D. J. Nesbitt. Pulsed IR heating studies of single-molecule DNA duplex dissociation kinetics and thermodynamics. *Biophysical Journal*, 106(1):220–231, 2014.

[214] E. D. Holmstrom and D. J. Nesbitt. Biophysical Insights from Temperature-Dependent Single-Molecule Förster Resonance Energy Transfer. *Annual Review of Physical Chemistry*, 67:441–465, 2016.

[215] K. J. Laidler and M. C. King. The development of transition-state theory. *Journal of Physical Chemistry*, 87(15):2657–2664, 1983.

[216] L. E. Morrison and L. M. Stols. Sensitive Fluorescence-Based Thermodynamic and Kinetic Measurements of DNA Hybridization in Solution. *Biochemistry*, 32(12):3095–3104, 1993.

[217] C. Chen, W. Wang, Z. Wang, F. Wei, and X. S. Zhao. Influence of secondary structure on kinetics and reaction mechanism of DNA hybridization. *Nucleic Acids Research*, 35(9):2875–2884, 2007.

[218] R. B. M. Schasfoort. Chapter 1. Introduction to Surface Plasmon Resonance. *Handbook of Surface Plasmon Resonance*, pages 1–26, 2017.

[219] H. H. Nguyen, J. Park, S. Kang, and M. Kim. Surface plasmon resonance: A versatile technique for biosensor applications. *Sensors*, 15(5):10481–10510, 2015.

[220] E. Helmerhorst, D. J. Chandler, M. Nussio, and C. D. Mamotte. Real-time and label-free biosensing of molecular interactions by surface plasmon resonance: A laboratory medicine perspective. *Clinical Biochemist Reviews*, 33(4):161–173, 2012.

[221] P. Schuck and H. Zhao. The Role of Mass Transport Limitation and Surface Heterogeneity in the Biophysical Characterization of Macromolecular Binding Processes by SPR Biosensing. *Methods Mol Biol*, 627:255, 2010.

[222] J. Homola. Present and future of surface plasmon resonance biosensors. *Analytical and Bioanalytical Chemistry*, 377(3):528–539, 2003.

[223] A. Madeira, E. Vikeved, A. Nilsson, B. Sjögren, P. E. Andrén, and P. Svenningsson. Identification of protein-protein interactions by surface plasmon resonance followed by mass spectrometry. *Current Protocols in Protein Science*, 19(21):1–9, 2011.

[224] H. F. Teh, W. Y. Peh, X. Su, and J. S. Thomsen. Characterization of protein-DNA interactions using surface plasmon resonance spectroscopy with various assay schemes. *Biochemistry*, 46(8):2127–2135, 2007.

[225] M. Geitmann and U. H. Danielson. Studies of substrate-induced conformational changes in human cytomegalovirus protease using optical biosensor technology. *Analytical Biochemistry*, 332(2):203–214, 2004.

[226] R. L. Rich, L. R. Hoth, K. F. Geoghegan, T. A. Brown, P. K. Lemotte, S. P. Simons, P. Hensley, and D. G. Myszka. Kinetic analysis of estrogen receptor/ligand interactions. *Proceedings of the National Academy of Sciences of the United States of America*, 99(13):8562–8567, 2002.

[227] O. L. B. Acevedo and D. Pauron. Protein-lipid Interaction Analysis by Surface Plasmon Resonance (SPR). *Bio-protocol*, 4(18), 2014.

[228] H. Zhang, L. Yang, B. Zhou, X. Wang, G. Liu, W. Liu, and P. Wang. Investigation of biological cellprotein interactions using SPR sensor through laser scanning confocal imagingsurface plasmon resonance system. *Spectrochimica Acta Part A: Molecular and Biomolecular Spectroscopy*, 121: 381–386, 2014.

[229] A. L. Chang, M. McKeague, J. C. Liang, and C. D. Smolke. Kinetic and equilibrium binding characterization of aptamers to small molecules using a label-free, sensitive, and scalable platform. *Analytical Chemistry*, 86(7):3273–3278, 2014.

[230] Y. Fang. Label-Free Cell-Based Assays with Optical Biosensors in Drug Discovery. *ASSAY and Drug Development Technologies*, 4(5):583–595, oct 2006.

[231] C. A. Wartchow, F. Podlaski, S. Li, K. Rowan, X. Zhang, D. Mark, and K. S. Huang. Biosensor-based small molecule fragment screening with biolayer interferometry. *Journal of Computer-Aided Molecular Design*, 25(7):669–676, 2011.

[232] J. Fransson, A. Teplyakov, G. Raghunathan, E. Chi, W. Cordier, T. Dinh, Y. Feng, J. Giles-Komar, G. Gilliland, B. Lollo, T. J. Malia, W. Nishioka, G. Obmolova, S. Zhao, Y. Zhao, R. V. Swanson, and J. C. Almagro. Human Framework Adaptation of a Mouse Anti-Human IL-13 Antibody. *Journal of Molecular Biology*, 398(2):214–231, 2010.

[233] J. Concepcion, K. Witte, C. Wartchow, S. Choo, D. Yao, H. Persson, J. Wei, P. Li, B. Heidecker, W. Ma, R. Varma, L.-S. Zhao, D. Perillat, G. Carricato, M. Recknor, K. Du, H. Ho, T. Ellis, J. Gamez, M. Howes, J. Phi-Wilson, S. Lockard, R. Zuk, and H. Tan. Label-Free Detection of Biomolecular Interactions Using BioLayer Interferometry for Kinetic Characterization. *Combinatorial Chemistry & High Throughput Screening*, 12(8):791–800, 2009.

[234] 2bind GmbH. Molecular Interactions. *https://2bind.com/bli*, 2020.

[235] V. Kamat and A. Rafique. Designing binding kinetic assay on the bio-layer interferometry (BLI) biosensor to characterize antibody-antigen interactions. *Analytical Biochemistry*, 536:16–31, 2017.

[236] J. M. Di Trani, S. De Cesco, R. O'Leary, J. Plescia, C. J. Do Nascimento, N. Moitessier, and A. K. Mittermaier. Rapid measurement of inhibitor binding kinetics by isothermal titration calorimetry. *Nature Communications*, 9(1), 2018.

[237] M. Bernetti, A. Cavalli, and L. Mollica. Protein-ligand (un)binding kinetics as a new paradigm for drug discovery at the crossroad between experiments and modelling. *MedChemComm*, 8(3): 534–550, 2017.

[238] R.-Y. Wang. Rapid Scan, Stopped-Flow Kinetics. *Encyclopedia of Inorganic and Bioinorganic Chemistry*, 2011.

[239] S. Martin and M. Schilstra. Rapid Mixing Kinetic Techniques. In *Protein-Ligand Interactions: Methods in Molecular Biology*, volume 1008. 2013.

[240] W. Bujalowski and M. Jezewska. Fluorescence Intensity, Anisotropy and Transient Dynamic Quenching Stopped-Flow Kinetics. In *Spectroscopic Methods of Analysis: Methods and Protocols in Molecular Biology*. 2012.

[241] E. L. Rachofsky and W. R. Laws. Kinetic models and data analysis methods for fluorescence anisotropy decay. *Methods in Enzymology*, 321(1979):216–238, 2000.

[242] G. M. Perez-Howard, P. A. Weil, and J. M. Beechem. Yeast TATA Binding Protein Interaction with DNA: Fluorescence Determination of Oligomeric State, Equilibrium Binding, On-Rate, and Dissociation Kinetics. *Biochemistry*, 34(25):8005–8017, 1995.

[243] J. Fernando Díaz, R. Strobe, Y. Engelborghs, A. A. Souto, and J. M. Andreu. Molecular recognition of taxol by microtubules: Kinetics and thermodynamics of binding of fluorescent taxol derivatives to an exposed site. *Journal of Biological Chemistry*, 275(34):26265–26276, 2000.

[244] E. L. Elson. Fluorescence correlation spectroscopy: Past, present, future. *Biophysical Journal*, 101 (12):2855–2870, 2011.

[245] L. Onsager. Reciprocal Relations in Irreversible Processes I. *Physical Review1*, 37:405–426, 1931.

[246] G. Bonnet, O. Krichevsky, and A. Libchaber. Kinetics of conformational fluctuations in DNA hairpin-loops. *Proc. Natl. Acad. Sci.*, 95(July):8602–8606, 1998.

[247] R. Rigler and J. Widengren. Fluorescence-based monitoring of electronic state and ion exchange kinetics with FCS and related techniques: from T-jump measurements to fluorescence fluctuations. *European Biophysics Journal*, 47(4):479–492, 2018.

[248] A. M. Lieto, R. C. Cush, and N. L. Thompson. Ligand-Receptor Kinetics Measured by Total Internal Reflection with Fluorescence Correlation Spectroscopy. *Biophysical Journal*, 85(5):3294–3302, 2003.

[249] S. Sterrer and K. Henco. Minireview: Fluorescence Correlation Spectroscopy (FCS) - A Highly Sensitive Method to Analyze Drug/Target Interactions. *Journal of Receptor and Signal Transduction Research*, 17(42007):511–520, 1997.

[250] M. Wachsmuth, C. Conrad, J. Bulkescher, B. Koch, R. Mahen, M. Isokane, R. Pepperkok, and J. Ellenberg. High-throughput fluorescence correlation spectroscopy enables analysis of proteome dynamics in living cells. *Nature Biotechnology*, 33(4):384–389, 2015.

[251] Y. Gao, L. K. Wolf, and R. M. Georgiadis. Secondary structure effects on DNA hybridization kinetics: A solution versus surface comparison. *Nucleic Acids Research*, 34(11):3370–3377, 2006.

[252] M. M. Baksh, A. K. Kussrow, M. Mileni, M. G. Finn, and D. J. Bornhop. Label-free quantification of membrane-ligand interactions using backscattering interferometry. *Nature Biotechnology*, 29(4): 357–360, 2011.

[253] G. Vauquelin, W. Huber, and D. C. Swinney. Experimental Methods to Determine Binding Kinetics. In *Thermodynamics and Kinetics of Drug Binding*, Methods and Principles in Medicinal Chemistry, pages 169–189. Wiley-VCH Verlag GmbH & Co. KGaA, 2015.

[254] D. Pörschke. Thermodynamic and kinetic parameters of an oligonucleotide hairpin helix. *Biophysical Chemistry*, 1:381–386, 1974.

[255] A. W. Peterson, R. J. Heaton, and R. M. Georgiadis. The effect of surface probe density on DNA hybridization. *Nucleic Acids Research*, 29(24):5163–5168, 2001.

[256] T. E. Ouldridge, F. Romano, J. P. K. Doye, S. Petr, and A. A. Louis. DNA hybridization kinetics : zippering , internal displacement and sequence dependence. *Nucleic Acids Researc*, 41(19):8886–8895, 2013.

[257] F. Crick and J. Watson. Molecular Structure of Nucleic Acids. *Nature*, 1953.

[258] A. Ianeselli, C. B. Mast, and D. Braun. Periodic Melting of Oligonucleotides by Oscillating Salt Concentrations Triggered by Microscale Water Cycles Inside Heated Rock Pores. *Angewandte Chemie - International Edition*, 58(37):13155–13160, 2019.

[259] A. Kornberg and T. A. Baker. *DNA Replication*. University Science Books, 2005.

[260] Y. Kafri, D. Mukamel, and L. Peliti. Why is the DNA denaturation transition first order? *Physical Review Letters*, 85(23):4988–4991, 2000.

[261] S. A. Gorski, J. Vogel, and J. A. Doudna. RNA-based recognition and targeting: Sowing the seeds of specificity. *Nature Reviews Molecular Cell Biology*, 18(4):215–228, 2017.

[262] D. Khodakov, C. Wang, and D. Y. Zhang. Diagnostics based on nucleic acid sequence variant profiling: PCR, hybridization, and NGS approaches. *Advanced Drug Delivery Reviews*, 105:3–19, 2016.

[263] Z. Xiao, D. Shangguan, Z. Cao, X. Fang, and W. Tan. Cell-specific internalization study of an aptamer from whole cell selection. *Chemistry - A European Journal*, 14(6):1769–1775, 2008.

[264] Y. Yin and X. S. Zhao. Kinetics and dynamics of DNA hybridization. *Accounts of Chemical Research*, 44(11):1172–1181, 2011.

[265] S. Xiao, D. J. Sharpe, D. Chakraborty, and D. J. Wales. Energy Landscapes and Hybridization Pathways for DNA Hexamer Duplexes. *Journal of Physical Chemistry Letters*, 10(21):6771–6779, 2019.

[266] M. T. Woodside, P. C. Anthony, W. M. Behnke-parks, K. Larizadeh, D. Herschlag, and S. M. Block. Direct Measurement of the Full, Sequence-Dependent Folding Landscape of a Nucleic Acid. *Science*, 314(November):1001–1005, 2006.

[267] J. SantaLucia. A unified view of polymer, dumbbell, and oligonucleotide DNA nearest-neighbor thermodynamics. *Proceedings of the National Academy of Sciences of the United States of America*, 95(4):1460–1465, 1998.

[268] C. Chen, W. Wang, J. Ge, and X. S. Zhao. Kinetics and thermodynamics of DNA hybridization on gold nanoparticles. *Nucleic Acids Research*, 37(11):3756–3765, 2009.

[269] M. Jerabek-Willemsen, T. André, R. Wanner, H. Marie, S. Duhr, P. Baaske, and D. Breitsprecher. MicroScale Thermophoresis : Interaction analysis and beyond. *Journal of Molecular Structure*, 1077:101–113, 2014.

[270] S. Sensale, Z. Peng, and H. C. Chang. Kinetic theory for DNA melting with vibrational entropy. *Journal of Chemical Physics*, 147(13), 2017.

[271] Y. Okahata, M. Kawase, H. Furusawa, and Y. Ebara. Kinetic Measurements of DNA Hybridization on an Oligonucleotide-Immobilized 27-MHz Quartz Crystal Microbalance. *Analytical Chemistry*, 70 (7):1288–1291, 1998.

[272] K. Bielec, K. Sozanski, M. Seynen, and Z. Dziekan. Kinetics and equilibrium constants of oligonucleotides at low concentrations. Hybridization and melting study. *Phys.Chem.Chem.Phys*, 21:10798–10807, 2019.

[273] D. Pörschke and M. Eigen. Co-operative non-enzymatic base recognition III. Kinetics of the helix-coil transition of the oligoribouridylic · oligoriboadenylic acid system and of oligoriboadenylic acid alone at acidic pH. *Journal of Molecular Biology*, 62(2):361–381, 1971.

[274] M. A. Mourão, J. B. Hakim, and S. Schnell. Connecting the dots: The effects of macromolecular crowding on cell physiology. *Biophysical Journal*, 107(12):2761–2766, 2014.

[275] Y. Phillip, E. Sherman, G. Haran, and G. Schreiber. Common crowding agents have only a small effect on protein-protein interactions. *Biophysical Journal*, 97(3):875–885, 2009.

[276] B. Liu. *Quantification of macromolecular crowding and ionic strength in living cells.* Phd thesis, University Groningen, 2018.

[277] R. J. Ellis. Macromolecular crowding: Obvious but underappreciated. *Trends in Biochemical Sciences*, 26(10):597–604, 2001.

[278] I. Schoen, H. Krammer, and D. Braun. Hybridization kinetics is different inside cells. *Proceedings of the National Academy of Sciences of the United States of America*, 106(51):21649–21654, 2009.

[279] L. E. Baltierra-Jasso, M. J. Morten, L. Laflör, S. D. Quinn, and S. W. Magennis. Crowding-Induced Hybridization of Single DNA Hairpins. *Journal of the American Chemical Society*, 137(51):16020–16023, 2015.

[280] R. Goobes, N. Kahana, O. Cohen, and A. Minsky. Metabolic buffering exerted by macromolecular crowding on DNA-DNA interactions: Origin and physiological significance. *Biochemistry*, 42(8):2431–2440, 2003.

[281] I. Smyrlaki, M. Ekman, A. Lentini, N. Rufino de Sousa, N. Papanicolaou, M. Vondracek, J. Aarum, H. Safari, S. Muradrasoli, A. G. Rothfuchs, J. Albert, B. Högberg, and B. Reinius. Massive and rapid COVID-19 testing is feasible by extraction-free SARS-CoV-2 RT-PCR. *Nature Communications*, 11(1):1–12, 2020.

[282] M. Reichl, M. Herzog, A. Götz, and D. Braun. Why Charged Molecules Move Across a Temperature Gradient : The Role of Electric Fields. *Physical Review Letters*, 198101(May), 2014.

[283] P. Reineck, C. J. Wienken, and D. Braun. Thermophoresis of single stranded DNA. *Electrophoresis*, 31(2):279–286, 2010.

[284] W. A. Kibbe. OligoCalc: An online oligonucleotide properties calculator. *Nucleic Acids Research*, 35(Web Server Issue):W43–W46, 2007.

[285] J. SantaLucia and D. Hicks. The thermodynamics of DNA structural motifs. *Annual Review of Biophysics and Biomolecular Structure*, 33:415–440, 2004.

[286] K. Tawa and W. Knoll. Mismatching base-pair dependence of the kinetics of DNA-DNA hybridization studied by surface plasmon fluorescence spectroscopy. *Nucleic Acids Research*, 32(8):2372–2377, 2004.

[287] W. H. Braunlin and V. A. Bloomfield. 1H NMR Study of the Base-Pairing Reactions of d(GGAATTCC): Salt Effects on the Equilibria and Kinetics of Strand Association. *Biochemistry*, 30(3):754–758, 1991.

[288] M. S. Searle and D. H. Williams. On the stability of nucleic acid structures in solution: enthalpy-entropy compensations , internal rotations and reversibility. *Nucleic Acids Research*, 21(9):2051–2056, 1993.

[289] X. Zhang, P. J. J. Huang, M. R. Servos, and J. Liu. Effects of polyethylene glycol on DNA adsorption and hybridization on gold nanoparticles and graphene oxide. *Langmuir*, 28(40):14330–14337, 2012.

Acknowledgement